Novel properties of interacting particles in small low-dimensional systems.

A Thesis
Presented to
The Academic Faculty

by

Igor A. Romanovsky

In Partial Fulfillment
of the Requirements for the Degree
Doctor of Philosophy

School of Physics
Georgia Institute of Technology
August 2006

Novel properties of interacting particles in small low-dimensional systems.

Approved by:

Dr. Uzi Landman, Advisor
School of Physics
Georgia Institute of Technology

Dr. Michael Pustilnik
School of Physics
Georgia Institute of Technology

Dr. Constantine Yannouleas
School of Physics
Georgia Institute of Technology

Dr. Leonid Bunimovich
School of Mathematics
Georgia Institute of Technology

Dr. Mei-Yin Chou
School of Physics
Georgia Institute of Technology

Date Approved: June 16, 2006

ACKNOWLEDGEMENTS

I wish to thank Professor Dr. Uzi Landman for the opportunity to study and work in his group in Georgia Institute of Technology, and for being my advisor for this thesis project. I would like to thank him for having confidence in me and for his continuous support and encouragement. I believe that all that knowledge that I gained while staying in his group, especially skills in numerical methods in Physics, will be very useful in my future work.

I want to thank Dr. Ilya Krive, Dr. Eduard Bogachek, and Dr. Constantine Yannouleas for supervising me during my work, for interesting discussions, for correcting my thesis and competent remarks. I want to thank all these people, who spend their time on me, who shared their knowledge and experience with me and from whom I learned most of what I know now.

I want to acknowledge Dr. David Luedtke for proof-reading of my thesis, for his patience correcting my English language mistakes.

Many thanks to all my friends from the Physics department and from other departments for making the good time at Georgia Tech.

TABLE OF CONTENTS

LIST OF TABLES

LIST OF FIGURES

SUMMARY

This work is about the unusual properties of several types of low dimensional small systems of interacting particles. We demonstrate that interaction between particles in the low dimensional small systems can lead to many unexpected effects. As typical cases we consider i) electrons in a quantum wire,considered within model of Luttinger liquid, ii) electrons in a superconducting state, and iii) atoms in a magneto-optical trap.

For the first case, using bosonization techniques, we calculate the thermopower of a Luttinger liquid wire with an impurity and find thermopower due to nonlinearities of dispersion relation for electrons.

For the second case, we considered nanoscopic superconductor - normal metal - superconductor (S/N/S) and superconductor-two dimensional electron gas - superconductor (S/2DEG/S) junctions. For these systems we predict the appearance of a phase dependent force and resonant phase dependent magnetization. We also considered plasma oscillations inside thin superconducting tubes and rings and predicted that the velocities of the plasmons in these systems are periodic functions of the magnetic flux.

Finally, by considering neutral atoms in a harmonic trap we discovered that strongly repelling atoms do not form Bose-Einstein condensate at zero temperature but tend to occupy different orbitals with small mutual overlap, forming crystallite structures similar to Wigner molecules of electrons inside a quantum dot.

The theoretical methods used (several of which are introduced here for the first time) vary depending on size and dimensionality. As a result, this thesis can be logically split into two separate parts. The first part (chapter 2) concerns finite-N systems (trapped bosons), and the second (chapters 3, 4, 5) - concerns 1D and 2D low-dimensional systems with an infinite number of particles, namely quantum wires, S/N/S contacts and superconducting cylinders and rings). The treatment of small finite-N systems requires methods that are markedly different from the methods used for treating the infinite-N low-dimensional

systems – the former have similarities with methods from chemistry, atomic, and nuclear physics – the latter are related to methods from solid state physics and from quantum field theory (bosonization). Whereas small finite-N systems require predominantly computational approaches (Hartree-Fock, projection via fast Fourier transform, variational wave functions, exact diagonalization, etc), treatment of the system with infinite number of particles is mostly analytical.

CHAPTER I

INTRODUCTION

Recently great experimental achievements were made in the area of creation and control of the parameters of small (nanoscopic) quasi-low-dimensional systems, such as ultrathin conducting wires, trapped ultracold atomic gases, and thin superconducting films. Although these systems differ from each other in many ways, they share a common characteristic - the size of the system in one, two, or all three dimensions, is of the order of the quantum mechanical wave length of the particles from which these systems are made of.

At low temperatures the above mentioned systems exhibit various interesting quantum phenomena. A large amount of literature appeared which is aimed at explaining the above phenomena. Because of mathematical difficulties encountered during solution of the physical models of the systems, researchers were forced to develop and refine new, and sometimes quite elegant approaches.

While there are several many-body Hamiltonians that can be solved exactly, the solution to the majority of other important models is unknown. The approaches to find the solution of strongly interacting systems can be divided into two classes. In the first case the original model is replaced by a simplified model that can be solved and then the missing details are added as small perturbations. The main idea of this approach is to calculate as many perturbative terms as possible, in an attempt to converge to the solution of the problem. In the second case, based on some general properties of the initial system, one writes a new Hamiltonian which, while not giving an exact solution of the initial problem in any order of perturbation theory, it can give some qualitatively correct results that agree with the intuitive understanding of the problem.

The mathematical difficulties of solution of a many-body problem originate from the interaction forces acting between the particles of the system. Attempts to take these forces into account using conventional perturbation approach, are doomed to fail in most cases.

Only in very rare cases can a system of strongly interacting particles be described starting from a system of free or weakly interacting particles (electrons in the metal are quite well described within the model of free Fermi gas although their interaction between each other and with ions of crystal lattice in no way can be considered to be weak). As a rule, if such a description is possible, it implies that the elementary excitations of the ground state of the system have the same statistics as the original elementary particles. For example, the Fermi gas model works very well because the properties of the elementary excitations, namely electrons and holes, are very similar to the properties of the bare electrons - both obey the Fermi statistics and a similar dispersion relation in the vicinity of the Fermi energy. In most cases, however, the properties of the elementary excitations have little in common with the properties of the elementary particles from which the system is built. Not only the strength (or sign, as in the case of superconductors) of the interaction can make a system behave in an unusual manner. Rather, the dimensionality of the system may also play an important role. If the size of the system in some direction becomes comparable to the wave length of the particles in the system then the motion of these particles in that particular direction becomes quantized. And if the temperature of the system is low enough, only very few of the lowest states (modes) are populated. Within one quantized state, particles behave very differently than they normally behave in the unrestricted bulk system. This is easily illustrated for a model of hard core particles on a string. Such particles cannot occupy the same location and therefore are unable to pass each other and exchange places. The motion of each particle would be correlated with the motion of its neighbors, and the lowest energy excitations of such particles will be similar to sound waves.

In this work we study, using various non-perturbative methods, different systems of highly-correlated particles. First, we consider the ground state of few strongly interacting bosons in rotating two-dimensional traps. The behavior of trapped bosons at low temperatures is a frontier topic in modern physics. Since the first successful realization of Bose-Einstein condensation of trapped cold alkali gases interest in these systems has been growing. Every year brings hundreds of new publications on this and related topics. Early experiments with cold atoms were able to realize systems of $10^4 - 10^7$ weakly interacting

particles in spherical or ellipsoidal traps and observe collective quantum phenomena related to the effect of Bose-Einstein condensation. Many of these effects can be successfully mathematically described by the mean field Gross-Pitaevskii equation.

Over the past decade experimental techniques in this area constantly improved, and currently the parameters of the cold trapped gases, as well as the shape of the traps, can be controlled with very high accuracy for a wide range of parameters. In particular, one can achieve a situation where the motion of the atoms in the trap is effectively two-dimensional, the number of atoms in the trap is small and the atoms are strongly repelling. The case of few strongly repelling atoms presents a new regime for atomic gas systems. In this thesis we show that under such conditions the Gross-Pitaevskii theory does not provide an adequate description of the ground state of the system. We show that one can construct a superior variational wave function, which has a lower energy than the Gross-Pitaevskii solution. Moreover, the variational wave function that we construct gives a lower energy than the Gross-Pitaevskii wave function even for weak repulsion - this finding is specific to a finite number of bosons. The Bose-Einstein condensate becomes the preferred variational ground state only for a large number of particles.

We consider two cases - the case of neutral bosons in rotating traps and the case of charged bosons in a magnetic field. We show that in both cases at the strong repulsion limit bosons localize at different orbitals, forming crystalline structures similar to the crystalline structures found earlier for electrons in quantum dots. This crystallization is "hidden", that is, it does not show up in the single-particle density, but manifests itself in several ways: the total angular momentum of the system is quantized in steps, with the magnitude of these steps depending on the symmetry of the crystallite. The total energy of the system of neutral bosons saturates (this happens because bosons start to behave as hard impenetrable spheres). The aforementioned crystalline structure consists of concentric polygonal rings centered about the center of the trap. The crystalline structure of the ground state wave function can be revealed by analyzing the two-particle conditional probability density, which has the form of $(N_r - 1)$ peaks (viewed from the location of one of the particles on the rth ring), where N_r is the number of particles in the rth polygonal ring. The rings rotate

independently of each other. The predictions that we make could be verified experimentally.

Secondly, we studied the thermoelectric properties of quantum wires. Quantum wires are conductors in which the motion of the electrons is free in only one direction, while it is quantized along the other two highly confined directions. The transport properties of a small wire with several transverse modes (each defining a 1D transport channel) can be modeled by adding the contributions of each of the channels. Because of the "nesting" effect, these one-dimensional wires can not be described within the Fermi-liquid theory (i.e. using the language of electrons and holes). Electron-like and hole-like excitations of the one-dimensional wire decay quickly, turning into charge density waves, similar to sound waves in an elastic medium, which are the actual elementary excitations for 1D conductors. There are several exactly solvable simplified models for one-dimensional wires. One of them is the Tomonaga-Luttinger model. We considered the thermopower of an infinite Luttinger liquid due to small nonlinearities of the dispersion relation for electrons and the thermopower due to a single nonmagnetic impurity. Applying bosonization techniques, we expressed the Hamiltonian of the systems in terms of Bose operators. Using perturbation theory in one case and the tunneling Hamiltonian method in the other case, we have found that the thermopower in both cases decreases if the strength of repulsion between the electrons increases. Moreover, we qualitatively analyzed the system of a finite Luttinger liquid connected to bulk leads and concluded that in this system the thermopower further decreases with the strength of the repulsion between electrons.

In the third part of the thesis we address the mechanical and magnetic properties of small superconductor – normal metal – superconductor (S/N/S) and superconductor - two-dimensional electron gas – superconductor (S/2DEG/S) junctions. The S/N/S junctions can be created, for example, in an experiment with a scanning tunneling microscope (STM), when the tip and the surface of the STM are cooled below the superconductor critical temperature. Then if the tip is pushed into the surface and is subsequently slowly retracted, a junction will be formed between the tip and the surface. Due to the small diameter of the junction, it will be in the normal state. The force that is required to stretch the junction depends on the quantum state of the conduction electrons. Since the transition from

the normal to the superconducting state affects the density of electron states, we expect the appearance of some additional forces related to superconductivity. Simple estimations show that the magnitude of these forces should be very small, way below the measurable limit. We demonstrate that these estimations are not accurate. The bound levels which form in the normal part of the S/N/S junction due to the appearance of Andreev reflection, and which are responsible for superconductivity induced oscillations of force in the S/N/S junction, are very sensitive to the phase difference of the order parameter in the two superconductor. For some special values of the phase difference when all transverse modes in the junction contribute to the force in unison, the contributions from different transverse modes in the junction add up. In the case of relatively thick normal part of a junction with many transverse modes the resulting total force can be much larger (100-1000 times) than the value obtained in the previous estimate. In addition to the force, we study magnetic response of the S/N/S junction. Due to the same resonance effect, the magnetization of the normal part of the junction (we assume that the magnetic field is applied only to the normal parts of the junction and is zero elsewhere) can be quite large ($\sim 100\mu_B$) and is detectable. In addition to the S/N/S junctions we considered S/2DEG/S junctions. Although experimentally S/2DEG/S system is very different from S/N/S system, its theoretical description is similar. The main differences between the theoretical models of the S/N/S and the S/2DEG/S junctions are the following: i) the effective masses of the electrons in the two-dimensional electron gas and in the bulk superconductor can differ greatly, ii) there are barriers at the interfaces between the bulk superconductors and the 2DEG. We considered the effects of these differences on the magnetization (the magnetic field is again applied locally to the 2DEG and is zero near superconductors). Since the amplitudes of both force and magnetization oscillations are withing a measurable range of values, our work provides the impetus for experimental investigations of these effects.

In the concluding chapter of this thesis we considered plasma oscillations in thin superconducting tubes and rings. Such superconducting thin structures can be formed by coating the surface of small capillary tubes with a superconducting material. Thin superconducting rings may be fabricated by etching of a thin superconducting layer made by evaporation of

superconducting material on the surface of a dielectric. Ordinary plasma oscillations can not exist in a bulk superconductor since the strong Coulomb repulsion will inevitably shift the frequency of these oscillations to values which are much higher than that corresponding to the superconductivity gap. In sufficiently thin structures the Coulomb interaction is not so effective and the plasma waves have an acoustic type of dispersion relation. The dispersion curve can be split into two regions - for small frequencies the dispersion relation is similar to that of plasma oscillations in a thin superconducting thread, and for higher frequencies the dispersion relation is similar to the dispersion relation in a thin superconducting plane. Tubes and rings are multiply-connected objects, which make it possible to study the Aharonov-Bohm effect for plasma oscillations. We derived a general expression for the plasma oscillations in rings and tubes and found that the frequency of the plasma oscillations is a periodic function of the magnetic flux with a period $hc/2e$, and that the the relative amplitude of the frequency or velocity variations due to the Aharonov-Bohm effect is proportional to $(\xi_0/R)^2$, where ξ_0 is the superconducting coherence length, and R is the radius.

The plan of the thesis is as follows. In the second chapter we address the ground state of a system of strongly repelling bosons in an external trapping potential. The third and fourth chapters are, respectively, about thermoelectric properties of quasi-low-dimensional wires and the magnetic and mechanical properties of S/N/S and S/2DEG/S junctions. In the final, fifth, part of the thesis we consider the problem of plasma oscillations in quantum cylinders and rings. Each of these parts has a brief review of the history of the subject, explanation of our approach and a short summary in which we discuss our results.

CHAPTER II

CRYSTALLINE PHASES OF REPELLING BOSONS IN TRAPS.

2.1 Introduction.

The great interest concerning the properties of bosonic particles at low temperature can be explained by the fact that under certain conditions at low temperatures bosons demonstrate a wealth of interesting quantum effects which are, in most cases, the manifestation of the phenomenon known as Bose-Einstein condensation. The phenomenon of Bose-Einstein condensation (BEC) was predicted by Einstein on the basis of a study made by Bose about photons. In a thermodynamical sense, when the condensation occurs, a large finite fraction of particles occupies the same state with the lowest energy. The prediction about the possibility of a system of particles, which obeying Bose statistics, to "condense" was made originally for the free particles. But later, after the observation of superfluidity of liquid ^4He, it was realized that BEC can occur also in particles with strong interactions. Many years later, BEC was experimentally produced in a completely different system - in trapped ultracold gases of neutral atoms. The first experimental realization of Bose-Einstein condensation in confined gases was achieved in 1995 [1]. The condensation of atoms was done in three stages: atoms were trapped in the magnetic trap, then laser-cooled, and then evaporatively cooled. Laser cooling and use of magnetic traps and other modern sophisticated techniques give researchers unprecedented control over the parameters of the system and allows one to control the motion of the atoms in the trap with very high precision. The condensates exhibit many interesting quantum phenomena like superfluidity and formation of vortices in rotating traps. Due to the possibility of manipulating the parameters of the traps with great accuracy in a wide range, ultracold trapped gases became a very popular subject of study among experimental physicists. From the theoretical point of view, due to

the low densities of the trapped gases and usually weak and the short-range character of the interaction potential between them, it is possible to simplify the mathematical model of such systems and apply different perturbation methods to them, and make theoretical predictions that agree very well with experimental data. Thus, weakly interacting ultracold atoms became an area where experiment and theory met together. As a result, in the decade, following the first experimental observation of Bose condensates, the properties of ultracold gases were extensively studied both experimentally and theoretically. Huge volume of literature has been produced. The first experiments were done with Rb atoms. Today many laboratories can create condensates with Rb, Na, Li, and H atoms. Although much theoretical and experimental work was directed toward the investigations of properties of neutral bosonic atoms, some preliminary theoretical studies were also done for the systems of particles interacting via a Coulomb potential, in particular for finite systems of a small number of bosons in a potential trap [2]. Such systems are realizations of Thomson's raisin cake model for atoms. From the experimental side, behavior of charged atoms in the traps is studied in great detail in cluster physics, where such systems are known as *quantised Thomson atoms*. Although those experiments are done only with fermion atoms, we believe that the same methods can be used with bosonic particles. For example, a bosonic Thomson atom can be realized by trapping alpha particles in a Paul trap.

The sizes of the magneto-optical traps and their shape can be very different. Moreover, cold atoms in the potential traps can be stirred up to induce uniform rotation [3]. Very popular are the experiments with quasi-low-dimensional traps and systems of few strongly interacting particles. Such systems are produced by loading Bose-Einstein condensate into an optical lattice. Optical lattice is formed by three mutually perpendicular (with mutually perpendicular polarizations) retroreflected laser beams. The optical potential depth is proportional to the intensities of the laser beams. One can create a situation when intensities of the two laser beams are very high, such that the motion of the atoms in two of the three directions is restricted. Two strong laser beams produce a two-dimensional array of tubes, and particles can move only in one direction - along the axis of the tubes. For sufficiently high intensities, hopping between the tubes becomes impossible, i.e. the system becomes

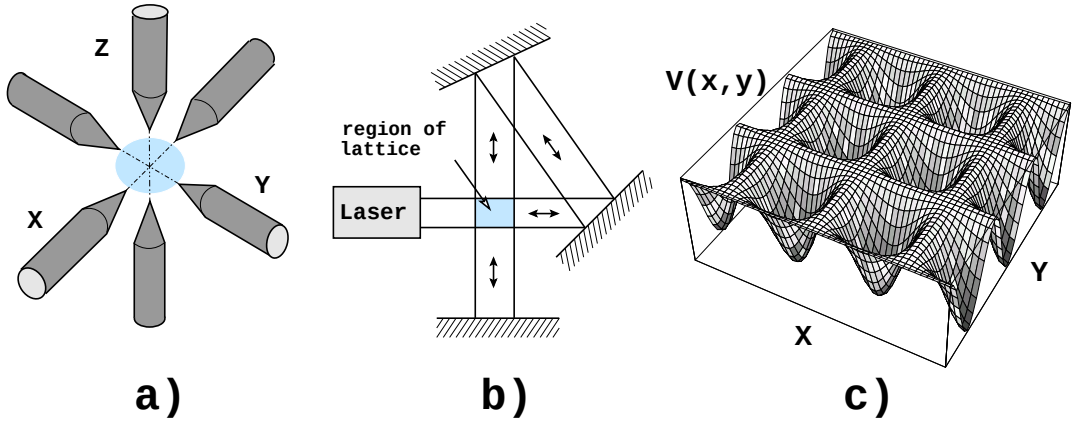

Figure 1: Optical crystal lattice. Optical crystal lattice is created by three mutually perpendicular standing waves Fig. a). One of the experimental schemes to produce an optical lattice is shown on the Fig. b). The effective external potential, which is formed by intersections of the laser beams has shape of the square lattice of wells, separated by the distance $\lambda/2$ (where λ is a wavelength of the laser light). The depth of the potential wells in the optical lattice can be changed by changing the intensity of the light.

effectively one-dimensional. Motion in the direction along the axis of the tubes can be additionally modulated by changing the intensity of the third beam. Such systems were experimentally realized and studied by the group of David Weiss [4] and were used to study the properties of Bose gases of strongly interacting particles. In the best experiments, tubes with geometric ratio (length of the tube versus its width) about 300 have been produced.

Another limiting case that one can think about is the situation when the intensity of one laser beam is much higher than the intensities of the beams in other two directions; then the atomic cloud is split into many pancake-shaped small clouds. By adjusting the intensities of laser beams, one can achieve a situation when each potential well contains only a few particles that move independently from the particles in other potential wells. In the vicinity of the bottom of each well, the potential can be roughly approximated by a harmonic potential. Thus one gets many identical harmonic wells with a few atoms per well. Each of these wells can be rotated independently using the same methods as those used to rotate Bose-Einstein condensates with thousands of particles. Although each potential well contains very few particles, due to big number of almost identical wells, the experimental signal from the system should be enhanced many times to the level when it can be used for

measurements.

The strength of interaction between the particles of the gas can be varied in a wide range and controlled with high accuracy. There are several ways to change the strength of interaction between the particles. The most popular is the method in which the scattering length of atoms is changed by the external magnetic field. The scattering length of the atoms depends on the magnetic field due to the effect of the Feshbach resonance. The mechanism of the Feshbach resonance is the following. For some atoms the interatomic potential is such that atoms can be in two different hyperfine states, one of which is a long-lived quasi-bound state and the other one is an open scattering state. The scattering state is also called an "open channel", and the bound state is called a "closed channel". The bound state exists in another part of the quantum-mechanical Hilbert space than the open scattering state. Due to the different magnetic moment of these two states, they have different Zeeman shift in a magnetic field. The Feshbach resonance occurs when the energy of the bound state is equal to the energy of a colliding pair of atoms. In the vicinity of the Feshbach resonance, the absolute value of the scattering length becomes very big. The increase of the scattering length happens because of the coupling of the open and closed channel. The closed and open channel can be coupled not only by shifting the levels in a magnetic field (magnetic Feshbach resonance), but also by shining light with a certain frequency on the atoms and thus initiating photoassociation transitions (optical Feshbach resonance).

2.2 The problem of few strongly repelling bosons.

In this part of the Dissertation, we study systems of strongly repelling bosons in rotating traps and develop new methods for their theoretical study. We show that strongly repelling bosons form a new state very different from the familiar Bose-Einstein condensate.

The problem of *weakly* interacting cold atoms in various potentials was studied very intensively over the past two decades. In this work we address a problem of theoretical description of *few strongly repelling bosons* in rotating quasi-two-dimensional harmonic and ring-shaped traps. We study the behavior of the ground state of such systems at different

parameters.

In order to proceed further and to discuss the ground state properties of few bosonic atoms in the traps we need to modify the definition of the Bose-Einstein condensation. The thermodynamical definition of condensation obviously cannot be used for a small number of particles. For a finite number of particles by Bose-Einstein condensation we understand the situation when *all* particles of the system occupy the same single-particle quantum state. This means that a many-particle wave function of the system, if described in the Fock space, is fully characterized by a single one-particle orbital.

2.3 Pseudopotential approximation. Coupling constant.

To start the description of the strongly repelling bosons, we should first specify the model for interaction potential. Let us consider a gas of cold neutral atoms. Let us assume that the range of the interaction potential is much smaller than the de Broglie wave length of the atoms. The specific shape of the interparticle potential in this case is not important, because all particles are spread out in the space and feel only an averaged effect of the potential of other particles. Interaction between particles can be characterized by a single parameter - the scattering length a, which is an effective diameter of the potential. The scattering from a short range (contact) potential in this limit can be viewed as scattering of hard spheres of diameter a. The Schrödinger equation for hard spheres in the center-of-mass system is

$$\begin{cases} (\nabla^2 + k^2)\psi(\mathbf{r}) = 0 & (r > a) \\ \psi(\mathbf{r}) = 0 & (r \leq a) \end{cases} \tag{1}$$

Therefore, the hard-sphere potential is set by imposing explicit boundary condition on the relative wave function of two interacting particles. Description of interacting potential by boundary conditions is very inconvenient for practical calculations. To simplify the problem even further the hard sphere potential is replaced by a fictitious and unphysical potential, (*pseudopotential*) which, however, gives correct amplitudes and phase shifts outside the sphere a and does not require any boundary conditions. In three dimensions for S-wave

scattering method of pseudopotentials gives the following approximation [5]

$$U_{3D}^{(2)}(r) = W_{3D}\delta(\mathbf{r})\frac{\partial}{\partial r}(r\ \bullet) \tag{2}$$

where parameter W_{3D} is called a *coupling constant*. Positive coupling constant corresponds to repulsive interaction between bosons and negative - to attractive. In full three dimensional systems coupling constant is given by the formula

$$W_{3D} = \frac{4\pi\hbar^2 a}{m} \tag{3}$$

where $a = a_{3D}$ is a atomic scattering length, $m = m_a/2$ is the reduced mass, and m_a is the mass of the single atom. Notice that in bulk 3D case coupling constant depends only on the parameters of the atoms and does not depend on parameters of the trapping potential.

In quasi-one and quasi-two dimensional systems expression for pseudopotential is simpler than in 3D case, namely short-range interaction can be modeled with the Dirac delta function

$$U^{(2)}(r) = W\delta(r) \tag{4}$$

Expressions for coupling constant for quasi-one and quasi-two-dimensional systems are not as simple as for pure 3D case. After calculation of the scattering amplitudes, taking into account the confinement potential, it turns out [6, 7, 8, 9] that to preserve the form of the equations, describing atoms in the traps, the expression for coupling constant in quasi-two-dimensional system should be modified. For quasi-two-dimensional trap coupling constant is given the the expression [7]

$$W_{2D} = \frac{2\sqrt{\pi}\hbar^2}{m}\frac{1}{l_\perp/a + (1/\sqrt{2\pi})\ln(1/\pi q^2 l_\perp^2)} \tag{5}$$

here $l_\perp = \sqrt{\hbar/m\omega_\perp}$ is the characteristic length of the confining potential in the direction perpendicular to the pancake, and q is the relative momentum of the colliding particles. In the limit $l_\perp >> a$ the logarithmic term in (5) is not important, and W is energy independent. On the other hand, if $l_\perp \sim a$, the logarithmic term becomes dominant, and the coupling constant can be approximately written as $W \approx -\frac{2\pi\hbar^2}{m}\frac{1}{\ln(a/l_\perp)}$. Figure 2 shows the effective strength of the interaction between particles in the quasi-two-dimensional trap as a function

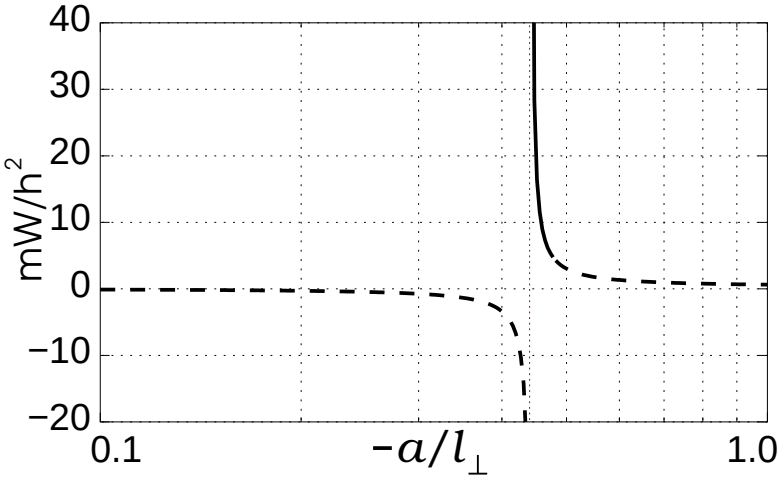

Figure 2: Effective strength of interaction in a quasi-two dimensional trap as a function of trap width. The effective interaction strength g between particles in quasi-two dimensional trap depends on their relative energy. For negative 3D scattering length a coupling constant g demonstrates resonant behavior. The resonance is achieved at $a^* = -\sqrt{2\pi} l_\perp / \ln(K\hbar\omega_\perp/\pi\epsilon)$ where ϵ is relative energy of colliding particles and $K \approx 0.915$. Parameters $l_\perp$ and $\omega_\perp$ are oscillator length and oscillator frequency in the tightly confined direction. Although the 3D scattering length is negative, the effective coupling constant at the vicinity of resonance can be positive and very large, which corresponds to strong repulsion between atoms.

of the ratio $a/l_\perp$. By deforming the confining potential, for attracting atoms, one can reach a regime when atoms repel each other.

In the quasi-one-dimensional (Q1D) case, the situation is similar. The coupling constant is

$$W_{1D} = -\frac{\hbar^2}{m a_{1D}} , \qquad a_{1D} = -\frac{l_\perp^2}{2a}\left(1 - C\frac{a}{l_\perp}\right) \tag{6}$$

where $l_\perp = \sqrt{\hbar/m\omega_\perp}$ is the width of the trap (which is assumed harmonic) in the transverse directions, and $\omega_\perp$ is the transverse frequency.

Notice, that in both quasi-one- and quasi-two-dimensional cases, the coupling constant depends on the confining potential. Therefore, by changing parameters of the confining potential, one can modify the coupling constant W. One can also modify the reduced mass m which also enters formulas (6) and (5). This is done by applying a weak beam along non-restricted directions. The periodic weak electromagnetic potential of the beam plays the same role as a crystal lattice in the metal with atoms instead of electrons. The effective

Table 1: Estimates for kinetic and interaction energy and expressions for coupling constant for the gas of neutral bosons in different dimensions. In this table variable n means local density of atoms. For each case definition of density is different. For 1D case n is number of particles per unit length, for 2D - per unit area and for 3D - per unit volume.

...	1D	2D	3D
$K \sim$	$\hbar^2 n^2/m$	$\hbar^2 n/m$	$\hbar^2 n^{2/3}/m$
$I \sim$	nW	nW	nW
W	$\frac{2\hbar^2 a}{m l_\perp}$	$\frac{2\pi\hbar}{m \ln(1/ka)}$	$\frac{4\pi\hbar^2 a}{m}$

mass of the atoms in such a system can differ very much from their real mass m_a.

2.4 Strength of repulsion and formation of boson molecules (Tonks Regime).

To characterize the strength of repulsion between atoms, we can introduce a dimensionless parameter $\gamma = I/K$, which is the ratio of interaction energy to the kinetic energy of the system. It turns out that the interaction strength γ depends not only on the coupling constant W, but also on the density n of the gas of atoms. As follows from the Table 1, the criterion of strong interaction. ($\gamma \gg 1$) is different for each case. For a 3D case, it is $n^{1/3}a \gg 1$, For 2D case strongly interacting regime is achieved when $n^{1/2}a \gg 1$; and for 1D, the condition is $a/(nl_\perp^2) \gg 1$. The 1D case is quite counterintuitive because the strongly interacting limit corresponds to low densities of the gas, i.e., the lower the density, the stronger the effective interaction between bosons.

For zero gamma (no repulsion) at zero temperature, all particles fall into the same state with the lowest energy, i.e., Bose-Einstein condensation occurs. At weak repulsion strength ($\gamma \ll 1$), bosons can still remain in the same orbital, though the orbital will be distorted by the interaction. At higher repulsion strength ($\gamma > 1$), bosons will minimize

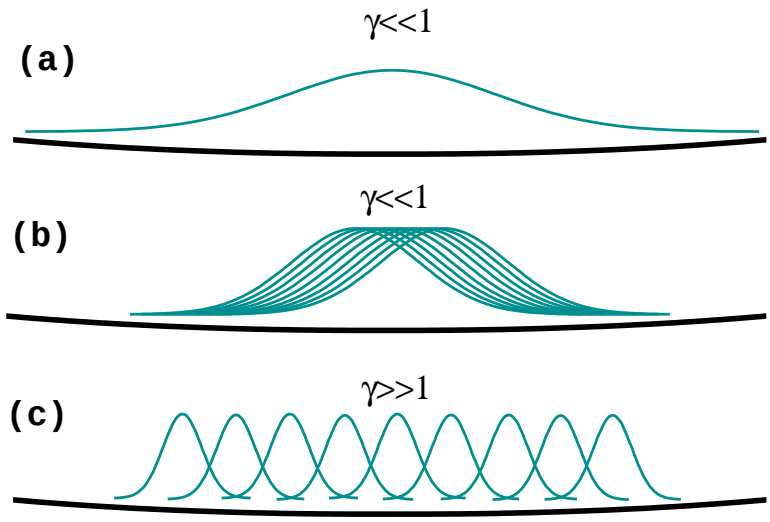

Figure 3: Gas of bosons at different values of repulsion strength. Tonks regime of Bose gas. In the strong repulsion limit **(c)** repulsion energy is minimized better if particles localize on different orbitals. Schematic pictures **(a)** and **(b)** show possible scenarios for Bose gas in the weak repulsion limit. When repulsion between particles is not very strong particles may choose between two possible ways to minimize their repulsion energy. Figure **(a)** corresponds to condensate regime of Bose gas and all other figures describe Tonk regime.

their repulsion energy either by deforming their common orbital or by going to different orbitals (see Fig.3c). In the latter case, we can say that the Bose condensate is destroyed and bosons start to behave like impenetrable spheres; in other words, bosons are prevented from occupying the same position in space. This behavior mimics the Pauli exclusion principle for fermions, causing the bosonic particles to exhibit fermionic properties. The first who reported this behavior was Giraredeau. In paper [10] in 1960, long before the first experimental realization of the system of trapped ultracold atoms, he showed that there is a one-to-one mapping of 1D impenetrable bosons to a system of free fermions. A little bit later two authors, Lieb and Liniger, considered a similar system, where bosons interacted via Dirac delta potential $U_0\delta(x-x')$. They studied the ground state and excitation spectrum of this system and found that 1D bosons in the strong repulsion limit $U_0 \to \infty$ indeed behave like fermions. Since the classical problem of gas of hard core particles (a prototype of the quantum mechanical problem) was solved by Tonks [11], the regime of the gas of strongly repelling bosons, which behave like fermions, is usually called the Tonks-Girardeau regime.

The results of the recent experiments [12, 4] confirmed the predictions made by Girardeau.

2.5 Hartree-Fock Method.

In general, the problem of few trapped interacting bosons cannot be solved exactly; one usually seeks an approximate solution. The approximate solution starts with an assumption about the form of the wave function of the system. By choosing the wave function in the certain form, one simplifies the problem significantly. One of the most popular mean field approaches is the Hartree-Fock approximation. An even simpler, but less accurate approximation is the Hartee approximation. In the Hartree approximation the wave function of N particles is taken in the form of the product of the orbitals $\phi_1,\ \phi_2,\ \phi_3,\ \ldots,\ \phi_N$, namely

$$\begin{aligned} |\Psi_N^H\rangle &= \phi_1(1)\phi_2(2)\phi_3(3)\ldots\phi_N(N) = \\ &= |1\rangle_1 \otimes |2\rangle_2 \otimes |3\rangle_3 \ldots \otimes |N\rangle_N = \\ &= |1\ 2\ 3\ldots\ N\rangle \end{aligned} \tag{7}$$

where we introduced for the orbitals a shorthand notation $\phi_i(x_k) = \phi_i(k) = |i\rangle_k$. Since our particles are indistinguishable bosons, the wave function should be symmetric relative to exchange of any two coordinates. The wave function that has the proper symmetry and is built from products of single-particle orbitals is called a Hartree-Fock wave function, i.e.,

$$|\Psi_N\rangle = \hat{S}(\phi_{i_1}(1)\phi_{i_2}(2)\phi_{i_3}(3)\ldots\phi_{i_N}(N)) = \sum_{P(i_n)} (|i_1 i_2 i_3 \ldots i_N\rangle), \tag{8}$$

were $\hat{S}$ is the symmetrization operator over all possible permutations $P(i_n) = [i_1 i_2 i_3 \ldots i_N]$ of the particles. For example, for $N = 3$ particles we will have

$$\begin{aligned} |\Psi_3\rangle = \phi_1(1)\phi_2(2)\phi_3(3) + \phi_1(1)\phi_3(2)\phi_2(3) + \phi_3(1)\phi_2(2)\phi_1(3) + \\ +\phi_2(1)\phi_1(2)\phi_3(3) + \phi_3(1)\phi_1(2)\phi_2(3) + \phi_2(1)\phi_3(2)\phi_1(3) \end{aligned} \tag{9}$$

In total there are $N!$ terms like $\phi_{i_1}(1)\phi_{i_2}(2)\phi_{i_3}(3)\ldots\phi_{i_N}(N)$ in the sum for the N particle wave function $|\Psi_N\rangle$, under the assumption that all orbitals are different.

The ground state of the system with Hamiltonian $\hat{H}$ is found by minimizing the expression for the total energy

$$E = \frac{\langle\Psi_N|\hat{H}|\Psi_N\rangle}{\langle\Psi_N|\Psi_N\rangle} \tag{10}$$

The drawback of the Hartree-Fock method is that it cannot properly treat correlations between particles. One of the ways to improve this is to use instead of anzats (8) an expression of the type

$$|\Psi_N\rangle = \hat{S}(\phi_{i_1}(1)\phi_{i_2}(2)\dots\phi_{i_N}(N))\prod_{i<k}^{N} f^{(2)}(i-k) = F^{(1)}F^{(2)} \tag{11}$$

The one-body term $F^{(1)} = \hat{S}(\phi_{i_1}(1)\phi_{i_2}(2)\dots\phi_{i_N}(N))$ is the Hartree-Fock term. And the term $F^{(2)} = \prod_{i<k}^{N} f^{(2)}(i-k)$ accounts for pair correlations between particles. This term should go to unity (uncorrelated value) at large distances, and should vanish at small distances if particles strongly repel. The disadvantage of this approach is that we do not know the form of the functions $f^{(2)}$ and should guess it. Fortunately, there are other ways to improve the Hartree-Fock solution. One of them is the method of projections which improves the wave function by restoring its symmetries of many-body Hamiltonian.

2.5.1 Restricted Hartree-Fock Method.

In the majority of cases the theoretical description of bosons in the trap, both numerical and analytical, is done within an approximation in which all particles are assumed to occupy the same orbital $\phi_i = \phi$ (using the language of quantum chemistry this approach can be called "Restricted Hartree-Fock" (RHF)), and therefore the energy (10) is minimized not over the space of functions (8) but over a space of functions of the type

$$\begin{aligned} |\Psi_N^{(RHF)}\rangle &= \phi(1)\phi(2)\phi(3)\dots\phi(N) = \\ &= |\phi\rangle_1 \otimes |\phi\rangle_2 \otimes |\phi\rangle_3 \dots \otimes |\phi\rangle_N \end{aligned} \tag{12}$$

In other words, it is assumed from the very beginning that the ground state of the system is a Bose-Einstein condensate. Obviously, this restricted mean field approximation works well when the interaction between particles is weak. The the RHF is expected to give a solution close to exact solution of the problem.

The Hamiltonian of N bosons in the trap can be written in the form

$$\hat{H} = \sum_{i=1}^{N} h_B(i) + \frac{1}{2}\sum_{i\neq j} U^{(2)}(i-j) \tag{13}$$

with

$$h_B(i) = -\frac{\hbar^2}{2m}\nabla_i^2 + U^{(1)}(i) \tag{14}$$

where $U^{(1)}(i) = U^{(1)}(x_i) = V_{ext}(\mathbf{r})$ is the interaction of bosons with the external confining potential, and $U^{(2)}(i-j) = U^{(2)}(\mathbf{r}_i - \mathbf{r}_j)$ is the potential of interparticle interaction, the double sum is taken over all pairs of different atoms.

After substitution of the expression for the wavefunction (12) into Eq. (10), the expectation value of the energy of the system of N bosons takes the form

$$\begin{aligned} E_N &= N\int d\mathbf{r}\left\{\frac{\hbar^2}{2m}|\nabla\phi(\mathbf{r})|^2 + U^{(1)}(\mathbf{r})|\phi(\mathbf{r})|^2\right\} + \\ &+ \frac{1}{2}N(N-1)\int d\mathbf{r}\int d\mathbf{r}'\phi^*(\mathbf{r})\phi^*(\mathbf{r}')U^{(2)}(\mathbf{r}-\mathbf{r}')\phi(\mathbf{r})\phi(\mathbf{r}')\ . \end{aligned} \tag{15}$$

The orbital $\phi(\mathbf{r})$ that minimizes expression (10) satisfies the equation

$$-\frac{\hbar^2}{2m}\nabla_{\mathbf{r}}^2\phi(\mathbf{r}) + U^{(1)}(\mathbf{r})\phi(\mathbf{r}) + (N-1)\left[\int d^3\mathbf{r}'\phi^*(\mathbf{r}')U^{(2)}(\mathbf{r}-\mathbf{r}')\phi(\mathbf{r}')\right]\phi(\mathbf{r}) = \mu\phi(\mathbf{r}) \tag{16}$$

where μ is a Lagrange multiplier which was introduced to take into account the normalization condition $\langle\Psi_N^{(RHF)}|\Psi_N^{(RHF)}\rangle = 1$. If the atoms are neutral, the interaction between them is short-range.

After substitution of (4) into the Eq.(16) one gets the so-called Gross-Pitaevskii Equation (GPE), which is also known under the name of Nonlinear Schrödinger Equation (NSE)

$$-\frac{\hbar^2}{2m}\nabla_{\mathbf{r}}^2\phi(\mathbf{r}) + U^{(1)}(\mathbf{r})\phi(\mathbf{r}) + (N-1)W|\phi(\mathbf{r})|^2\phi(\mathbf{r}) = \mu\phi(\mathbf{r}) \tag{17}$$

The Gross-Pitaevskii equation was widely investigated in theoretical physics (see, for example Ref. [13]). This equation predicts many important phenomena in weakly interacting condensates. One of them is the appearance of vortices in rotating condensates. The expression for the energy (15) with the potential (4) is simply given by

$$E_N = N\int d\mathbf{r}\left\{\frac{\hbar^2}{2m}|\nabla\phi(\mathbf{r})|^2 + U^{(1)}(\mathbf{r})|\phi(\mathbf{r})|^2 + \frac{1}{2}(N-1)W|\phi(\mathbf{r})|^4\right\} \tag{18}$$

In the limit $l_\perp \sim a$ for large number of particles and at high densities of particles, the interaction between particles significantly depends on local density to take this dependence

into account some authors [14] prefer to use another mean-field equation instead of Eq. (17), namely

$$-\frac{\hbar^2}{2m}\nabla^2_{\mathbf{r}}\phi(\mathbf{r}) + U^{(1)}(\mathbf{r})\phi(\mathbf{r}) + \frac{\hbar^2}{2m}\frac{8\pi}{|\ln|\phi|^2a^2|}|\phi(\mathbf{r})|^2\phi(\mathbf{r}) = \mu\phi(\mathbf{r}) \ . \tag{19}$$

Although equation (19) provides a better description for bosons in 2D traps than Eq.(17), it does not give any qualitatively new results, and like equations (17) and (16), it cannot describe the regime of strong repulsion since it does not permit localization of particles on different orbitals. Eq.(19) better describes opposite case of very weak repulsion or the case of attractive forces between bosons.

2.5.2 The Unrestricted Hartree-Fock Method.

Repulsion forces particles to occupy different orbitals. In the limit of infinite interaction between particles, these orbitals should be orthogonal to each other. The Restricted Hartree-Fock method, which uses wave function in the form given by Eq. (12), assumes that particles occupy the same orbital. Although this assumption is good for weakly interacting particles, it is definitely wrong when the interaction becomes strong. To describe a system of bosons in the limit of strong repulsion, we must use expression (8) for the wave function.

The following results are derived following the same logic as for fermions except that due to different statistics we do not use determinants - the determinants are being replaced with permanents. For example, the norm of a N-particle wave function $|\Psi_N\rangle$ for bosons can be written in terms of the permanents of the overlap matrix

$$\langle\Psi_N|\Psi_N\rangle = N!\sum_{P(i_n)}(1|i_1)(2|i_2)\dots(N|i_N) = N!\ \mathrm{perm}(\mathbf{S}) \tag{20}$$

where the sum in (20) is taken over all permutations $P(i_n)$ of the indexes $i_1, i_2, \dots, i_N$ and $\mathrm{perm}(\mathbf{S}) = \sum\limits_{P(i_n)} s_{1,i_1}s_{2,i_2}\dots s_{N,i_N}$ is the permanent of the overlap matrix $\mathbf{S}$, elements of which are $s_{ij} = (i|j) = \int \phi_i^*(\mathbf{r})\phi_j(\mathbf{r})d\mathbf{r}$. One can easily find the general expressions for the matrix elements of the one- and two- particle operators. For one-particle operators we have

$$\langle\Psi_N|h_B|\Psi_N\rangle = \sum_{P(i_n)P(j_m)}\langle i_1 i_2\dots i_N|h_B|j_1 j_2\dots j_N\rangle =$$

$$= \sum_{k,l}(k|h_B|l) \sum_{P(i_n)P(j_m)} \langle i_1 i_2 \dots i_{k-1} i_{k+1} \dots i_N | j_1 j_2 \dots j_{l-1} j_{l+1} \dots j_N \rangle =$$
$$= (N-1)! \sum_{k,l}(k|h_B|l) \sum_{P(j_m)} \langle \dots, k-1, k+1, \dots | \dots, j_{l-1}, j_{l+1}, \dots \rangle =$$
$$= (N-1)! \sum_{k,l}(k|h_B|l) \mathrm{perm}(\mathbf{S}_l^k) \tag{21}$$

here $(k|h_B|l) = \int d\mathbf{r} \phi_k^*(\mathbf{r}) h_B \phi_l(\mathbf{r})$ and $\mathbf{S}_l^k$ is the minor of the overlap matrix, corresponding to the element kl, i.e. the matrix that we get after eliminating the kth row and lth column from the original matrix $\mathbf{S}$. Similarly we can prove that

$$\langle \Psi_N | U^{(2)} | \Psi_N \rangle = (N-2)! \sum_{i \neq k,\ l \neq m} (ik|U^{(2)}|lm) \mathrm{perm}(\mathbf{S}_{lm}^{ik}) \tag{22}$$

where $(ik|U^{(2)}|lm) = \int d\mathbf{r}_1 \int d\mathbf{r}_2 \phi_i^*(\mathbf{r}_1) \phi_k^*(\mathbf{r}_2) U^{(2)}(\mathbf{r}_1 - \mathbf{r}_2) \phi_l(\mathbf{r}_1) \phi_m(\mathbf{r}_2)$ and $\mathbf{S}_{lm}^{ik}$ is the double-minor of the matrix $\mathbf{S}$ i.e. the matrix that we get from original overlap matrix $\mathbf{S}$ after removing rows i, k and columns l, m. Since all particles are indistinguishable, there are totally N terms $\langle \Psi_N | h_B | \Psi_N \rangle$ and $N(N-1)$ terms $\langle \Psi_N | U^{(2)} | \Psi_N \rangle$ in the Hamiltonian, therefore the final expression for the matrix element $\langle \Psi_N | \hat{H} | \Psi_N \rangle$ is

$$\langle \Psi_N | \hat{H} | \Psi_N \rangle = N! \sum_{k,l}(k|h_B|l) \mathrm{perm}(\mathbf{S}_l^k) + \frac{N!}{2} \sum_{i \neq k,\ l \neq m} (ik|U^{(2)}|lm) \mathrm{perm}(\mathbf{S}_{lm}^{ik}) \tag{23}$$

The total energy $E = \langle \Psi_N | \hat{H} | \Psi_N \rangle / \langle \Psi_N | \Psi_N \rangle$ of the system of N bosons described by a single permanent $|\Psi_N\rangle$ in potential well can be written as

$$E = \frac{1}{\mathrm{perm}(\mathbf{S})} \left(\sum_{k,l}(k|h_B|l) \mathrm{perm}(\mathbf{S}_l^k) + \frac{1}{2} \sum_{i \neq j, k \neq l} (ij|U^{(2)}|kl) \mathrm{perm}(\mathbf{S}_{kl}^{ij}) \right) \tag{24}$$

One has to emphasise that expressions (20)-(24) correspond to Hartree-Fock wave function (8), which is a single permanent of the one-particle orbitals. These expressions involve only matrix elements between equal many-body wave functions. Further in the Thesis we describe a new method, based on the Hartree-Fock method, which gives better results than the Hartree-Fock method. This new method requires calculation of the expressions (which are not shown here because they are more cumbersome) for the matrix elements and overlaps between non-equal bosonic many-body wave functions.

2.5.3 Difficulties of self-consistent unrestricted Hartree-Fock for bosons.

Inspired by the usefullness of the self-consistent Hartree-Fock method for fermions, one can try to build a Hartree-Fock method for bosons. However, very soon one realizes that this is not so simple. In this paragraph we describe why the self-consistent Hartree-Fock method can not be reduced to the simple eigenvalue problem as in the case of fermions.

We start with equation (10). In order to get the ground state of the system, we should find the minimum of the quantity (10). Since orbitals should satisfy the normalization condition $\langle m|m\rangle = \int \phi_m^*(x)\phi_m(x)dx = 1$, the problem reduces to minimization of the functional

$$L = \langle\Psi_N|H|\Psi_N\rangle/\langle\Psi_N|\Psi_N\rangle - N\sum_m \lambda_m(\langle m|m\rangle - 1). \tag{25}$$

Notice at first that since bosons (unlike fermions) can occupy the same state, orbitals are not necessarily mutually orthogonal, i.e. scalar products $\langle m|k\rangle$ may not be equal to zero even if $m \neq k$. The first obvious consequence of this fact is that equation (25) has only N free parameters, instead of $N(N+1)/2$ as in the case of fermions. To understand better the differences between bosons and fermions, let us consider first the simplest case of only $N = 2$ particles. The Hamiltonian for two bosons is:

$$H = \hat{h}(1) + \hat{h}(2) + U^{(2)}(1-2)\ , \tag{26}$$

where $h(1)$ is the single particle Hamiltonian, and the therm $U^{(2)}$ describes interparticle interaction. The wave function for two indistinguishable bosons is simply

$$|\Psi_2\rangle = \phi_1(1)\phi_2(2) + \phi_1(2)\phi_2(1). \tag{27}$$

Taking into account the different symmetry relations between the matrix elements, such as $\langle i|\hat{h}_1|k\rangle = \langle i|\hat{h}_2|k\rangle = \langle i|\hat{h}|k\rangle$ and $\langle 12|U^{(2)}|12\rangle = \langle 21|U^{(2)}|21\rangle$, $\langle 21|U^{(2)}|12\rangle = \langle 12|U^{(2)}|21\rangle$, we can write the matrix elements of the Hamiltionan in the form

$$\langle\Psi_2|H|\Psi_2\rangle = 2\langle 2|h|2\rangle\langle 1|1\rangle + 2\langle 2|h|1\rangle\langle 1|2\rangle + \tag{28}$$

$$+2\langle 1|h|2\rangle\langle 2|1\rangle + 2\langle 1|h|1\rangle\langle 2|2\rangle + 2\langle 12|U|12\rangle + 2\langle 12|U|21\rangle. \tag{29}$$

The function that we should minimize for this specific case is

$$L = \frac{\langle \Psi_2 \mid H \mid \Psi_2 \rangle}{\langle \Psi_2 | \Psi_2 \rangle} + \lambda_1(\langle \phi_1 | \phi_1 \rangle - 1) + \lambda_2(\langle \phi_2 | \phi_2 \rangle - 1), \tag{30}$$

and the variational procedure results in the system of two equations

$$\begin{cases} \Gamma\Big(s_{11}\hat{h} + w_{22}\Big)|\phi_1\rangle + \Gamma\Big(s_{21}\hat{h} + w_{21} + \mu_{21}\Big)|\phi_2\rangle = \lambda_1|\phi_1\rangle \\ \\ \Gamma\Big(s_{22}\hat{h} + w_{11}\Big)|\phi_2\rangle + \Gamma\Big(s_{12}\hat{h} + w_{12} + \mu_{12}\Big)|\phi_1\rangle = \lambda_2|\phi_2\rangle \end{cases} \tag{31}$$

where

$$s_{ik} = \langle i|k\rangle \ , \qquad \mu_{ik} = \langle i|\hat{h}|k\rangle - E s_{ik} \ , \qquad \Gamma = 1/\left(1 + |s_{12}|^2\right)$$

$$\sigma_{ik} = \gamma s_{ik} = s_{ik}/\left(1 + |s_{12}|^2\right) \ , \qquad w_{ik} = \int dy \phi_i^*(y) U(x-y) \phi_k(y) \tag{32}$$

$$\tag{33}$$

For the energy we have

$$E = \Gamma \sum_{i,k=1}^{2} s_{ik}\langle i|\hat{h}|k\rangle + \langle 12|U|12\rangle + \langle 12|U|21\rangle.$$

To write these equations in matrix form, we need to introduce a basis of orthonormal functions $\{\theta_\alpha\}$ and expand the orbitals in terms of these functions

$$\phi_l(x) = \sum_{\alpha=1}^{k} C_l^\alpha \theta_\alpha(x). \tag{34}$$

After substitution of the expansions of the orbitals into the equation (31), we get

$$\begin{cases} \Gamma \sum\limits_\beta \Big[(s_{11}h^{\alpha\beta} + g_2^{\alpha\beta})C_1^\beta + (s_{21}h^{\alpha\beta} + \mu_{21}\Delta^{\alpha\beta})C_2^\beta\Big] = \lambda_1 C_1^\alpha \\ \\ \Gamma \sum\limits_\beta \Big[(s_{12}h^{\alpha\beta} + \mu_{12}\Delta^{\alpha\beta})C_1^\beta + (s_{22}h^{\alpha\beta} + g_1^{\alpha\beta})C_2^\beta\Big] = \lambda_2 C_2^\alpha, \end{cases} \tag{35}$$

$$h^{\alpha\beta} = \int dx \ \theta_\alpha^*(x)\hat{h}(x)\theta_\beta(x) \ , \quad U^{\alpha\beta\gamma\delta} = \int dx \int dy \ \theta_\alpha^*(x)\theta_\beta^*(y)U(x-y)\theta_\gamma(x)\theta_\delta(y),$$

$$g_i^{\alpha\beta} = \sum_{\gamma\delta}(U^{\alpha\gamma\delta\beta} + U^{\alpha\gamma\beta\delta})(C_i^{\gamma})^* C_i^{\delta}\ , \qquad s_{ik} = \sum_{\alpha}(C_i^{\alpha})^* C_k^{\alpha},$$

$$\mu_{ik} = \sum_{\alpha\beta}(C_i^{\alpha})^* h^{\alpha\beta} C_k^{\beta} - E\sum_{\alpha}(C_i^{\alpha})^* C_k^{\alpha}, \tag{36}$$

$$E = \Gamma\Big(\sum_{ik}\sum_{\alpha\beta} s_{ik} h_{\alpha\beta}(C_i^{\alpha})^* C_k^{\beta} + \sum_{\alpha\beta\gamma\delta} U_{\alpha\beta\gamma\delta}(C_1^{\alpha})^*(C_2^{\beta})^*\Big(C_1^{\gamma}C_2^{\delta} + C_2^{\gamma}C_1^{\delta}\Big)\Big).$$

The system (35) of Hartree-Fock equations for bosons can be written in the form

$$\begin{cases} F_{11}^{\alpha\beta} C_1^{\beta} + F_{21}^{\alpha\beta} C_2^{\beta} = \lambda_1 C_1^{\alpha} \\ F_{12}^{\alpha\beta} C_1^{\beta} + F_{22}^{\alpha\beta} C_2^{\beta} = \lambda_2 C_2^{\alpha} \end{cases}, \tag{37}$$

which can be rewritten in compact form

$$\sum_k \sum_{\nu} F_{ik}^{\mu\nu} C_k^{\nu} = \lambda_i C_i^{\mu}. \tag{38}$$

This equation is similar to the system of Roothaan equations for fermions, namely [15]

$$\sum_{\nu} F^{\mu\nu} C_i^{\nu} = \lambda_i C_i^{\mu}, \tag{39}$$

where $F^{\mu\nu}$ are the matrix elements of the Fock operator $f(1) = h(1) + \sum_b \Big(J_b(1) - K_b(1)\Big)$. The obvious difference between (38) and (39) is that the equations for different bosonic orbitals i are coupled, whereas for fermions one has a separate equation for each index i. Mixing of the bosonic orbitals happens because of the absence of Pauli exclusion principle for bosons. In fact, several or all bosons can occupy the same state. In the case of fermions, orthogonalization of orbitals is achieved using unitary transformations. Indeed, the wave function of the system of fermions is the Hartree-Fock approximation is a determinant made of orbitals, $|\Psi\rangle = \det(\mathbf{A})$. A change of the basis is equivalent to the matrix transformation $\mathbf{A}' = \mathbf{AU}$, and therefore, using the property of the determinants, $\det(\mathbf{AB}) = \det(\mathbf{A})\det(\mathbf{B})$, we can write $|\Psi'\rangle = \det(\mathbf{A}') = \det(\mathbf{AU}) = \det(\mathbf{U})\det(\mathbf{A}) = \det(\mathbf{U})|\Psi\rangle = e^{i\phi}|\Psi\rangle$, i.e. a unitary transformation on the orbitals changes the HF wave function only by a phase factor, which cannot affect the physical observables. Thus, in order to orthogonalize the orbitals of the Hartree-Fock wave function for fermions one needs to find a proper unitary transformation.

Orthogonalization of the orbitals in the case of bosons is not as simple as for fermions. If some state is occupied by more than one particle, then the orbitals are not linearly

independent, which in turn means that the system should be described by a smaller basis ϕ'_μ, where $\mu = 1, 2, \ldots, M < N$. A transformation $\mathbf{X}$ that orthogonolizes the orbitals, automatically reduces the number of orbitals. It is also unclear how to build in a reduced basis an orthogonalization procedure that does not spoil the many-body wave function $|\Psi\rangle$, which in the case of bosons is a *permanent* of the matrix of the orbitals, $|\Psi\rangle = \mathrm{perm}(A)$. Indeed, unlike the case of determinant, the permanent of a product of matrices is not equal to the product of permanents $\mathrm{perm}(\mathbf{AB}) \neq \mathrm{perm}(\mathbf{A})\mathrm{perm}(\mathbf{B})$. Thus, methods of orthogonalization using unitary transformations that worked for fermions are not applicable to bosons. One of the possible ways around this problem is to use method developed by Goddard [16, 17, 18] His method does not require orthogonalization of the basis but is very complicated, and as a result it is used in quantum chemistry for only a small number of cases, in particular for systems involving a small number of valence electrons forming pairwise covalent bonds. Moreover, the self-consistent solution of the equation (38) in its original form is computationally much more expensive than the solution of the corresponding Hartree-Fock equation for fermions (39), especially in the case of more than two particles, because the self-consistent procedure involves recomputation of the permanents of large matrices at each iteration.

2.6 Projection techniques.

The wave function of a system must have the same symmetry as the many-body Hamiltonian. If the Hamiltonian $\hat{H}$ of a system is invariant under some transformations $\{\hat{S}\}$, its wave function should also be invariant under the same transformations. However, when solving the Schrödinger equation in the mean field approximation, many times, instead of getting a single solution with correct symmetry one gets a manifold of solutions $|\psi_i(\mathbf{r})\rangle$. These multiple mean field solutions have the same energy, but their symmetry is lower than that of the Hamiltonian (symmetry breaking). Moreover any two of the solutions $|\psi_i(\mathbf{r})\rangle$ are related to each other by a symmetry transformation which commutes with the Hamiltonian ($|\psi_i(\mathbf{r})\rangle = \hat{S}_{ik}|\psi_k(\mathbf{r})\rangle$). Symmetry breaking presents a dilemma, but this dilemma can be resolved. The solution with correct symmetry $|\Psi_S(\mathbf{r})\rangle$ can be constructed from mean field

solutions using projection techniques [19, 20, 21]. The symmetric wave function is a linear combination of different broken-symmetry mean-field solutions $|\psi_i(\mathbf{r})\rangle$:

$$|\Psi_S(\mathbf{r})\rangle = \sum_i f_i |\psi_i(\mathbf{r})\rangle, \tag{40}$$

where f_i are proper coefficients, chosen in such a way as to minimize the expectation value of the Hamiltonian. In the case of breaking of a continuous symmetry, the sum over discrete index i is replaced by the integral over the continuous variable (for the rotational symmetry in two dimensions, it is the azimutal angle θ around the axis of rotation). We will discuss this method in detail below when we restore the rotational symmetry of the many-body variational wave function of the ground state.

2.7 Going beyond the mean-field. Two Step Method.

We describe the strongly repelling bosons through symmetry breaking at the unrestricted Hartree-Fock mean-field level followed by a post-Hartree-Fock symmetry restoration, thus taking into account correlations beyond the GP solution. This two-step method, which has not been applied yet to bosonic many-body systems, is successfully used to describe strongly correlated electrons in 2D semiconductor quantum dots [22, 23, 24, 25, 24].

2.8 Step I. Choice of the orbitals. Symmetry breaking.

Since the self-consistent Hartree-Fock method appears to be computationally unfeasible, we describe our system using non-selfconsistent unrestricted Hartree-Fock. The lack of self-consistency is compensated by a very good initial guess for the form of the atomic orbitals. Further improvements of the many-body wave function are achieved via variations of the parameters of the single particle orbitals. Because of the strong repulsion, bosons avoid occupying the same position in space, i.e. they occupy different orbitals. On the other hand, if the repulsion is not very strong, the shape of the orbitals of the interacting bosons not very different from the shape of the orbitals of free bosons. Thus we assume that the interaction between atoms only modifies some parameters and the position of the orbitals, but their shape remains essentially the same. In other words, we model the atomic orbitals

of interacting atoms by displaced and deformed orbitals of free atoms. This approach turns out, at the end, to be a really good approximation.

In the following we will consider the orbitals and energy spectrum of a system of bosonic atoms in harmonic trap in two different situations: i) stationary frame and ii) in a frame that rotates around the symmetry axis of the external parabolic well.

2.8.1 Charged particles in a magnetic field in harmonic trap.

The Hamiltonian of a single charged atom in parabolic potential well in magnetic field is given by the formula

$$\hat{H} = \frac{\hbar^2}{2m_a}\Big(\hat{\mathbf{p}} - \frac{e}{c}\mathbf{A}\Big)^2 + \frac{m_a\omega_0^2}{2}\mathbf{r}^2. \tag{41}$$

In the symmetric Landau gauge $\mathbf{A} = \frac{1}{2}[\mathbf{B}, \mathbf{r}]$ this Hamiltonian can be written in the form

$$\hat{H} = -\frac{\hbar^2}{2m_a}\left(\frac{\partial^2}{\partial x^2} + \frac{\partial^2}{\partial y^2}\right) - i\hbar\frac{\omega_c}{2}\left(x\frac{\partial}{\partial y} - y\frac{\partial}{\partial x}\right) + \frac{m_a\tilde{\omega}^2}{2}(x^2 + y^2)\ , \tag{42}$$

where $\omega_c = eB/m_ac$ is the cyclotron frequency, and $\tilde{\omega} = \sqrt{\omega_0^2 + \omega_c^2/4}$ is the new effective confinement. Introducing the characteristic length $l_A = \sqrt{\hbar/m_a\tilde{\omega}}$, in the dimensionless polar coordinates (ρ, φ) where the radius ρ is defined as $\rho = r^2/l_A^2$, and the angle φ is such that $\tan\varphi = y/x$, the eigenfunctions of Eq.(42) can be expressed via associated Laguerre polynomials $L_n^{(\alpha)}(x)$

$$\begin{gathered}\psi(\rho,\varphi) = R(\rho)e^{il\varphi} \quad , \quad R(\rho) = \rho^{|l|/2}e^{-\rho/2}L_n^{(|l|)}(\rho) \\ L_n^{(\alpha)}(x) = \frac{x^{-\alpha}e^x}{n!}\frac{d^n}{dx^n}\left(x^{n+\alpha}e^{-x}\right)\ .\end{gathered} \tag{43}$$

The spectrum of single-particle energies that corresponds to wave functions (43) is shown in Fig.4, and is known in the literature as the Darwin-Fock spectrum:

$$\frac{E_n^l}{\hbar\omega_0} = (2n + |l| + 1)\sqrt{1 + \left(\frac{\eta}{2}\right)^2} - \frac{l}{2}\eta\ , \qquad \eta = \omega_c/\omega_0\ . \tag{44}$$

If the magnetic field is very strong, $\omega_c \gg \omega_0$, we can approximately neglect the external confining potential, and the spectrum of energies (44) reduces to the spectrum of levels of

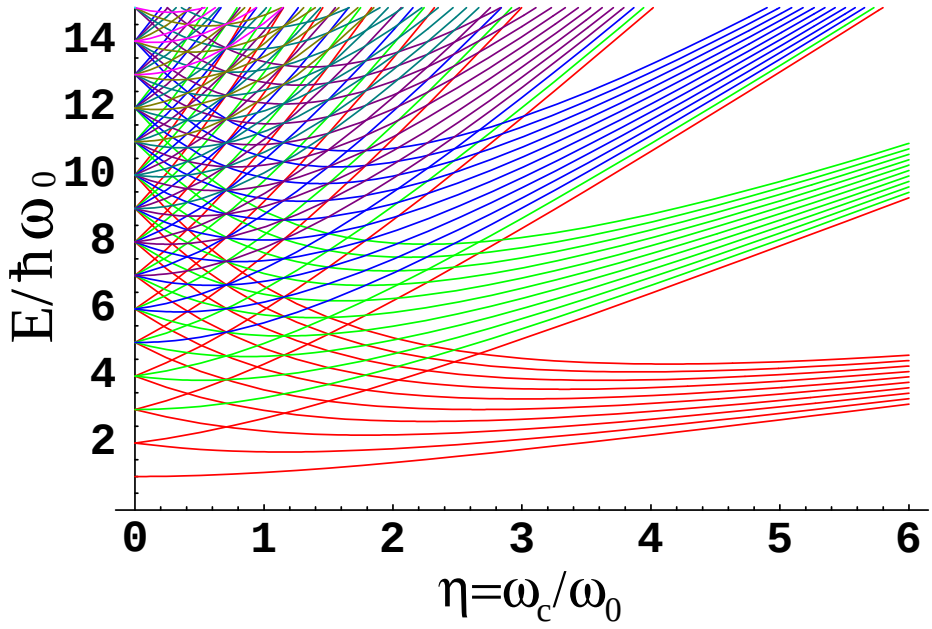

Figure 4: Spectrum of energy levels of a single atom in harmonic potential as a function of magnetic field (Eq. (44)). Different colors correspond to different indexes n. For the strong magnetic field ($\omega_c \sim \omega_0$), when the influence of the trap potential is small but still can not be neglected, the energy level form Landay bands (LB), with energy of each band approaching the energy of some specific Landau level (LL)

a free particle in a strong magnetic field, i.e., to the Landau spectrum (LS).

$$E_n = \hbar\omega_c \left(n + \frac{1}{2} \right) \ . \tag{45}$$

Each level of the Landau spectrum is infinitely degenerate. Each Landau level contains levels with all possible angular momenta. The distance between levels in the Landau spectrum grows with the magnetic field. For finite strengths of the field ($\omega_c \sim \omega_0$), when the influence of the trap can not be neglected, the energy levels form Landau bands (LB), with energy of each band approaching the energy of some specific Landau level (LL) (see Fig.4). The distance between levels within each band decreases with increasing magnetic field. For strong fields the energy levels withing the Landau bands are so close that any small perturbation strongly mixes them. From the Eq.(44) and Fig. (4), one can see that for the free noninteracting particles the lowest state in the spectrum is always a state with zero angular momentum. But if there is some even small perturbation, then, in a sufficiently strong field, one may achieve a situation when some other state, with nonzero l becomes

lower than the state with zero l.

The wave function of the lowest Darwin-Fock level (which corresponds to zero angular momentum l and zero node number n, and has energy $E_0^0 = \hbar\sqrt{\omega_0^2 + (\omega_c/2)^2}$ is given by the expression

$$\psi(\mathbf{r}) = \frac{1}{\sqrt{\pi}\sigma} \exp\left(-\frac{1}{2\sigma^2}(x^2 + y^2)\right), \tag{46}$$

where $\sigma = \sqrt{\hbar/(m\tilde{\omega})}$ is an effective oscillator length, with $\tilde{\omega} = \sqrt{\omega_0^2 + \omega_c^2/4}$. On the other hand, the wave function of the lowest Landau level, corresponding to the ground state energy $E_0 = \hbar\omega_c/2$ can be written in the form

$$\psi(\mathbf{r}) = \frac{1}{\sqrt{2\pi}l_B} \exp\left(-\frac{1}{4l_B^2}((x-X)^2 + (y-Y)^2) - \frac{i}{2l_B^2}(xY - yX)\right) , \tag{47}$$

where $l_B = \sqrt{\hbar c/eB} = \sqrt{\hbar/m\omega_c}$ is the Larmor radius, and $\mathbf{R} = (X, Y)$ is an arbitrary shift of coordinates since in this ($\omega_c \gg \omega_0$) limit all points of the space are equivalent (no confinement). Notice, that this wave function can be considered as a ground state wave function of the unperturbed system and it can be used for calculations of the spectrum in the strong magnetic fields, where an external potential is treated as a small perturbation. Equations (46) and (47) suggest us that, in a first approximation, orbitals of the interacting bosons can be described by the expression

$$\psi_i(x, y) = \frac{1}{\sqrt{\pi\lambda^2}} \exp\left(-\frac{1}{2\lambda^2}((x-X_i)^2 + (y-Y_i)^2) - \frac{i}{2l_B^2}(xY_i - yX_i)\right) , \tag{48}$$

where λ, the width of the orbital, is a variational parameter. λ as well as coordinates of the shift, X_i and Y_i, must be determined by minimizing the energy (10) of the system. In the weak magnetic field, the width λ should be approximately equal to the oscillator length l_0, whereas for strong fields λ, it approaches the value $\sqrt{2}l_B$.

2.8.2 Neutral particles in a rotating harmonic trap.

There are very many analogies between the system in a rotating frame and the system in a magnetic field. In a rotating frame, the effect of rotation manifests itself in the form of Coriolis and centrifugal force. The Coriolis force is

$$\mathbf{F}_{cor} = 2m[\mathbf{v}, \mathbf{\Omega}] . \tag{49}$$

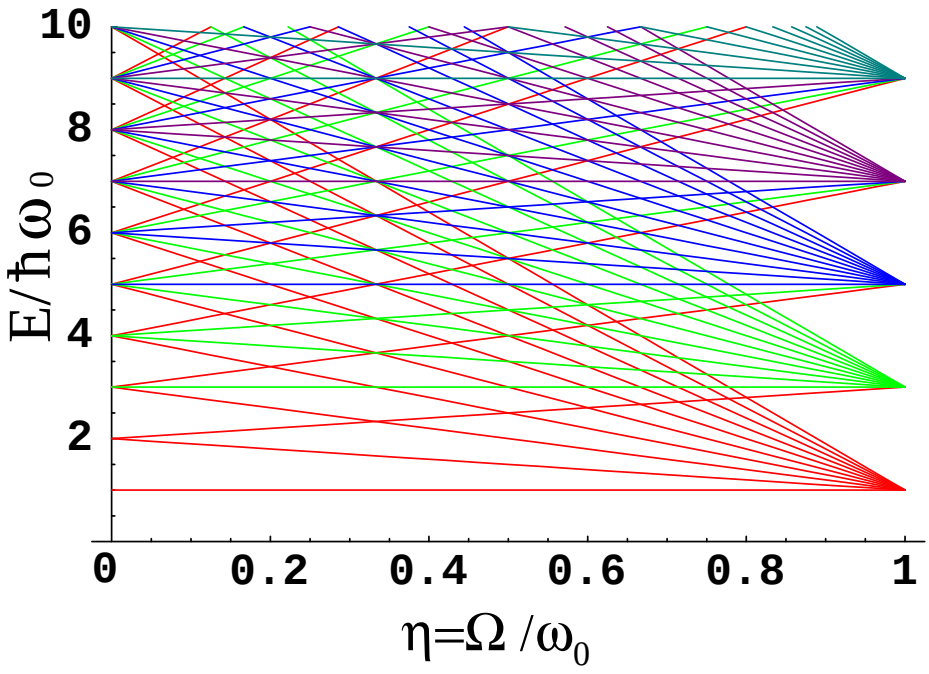

Figure 5: Spectrum of energy levels of a single atom in harmonic potential in the rotating frame as a function of frequency of rotation Ω (Eq. (55)). Different colors correspond to different indexes n.

This fictitious velocity-dependent force is analogous in form to the Lorentz force on the charged particle in the presence of a magnetic field,

$$\mathbf{F}_{lor} = \frac{e}{c}[\mathbf{v}, \mathbf{B}] \ . \tag{50}$$

Comparing the previous two formulas, we can relate the strength of the magnetic field to the angular velocity of rotation

$$\mathbf{B} \to \frac{2mc}{e}\mathbf{\Omega}. \tag{51}$$

The applicability of this analogy becomes even more apparent if we recall that the canonical momentum in the rotating frame is given by

$$\mathbf{P} = \mathbf{p} + m[\mathbf{\Omega}, \mathbf{r}] \ , \tag{52}$$

whereas for a charged particle in the magnetic field the canonical momentum is

$$\mathbf{P} = \mathbf{p} + (e/c)\mathbf{A} \ , \tag{53}$$

where, for the spatially uniform magnetic field $\mathbf{B}$, the vector potential is $\mathbf{A} = [\mathbf{B}, \mathbf{r}]/2$. The Hamiltonian of the particle in the rotating frame in a parabolic confining potential is

$$\hat{H} = -\frac{\hbar^2}{2m_e}\left(\frac{\partial^2}{\partial x^2} + \frac{\partial^2}{\partial y^2}\right) + i\hbar\Omega\left(x\frac{\partial}{\partial y} - y\frac{\partial}{\partial x}\right) + \frac{m_e}{2}{\omega_0}^2(x^2 + y^2)\ , \tag{54}$$

where Ω is the frequency of rotation and ω_0 is the frequency of the confining potential. The spectrum of a particle in the rotating frame is obtained similarly to (44) and is shown in Fig.5

$$\frac{E}{\hbar\omega_0} = (2n + |l| + 1) + l\frac{\Omega}{\omega_0} \tag{55}$$

Repeating the same arguments that led us to expression (48), we can write the expression for the orbitals in the rotating frame as

$$\psi_i(x, y) = \frac{1}{\sqrt{\pi\lambda^2}}\exp\left(-\frac{1}{2\lambda^2}((x - X_i)^2 + (y - Y_i)^2) + \frac{i}{2l_\Omega^2}(xY_i - yX_i)\right)\ . \tag{56}$$

The only difference between (56) and (48) is that instead of $l_B = \sqrt{\hbar/m\omega_c}$, one has $l_\Omega = \sqrt{\hbar/2m\Omega}$. In the same sense as for magnetic fields, one can say that at $\Omega = \omega_0$ the system is in the lowest Landau level.

2.9 Step II. Restoration of rotational symmetry.

The second step of our method is an improvement of the mean-field solution via projection of the many-body wave function on a state with good total angular momentum. After this step, the symmetry of the projected wave function is the same as the symmetry of the Hamiltonian. The specific value of the angular momentum for which the projection should be made is determined from the condition that energy calculated for the projected wave function is minimal. Methods of restoration of symmetries are widely used in nuclear theory (See Ref. [20]). The formula (40) for a rotationally invariant 2D Hamiltonian reads

$$|\Psi_S(\mathbf{r})\rangle = \int_0^{2\pi} d\theta f(\theta)|\psi(\theta, \mathbf{r})\rangle, \tag{57}$$

where the wave function $|\psi(\theta, \mathbf{r})\rangle$ is produced by means of a rotation by an angle θ from the function $|\psi(0, \mathbf{r})\rangle = |\Psi_{MF}(\mathbf{r})\rangle$. The weight $f(\theta)$ is chosen in such a way as to minimize

the expectation value of the Hamiltonian. Namely, the form of the $f(\theta)$ is determined from the equation

$$\delta \frac{\langle \Psi_S | \hat{H} | \Psi_S \rangle}{\langle \Psi_S | \Psi_S \rangle} = 0 \qquad \text{or, equivalently} \qquad \delta \langle \Psi_S | \hat{H} | \Psi_S \rangle - \epsilon \delta \langle \Psi_S | \Psi_S \rangle = 0 \tag{58}$$

Substituting relation (57) into (58) we get an integral equation for $f(\theta)$

$$\int_0^{2\pi} h(\theta' - \theta) f(\theta) d\theta - \epsilon \int_0^{2\pi} n(\theta' - \theta) f(\theta) d\theta = 0 \tag{59}$$

where

$$h(\theta' - \theta) = \langle \psi(\theta') | \hat{H} | \psi(\theta) \rangle \qquad \text{and} \qquad n(\theta' - \theta) = \langle \psi(\theta') | \psi(\theta) \rangle \tag{60}$$

are functions only of differences between angles. The integral equation (59) has solutions $f(\theta) = Ce^{im\theta}$, with an arbitrary constant C and integer parameter m. If we insert this $f(\theta)$ into (59), and make substitution of variables $\theta' - \theta = \xi$, we get

$$e^{im\theta'} \left(\int_{\theta'-2\pi}^{\theta'} h(\xi) e^{-im\xi} d\xi - \epsilon_m \int_{\theta'-2\pi}^{\theta'} n(\xi) e^{-im\xi} d\xi \right) = 0. \tag{61}$$

The functions $h(\xi)$ and $n(\xi)$ are periodic in ξ with period 2π; therefore, the two integrals in (61) are just scalar numbers and, provided the parameter ϵ_m is chosen as

$$\epsilon_m = \frac{\int_0^{2\pi} h(\theta') e^{-im\theta'} d\theta'}{\int_0^{2\pi} n(\theta') e^{-im\theta'} d\theta'} , \tag{62}$$

the left and right hand sides of the equation (61) become identical. Thus, functions $f(\theta) = Ce^{im\theta}$ are indeed solutions of (59). Moreover they form a complete orthogonal basis, and therefore there is no other solutions to equation (59). As a result, the symmetry-restored wave function can be written as

$$|\Psi_S(\mathbf{r})\rangle = \frac{1}{2\pi} \int_0^{2\pi} d\theta e^{im\theta} |\psi(\theta, \mathbf{r})\rangle. \tag{63}$$

If we take into account the properties of the angular momentum operator, namely that operator of angular momentum is a generator of rotations,

$$|\psi(\theta, \mathbf{r})\rangle = e^{-i\theta \hat{L}} |\psi(0, \mathbf{r})\rangle = \hat{R}(\theta) |\psi(0, \mathbf{r})\rangle, \tag{64}$$

the symmetric wave function can be represented in the form

$$|\Psi_S(\mathbf{r})\rangle = \frac{1}{2\pi}\int_0^{2\pi} d\theta e^{i\theta(m-\hat{L})}|\psi(0,\mathbf{r})\rangle = \hat{P}_m|\Psi_{MF}(\mathbf{r})\rangle \tag{65}$$

Thus, multiplying the wave function $|\psi(\theta,\mathbf{r})\rangle$ with the weight $f(\theta) = e^{im\theta}/2\pi$ and carrying out the integration is equivalent to applying the projection operator

$$\hat{P}_m = \frac{1}{2\pi}\int_0^{2\pi} d\theta e^{i\theta(m-\hat{L})} = \delta(m-\hat{L}) \tag{66}$$

which extracts from the function $|\psi(0,\mathbf{r})\rangle$ only states with a given angular momentum $\hat{L} = m$. The wave function $|\Psi_S(\mathbf{r})\rangle$ gives an energy lower than the energy of $|\psi(\theta,\mathbf{r})\rangle$. To see why the operation of projection lowers the energy, we can expand the mean field wave function $|\Psi_{MF}(\mathbf{r})\rangle = |\psi(0,\mathbf{r})\rangle$ in terms of the eigenfunctions $\psi_m(\theta) = \langle\theta|m\rangle = e^{im\theta}/\sqrt{2\pi}$ of angular momentum, namely

$$\Psi_{MF}(\mathbf{r}) = \sum_m a_m(r)\psi_m(\theta) \tag{67}$$

Then, since, the wave functions ψ_m with different indices m are orthogonal, we can express the matrix elements as a sum of squares of absolute values of amplitudes a_m:

$$\langle\Psi|\hat{H}|\Psi\rangle = \sum_m \epsilon_m|a_m(r)|^2 = \epsilon_0 n_0 + \epsilon_1 n_1 + \epsilon_2 n_2 + \ldots \tag{68}$$

$$\langle\Psi|\Psi\rangle = \sum_m |a_m(r)|^2 = n_0 + n_1 + n_2 + \ldots, \tag{69}$$

where $\epsilon_0, \epsilon_1, \epsilon_2, \ldots$ are the energies for states with different angular momenta. Thus, energy of the unprojected wave function is

$$E_{MF} = \frac{\langle\Psi_{MF}|\hat{H}|\Psi_{MF}\rangle}{\langle\Psi_{MF}|\Psi_{MF}\rangle} = \frac{\epsilon_0 n_0 + \epsilon_1 n_1 + \epsilon_2 n_2 + \ldots}{n_0 + n_1 + n_2 + \ldots} \tag{70}$$

On the other hand, the energy of the projected state is

$$E_S(m) = \frac{\langle\Psi_S|\hat{H}|\Psi_S\rangle}{\langle\Psi_S|\Psi_S\rangle} = \frac{\langle\hat{P}_m\Psi|\hat{H}|\hat{P}_m\Psi\rangle}{\langle\hat{P}_m\Psi|\hat{P}_m\Psi\rangle} = \frac{\langle\Psi|\hat{H}|\hat{P}_m\Psi\rangle}{\langle\Psi|\hat{P}_m\Psi\rangle} = \epsilon_m \tag{71}$$

where we used the fact that the projection operator P_m commutes with the Hamiltonian of the system, i.e. $P_m\hat{H} = \hat{H}P_m$, and that $P_m^2 = P_m$. If we assume that wave function with angular momentum m has the lowest energy, then from inequality

$$\epsilon_m(n_0 + n_1 + n_2 + \ldots + n_m + \ldots) < \epsilon_0 n_0 + \epsilon_1 n_1 + \epsilon_2 n_2 + \ldots + \epsilon_m n_m + \ldots \tag{72}$$

we conclude that energy of projected ground state function is smaller than energy of unprojected function $E_S(m) < E_{MF}$.

The energy, obtained by minimization of the expectation value of the energy of an arbitrary trial wave function is, according to the variational principle, an upper bound to the true ground state energy. Thus the minimization with projected wave function gives not just smaller energy, but one, which is closer to the true ground state energy than the energy obtained by varying the unprojected wave function.

The projection of the wave wave function can be done in two different ways. One can minimize the expectation value of energy using unprojected wave function, and then, perform the operation of projection, and calculate the energy of projected wave function. This approach is called *minimization before projection* (MBP). The second way, which is known as *minimization after projection* (MAP), is to use the energy of the projected wave function during minimization. This requires the projection to be carried out at every step of minimization procedure and, therefore takes more time, but energies obtained are better than obtained by the first method.

2.10 Two-step method versus other methods.

Earlier attempts [26, 27, 28] to describe the systems of few bosons in the rotating frame of reference were inspired by the success of the theory of integer and fractional quantum Hall effect. The main idea behind these attempts was to apply the concepts and the methods previously used for highly correlated electrons in strong magnetic field to the systems of highly correlated trapped bosons in rotating frames. In these works, the system of trapped bosons is considered in the *limit of rapid rotation*, i.e., when all particles are restricted to the lowest Landau level. Limit of rapid rotation corresponds to angular frequencies Ω that are close to the frequency of harmonic confinement ω_0. In this limit external potential is almost canceled by the centrifugal potential of rotation. Taking into account only the lowest Landau level, and neglecting all other levels, considerably simplifies the problem for such methods as exact diagonalization, or Hartree Fock. Further simplifications are achieved by constructing explicit relations for many-body wave functions, based on general principles of

symmetry and taking into account specific properties of the interaction potential between particles. The many-body wave function, used by the authors of [26, 27, 28], has the general form

$$\Phi_\nu(z_1,\ldots,z_N) = P(z_1,\ldots,z_N)\prod_k e^{-|z_k|^2/4l_B^2} \tag{73}$$

where $P(z_1,\ldots,z_N)$ is an homogeneous function of the atomic coordinates $z_k = x_k + iy_k$. Due to the symmetry properties of the bosonic wave function, function $P(z_1,\ldots,z_N)$ should be symmetrical under interchange of coordinates of any two particles. For the hard-core bosons $P(z_1,\ldots,z_N)$ is usually chosen in the form

$$P(z_1,\ldots,z_N) = Q(z_1,\ldots,z_N)\prod_{i<j}(z_i - z_j)^{2m} \tag{74}$$

where $Q(z_1,\ldots,z_N)$ is some totally symmetric homogeneous polynomial of coordinates $z_1,\ldots,z_N$, and m is an integer number. Relation (74) is chosen in such way in order to make all formulas for boson similar to the formulas for fermions. The wave function (73), (74) is symmetric and it becomes zero if coordinates of any two particles are the same. This property of the wave function correctly reflects the fact that bosons are strongly repelling and, as a result, avoid each other. The ground state of the system, which is the state with the lowest possible total angular momentum has $Q(z_1,\ldots,z_N) = 1$, and mathematically is the same as Laughlin wave function for bosons in the fractional quantum Hall effect for filling factors $\nu = 1/2m$:

$$\Phi_{2m}(z_1,\ldots,z_N) = \prod_{j<k}(z_j - z_k)^{2m}\exp\left[-\frac{1}{4l_B^2}\sum_i |z_i|^2\right] \tag{75}$$

Notice that analogies between fermions and bosonic systems were explicitly introduced on the stage of building the anzats of the many-body wave function. Function (75) describes bosons in the limit of strong repulsion, but it may not be accurate if repulsion is not very strong when there still exist some nonzero probability of the particles to occupy the same orbital.

The more general theory that takes into account other forms of many-body wave function of the ground state is a theory of *composite bosons*. In this theory, like in the theory

of *composite fermions*, strongly interacting particles in high magnetic field (or at high frequencies of rotation $\Omega \sim \omega_0$) transform into a new kind of weakly interacting particles in a weaker effective magnetic field (smaller frequencies of rotation). Bosons transmute into composite bosons by capturing $2m$ vortices because that is how they screen the repulsive interaction between them. The interaction between composite bosons is weak because most of the interaction was screened out. The many-body wave function of the ground state is given by the relation

$$\Phi^{CB}_{2m,L}(z_1,\ldots,z_N) = \hat{\mathcal{P}}_{LLL} \prod_{j<k} (z_j - z_k)^{2m}\, \Psi^0_{\nu^*,L^*} \tag{76}$$

here $\Psi^0_{\nu^*,L^*}$ is the wave function of N *noninteracting* bosons of total angular momentum $L^* = L - 2mN(N-1)$; it is constructed from the Darwin-Fock orbitals $\psi_{p,l}(z)$, where p is the principal quantum number, and l is an angular quantum number. To take into account Bose statistics, the product of single-particle orbitals should be properly *symmetrized* so that interchange of coordinates of any two particles will not change the wave function. In fact, wave function $\Psi^0_{\nu^*,L^*}$ can be written as a *permanent* of the single particle orbitals.

Factor $q(z_1,\ldots,z_N) = \prod_{j<k} (z_j - z_k)^{2m}$, in front of the $\Psi^0_{\nu^*,L^*}$, which is called in the literature *"Jastrow factor"*, is introduced to represent strong repulsion between particles. For any integer number m this factor is a totally symmetric function of coordinates z_i, and it can be viewed as the consequence of the attachment of $2m$ vortices to each boson $\Psi^0_{\nu^*,L^*}$ to convert it into composite boson. Whereas in the limit of rapid rotation all bosons occupy lowest Landau level, the composite bosons may occupy several Landau levels. The filling factor for composite bosons is related to the filling factor of real particles via $\nu = \nu^*/(4m\nu^* + 1)$. The projection operator $\hat{\mathcal{P}}_{LLL}$ was introduced to guarantee that composite boson is restricted only to the lowest Landau level (in general function $\Psi^0_{\nu^*,L^*}$ is not in the lowest Landau level).

Laughlin-type state (75) is an exact ground state for the particles interacting via short-range potential in the lowest Landau level [29]. The situation with the composite boson wave function is similar. For long-range interactions, like Coulomb interaction, the Laughlin state or composite bosons wave function are just approximations to the real wave function.

This means that Laughlin and composite bosons wave function are good only for qualitative description of the system, but cannot be good quantitatively, especially for frequencies of rotation not very close to the critical frequency. For Coulomb interactions one should use other, better approximations.

Besides these difficulties of the Laughlin and composite boson theories, there is one more problem, which was neglected and forgotten for a long time, but recently attracted attention again. This problem is related to the validity of the lowest Landau level approximation. As was noticed in the paper [30], the Lowest Landau Level approximation is valid only in the weakly interacting regime. The criteria for the lowest Landau level approximation are, in general, too restrictive. At high strengths of repulsion between particles energy levels from other Landau levels can approach very close to the lowest Landau level and thus should not be ignored. The importance of higher Landau levels can be estimated by comparing critical frequencies of rotation for different ground states. Using exact diagonalization method authors of [30] found that for contact potential, critical interaction strength γ_c, at which differences of the critical frequencies exceeds 10%, is of the order $\gamma \sim 1$, and decreases with the number of particles in the system. This means that for $\gamma \gg 1$ Lowest Landau level approximation becomes inappropriate.

In our two-step method many of these problems are avoided. We construct the many body projected wave function from the displaced orbitals (48) or (56). Like the Laughlin wave function or composite the boson wave function, our wave function has good angular momentum. Unlike the case of the wave functions (75) or (76), we do not explicitly restrict bosons from occupying the same orbital. The arrangement of atoms and values of the overlaps of the orbitals are determined during variation and, therefore, should give a better wave function, especially if the repulsion is very strong. Our wave function does not restrict particles to the lowest Landau level. As shown in the Appendix C, unless the width of the orbitals is equal to $\lambda = \sqrt{2}l_B$ (or $\lambda = \sqrt{2}l_\Omega$), the many body wave function always contains contributions from higher Landau levels. Since the width of the orbitals is also a variational parameter, our wave function will be more accurate at high strengths of repulsion than wave functions (75) or (76).

2.11 Results of Calculations.

2.11.1 Neutral and charged bosons in the laboratory frame.

Let us first consider a simple case of a system of N neutral bosons trapped in a harmonic trap in the laboratory frame. The Hamiltonian of a such system is

$$\hat{H} = -\frac{\hbar^2}{2m_e}\left(\frac{\partial^2}{\partial x^2} + \frac{\partial^2}{\partial y^2}\right) + \frac{m_e}{2}{\omega_0}^2(x^2 + y^2) \ , \tag{77}$$

The wave function of the system in this case can be taken to be real. The single-particle orbitals according to the discussion in the previous chapter are approximated by simple Gaussians

$$\psi_i(x, y) = \frac{1}{\sqrt{\pi\lambda^2}} \exp\left(-\frac{1}{2\lambda^2}((x - X_i)^2 + (y - Y_i)^2)\right) \ , \tag{78}$$

and, therefore, the trial wave function of N bosons is automatically real. After substitution of the orbitals (78) into the expression for energy (24), and performing the variation over parameters X_i, Y_i and λ, we get an unrestricted mean-field many-body wave function $|\Phi_{UBHF}\rangle$ of the ground state. The single-particle density, which corresponds to this wave function (see Appendix B), is shown in Fig. 8. Although Hamiltonian (77) is symmetric toward rotation around the axis z (which intersects xy plane at the point $(0, 0)$), the wave function $|\Phi_{UBHF}\rangle$ does not have this circular symmetry and does not have good total angular momentum. To restore the symmetry we have to perform a projection on the state with given angular momentum. Since in the stationary frame without a magnetic field both clockwise and counterclockwise directions of rotation are equivalent, the ground state of the system has zero angular momentum, and according to Eq.(63), the projected (PRJ) Hartree-Fock wave function can be written as

$$|\Psi_{PRJ}(\mathbf{r})\rangle = \frac{1}{2\pi}\int_0^{2\pi} d\theta |\Psi_{UBHF}(\theta, \mathbf{r})\rangle \tag{79}$$

The expression for the energy of the projected function is according to (62)

$$E_{PRJ} = \frac{\langle\Psi_{PRJ}|\hat{H}|\Psi_{PRJ}\rangle}{\langle\Psi_{PRJ}|\Psi_{PRJ}\rangle} = \left(\int_0^{2\pi} h(\theta')d\theta'\right) / \left(\int_0^{2\pi} n(\theta')d\theta'\right) \ , \tag{80}$$

where $h(\theta) = \langle\Psi_{UBHF}(0)|\hat{H}|\Psi_{UBHF}(\theta)\rangle$ and $h(\theta) = \langle\Psi_{UBHF}(0)|\Psi_{UBHF}(\theta)\rangle$. Energies of the

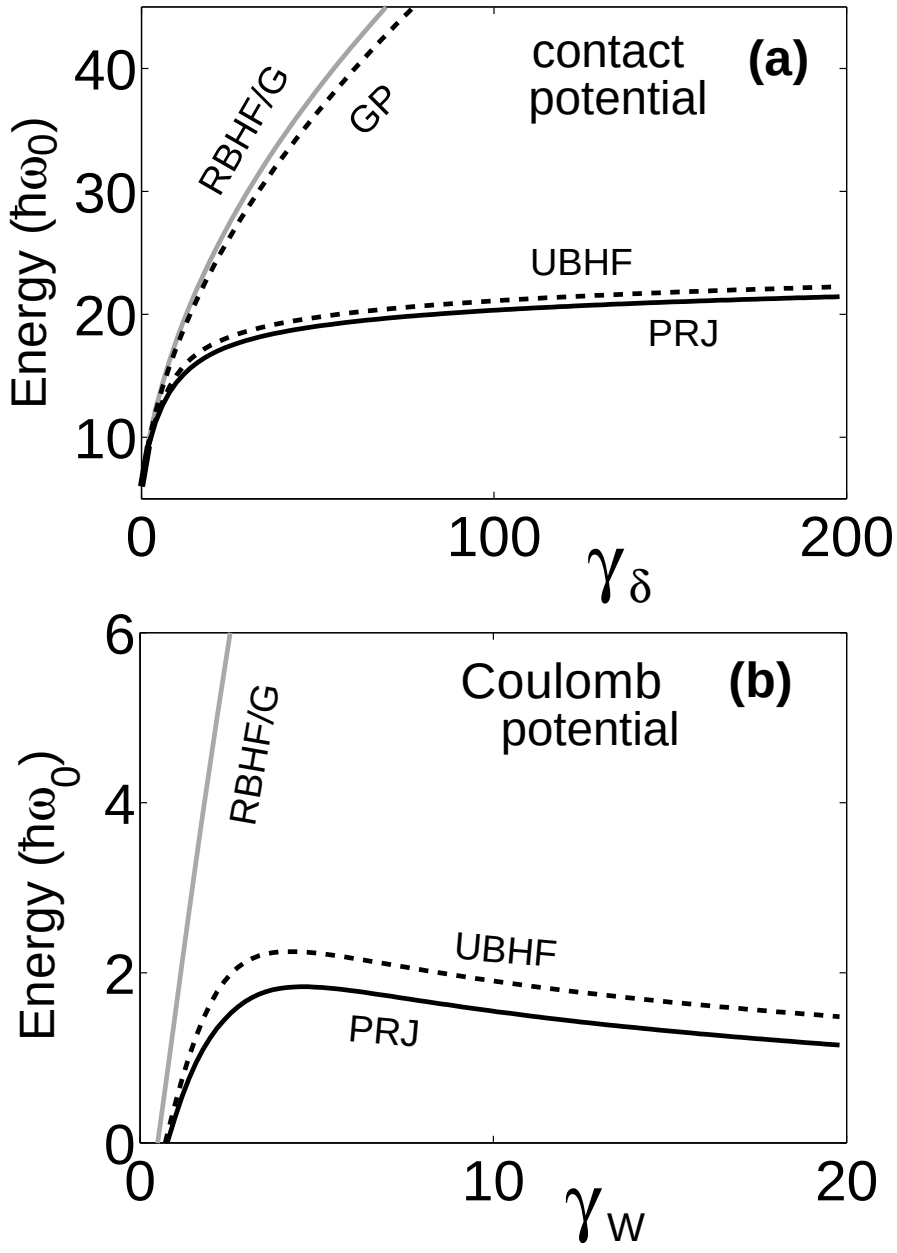

Figure 6: Total energies of the system of six strongly interacting neutral and charged bosons in harmonic trap as a function of interaction strength γ for various approximation levels. Energies in units of $\hbar\omega_0$. The top figure shows results for neutral bosons. The lowest energy configuration for six neutral bosons is (1,5). Notation: RBHF/G - Restricted Bose-Hartree-Fock energy, with the common orbital ϕ_0 approximated by a Gaussian centered at the trap origin. GP - Gross-Pitaevskii energy; PRJ - energy of the symmetry-restored state obtained via projection of the unrestricted Bose-Hartree-Fock (UBHF) state. The bottom figure shows results for charged bosons. The energies for the charged bosons are referred to the classical energies of point charges in their equilibrium (1,5) configuration.

unprojected and projected wave function are shown in Fig.6. Notice that, as was proven above, the energy of projected wave function is always smaller than the energy of the unprojected wave function. For the stationary frame and without magnetic field the gain in the energy is not very large, but, we will see later that in the rotating frame (and for magnetic field) for the angular momenta which are not zero the gain in energies is larger. For $N = 6$ it turns out that for both cases of the projected and unprojected wave function, the ground state of the system corresponds to a (1,5) crystalline configuration of the bosons, i.e. there is one boson in the center and the remaining five bosons surround it, forming a regular pentagon. The Gross-Pitaevskii energies are slightly smaller than the energies $E_{RBHF/G}$ of restricted Bose-Hartree-Fock with a common orbital approximated by a Gaussian, this is due to the self-consistent nature of GP solution: the shape of the Gross-Pitaevskii solution can significantly deviate from the Gaussian form at high repulsion strengths. As it can be seen from Fig.6 for neutral bosons, both $E_{RBHF/G}$ and E_{GP} exhibit unphysical behavior for high repulsion strengths - i.e., energies of the restricted mean-field methods diverge as $\gamma_\delta \to \infty$. This behavior contrasts sharply with that of the unrestricted Hartree-Fock energies, E_{UBHF} and those of the projected states E_{PRJ}, which saturate as $\gamma_\delta \to \infty$. In fact, a value close to saturation is achieved already for $\gamma_\delta(\gamma_W) \sim 10$. We have checked that for all cases with $N = 2 - 14$, the total energies exhibit similar behavior. The saturation of UBHF energies is associated with the ability of the trapped bosons to minimize their energy of interaction by occupying different positions in space, thus minimizing their mutual overlap. For $N \leq 5$ the preferred UBHF crystalline arrangement is a single ring [usually denoted as (0,N)]. N=6 is the first case having one boson at the center and [designated as (1,N-1)] and the (0,6) arrangement is a higher energy isomer. For numbers of particles $N \geq 8$, the situation becomes more complicated. The structure of the bosonic molecules in these cases cannot in general be reduced to the series of the rings with symmetrical arrangement of the particles on them. For strong enough interaction between atoms, they start to behave like impenetrable circles with radius $\lambda \sim l_0$ and the problem of finding the optimal configuration with the lowest energy is similar to the problem of dense packing of circles on the 2D plane. The saturation of energy of strongly interacting bosons is a manifestation of the fermionization

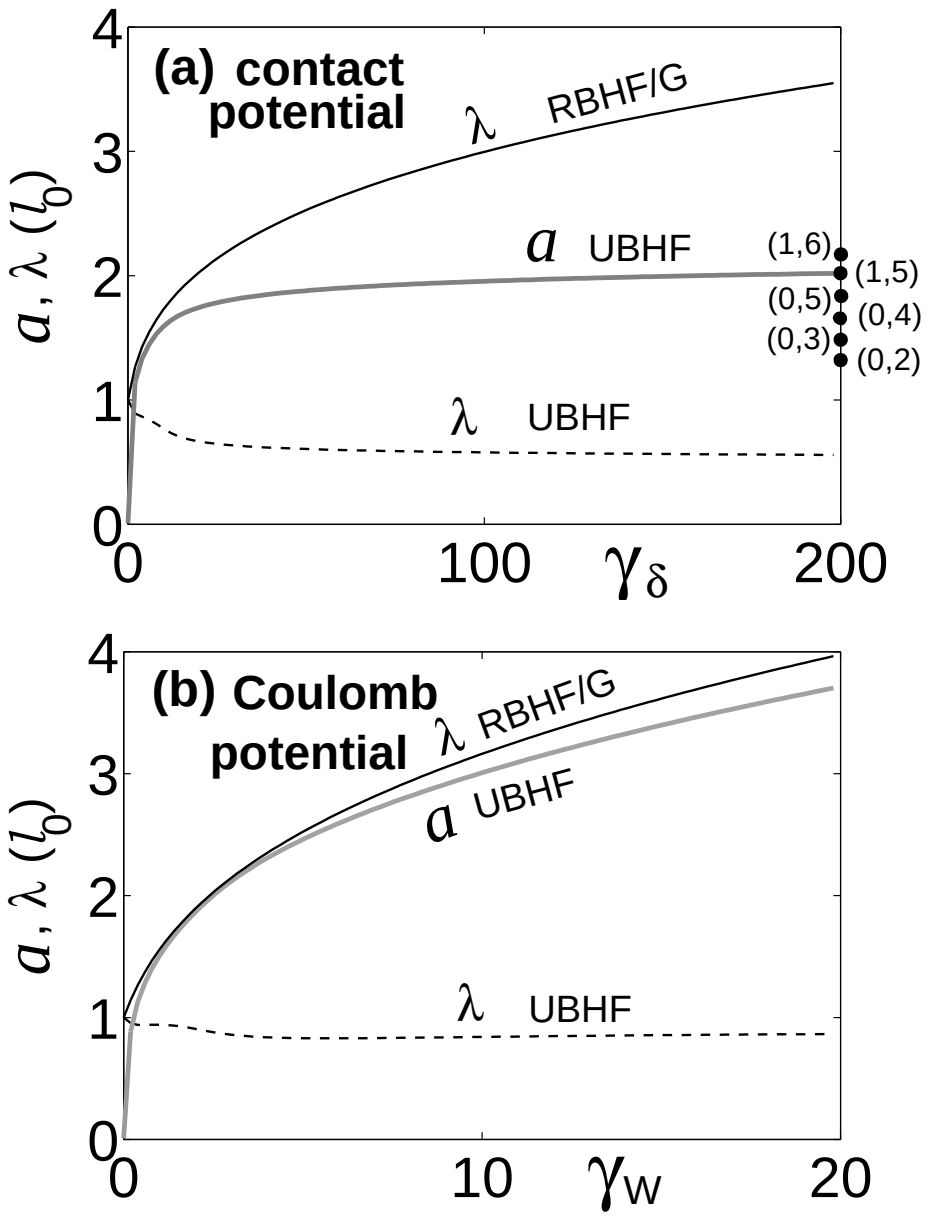

Figure 7: Variationally determined widths (λ) and ring radii (a) for $N = 6$ harmonically confined 2D bosons as a function of (a) γ_δ and (b) γ_W, obtained according to various approximations. RBHF/G - corresponds to the restricted Bose-Hartree-Fock where the single orbital is approximated by Gaussian. UBHF - unrestricted Bose-Hartree-Fock, particles occupy different orbitals modeled by shifted gaussians.

phenomenon. The similar energy saturation has been shown in 1D for the Tonks-Girardeau gas [10, 31]. Saturation of the energy and the length of the trapped atom cloud (and thus the saturation of the interparticle distance) has been measured recently for the gas of neutral atoms trapped in long cigar-shaped traps [4] (compare, in particular, Fig. 3 and Fig. 4 of [4] with our figure 6).

For the Coulomb potential the displayed energies have been referenced to the classical energy E_{cl} (plus zero point energy of noninteracting bosons) of six trapped point charges in the (1,5) configuration, since the total energy of a Wigner crystallite (independently of whether it consists of bosons or fermions) is expected to approach the classical limit E_{cl} as $\gamma_W \to \infty$. We see again that $E_{RBHF/G}$ (i.e. restricted Hartree-Fock with a common orbital in form of a Gaussian) diverges as $\gamma_W \to \infty$. In contrast, the unrestricted HF energies grow much slower and approach slowly to E_{cl}. We checked that a similar behavior is exhibited by the total energies of $N = 2 - 14$ charged bosons.

In Fig.7 we display for the $N = 6$ bosons the radii of the polygonal rings a and width λ of the Gaussian orbitals obtained in various approximations, as a functions of γ_δ (a) and γ_W (b). For the contact potential in the RBHF/G approximation the width of the orbital keeps increasing continuously as $\gamma_\delta \to \infty$ (this reflects the unsuccessful attempt of the common orbital to minimize the mutual repulsion between the bosons by spreading out as far as possible). In contrast, the unrestricted width λ_{UBHF} associated with the displaced Gaussian orbitals (that corresponds to lower energies, see Fig.6) saturate to a constant value. Similar behaviors are also exhibited by $\lambda_{RBHF/G}$ and λ_{UBHF} in the case of the Coulomb force, see Fig.7 (b). The radii a associated with the pentagonal ring of localized orbitals, however, exhibit different behavior depending whether the repulsive force is a contact or a Coulomb one. In the Coulomb case, the radii a_{UBHF} keep increasing with γ_W approaching equilibrium radius of six classical point charges in a harmonic trap in the (1,5) configuration. In contrast, for a repulsive contact potential the radii a_{UBHF} saturate to a constant value $\approx 2l_0$ The different behavior of the boson positions in the UBHF crystallite is a natural consequence of the long-range character of the Coulomb potential versus the short-range contact potential.

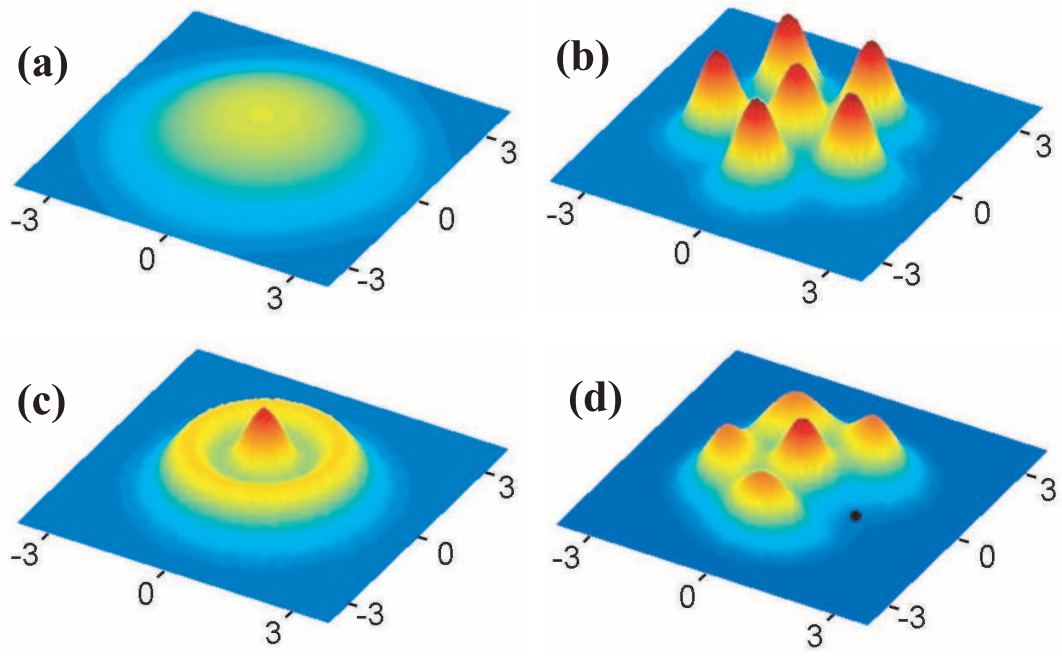

Figure 8: Four single-particle densities for $N = 6$ 2D harmonically trapped neutral bosons with a contact interaction and $\gamma_\delta = 25$. **(a)** Single orbital self-consistent Gross-Pitaevskii wave function. This solution was obtained using fastest descent method. As strength of repulsion increases, the wavefunction spreads out trying to minimize the total energy of the system. Although GP wave function has the same symmetry as Hamiltonian (77), due to the restriction that all orbitals should be the same, energy of the wave function is very hight for high repulsion strengths. **(b)** Probability density of unprojected Bose-Hartree-Fock wave function. The overlap between different humps (orbitals) becomes negligible for high repulsion strengths. The wave function does not have a circular symmetry of the Hamiltonian, and therefore, does not have good angular momentum. **(c)** The projected (symmetry-restored) wave function. The crystalline structure of the outer ring is now hidden, but it can be revealed in the conditional probability distribution (see Fig. (d)). Notice that the width of the projected wave function is smaller than the width of self-consistent Gross-Pitaevskii wave function. **(d)** Conditional probability $P(x|x_0)$ distribution for bosons in the trap, calculated using projected wave function. The observation point is denoted by a black dot.

2.11.2 Bosons in rotating traps and under a magnetic field.

Results of the previous paragraph are rather intuitive: bosons behave exactly in the same way as we expect the classical particles should behave in the same situation. However, one should keep in mind that our solution is not classical and that the wave function obtained via our two-step method takes into account correlations beyond mean field. The merits of our approach will become obvious when we try to use our two-step method to build a wavefunction of bosons in the rotating frame of reference or (if bosons are charged) in a magnetic field.

For applications, we consider two kinds of systems: bosons in the quasi-one dimensional rotating rings and bosons in the rotating harmonic traps. Problem of bosons in a ring is interesting for us because it is analogous to the well studied problem for electrons in the ring-shaped quantum dots [32]. Ring structures with bosonic particles are recently being realized in experiments [33]; however, at the present time, those ring traps are very big and contain a large number of particles. There are some ideas, however, about how to make smaller traps. For example, the authors of Ref. [34] propose a method to create a 1D stack of ring traps through interference of two counter propagating beams with modulated intensities.

In our calculations we assume that the potential of the ring trap has the functional form

$$U^{(1)}_{ring}(R) = \frac{m\omega_0^2}{2}(R - R_0)^2. \tag{81}$$

This specific functional form is such that the case of harmonic trap is just a limiting case of this potential when the radius R_0 of the ring is set to zero. The external potential (81) is thus a generalization of harmonic potential. The potential (81) represents a soft-walled ring. This ring can be destroyed by rotation. The angular velocity that destroys the ring is $\Omega = \omega_0$. As well as for the harmonic trap, one can introduce an oscillator length $l_0 = \sqrt{\hbar/(m\omega_0)}$ and measure of energy in terms of $\hbar\omega_0$; then the only free parameter that characterizes the ring is the dimensionless radius $r_0 = R_0/l_0$.

A more general potential for the ring trap with radius r_0 can be specified by the formula

$$U^{(1)}_{ring}(R) = \frac{\hbar\omega_0}{2}\frac{(R - R_0)^n}{l_0^n} \tag{82}$$

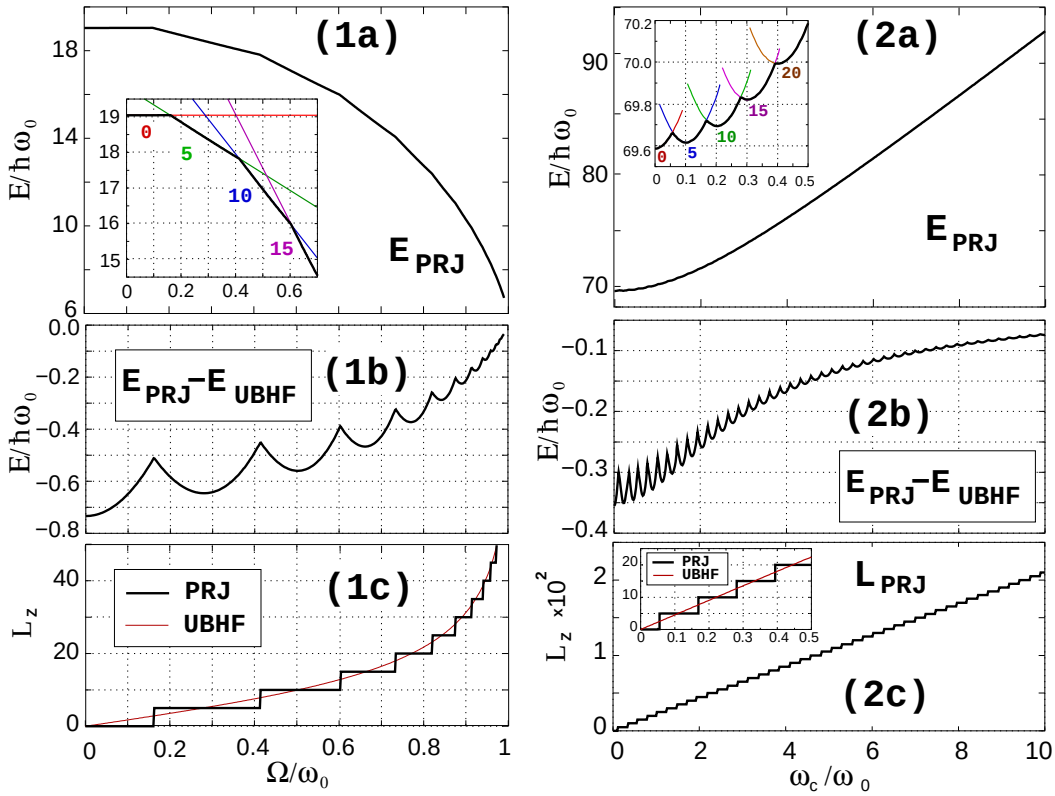

Figure 9: Six bosons in the rotating harmonic trap and in the magnetic field. **1(a,b,c)** Neutral bosons in the rotating trap. Interaction strength between particles is $\gamma_\delta = 50$. **1(a)** graph shows the total energies of the system of six neutral bosons in (1,5) configuration as a function of rotation frequency. Inset shows magnified region for small frequencies of rotation. Energy curve consists from line segments. Each segment corresponds to different angular momentum of the system. **1(b)** graph shows differences between energy of projected wave function and energy of unprojected wave function. And the **1(c)** graph shows absolute value of the total angular momentum of the system. Angular momentum of the system grows in steps. The height of each step is equal to the number of the bosons on the outer shell of the bosonic crystallite. **2(a,b,c)** Charged bosons in the harmonic trap in the external magnetic field. Interaction strength between particles is $\gamma_W = 10$. First graph shows the total energy of the system as a function of cyclotron frequency. As well as for the case of neutral bosons, energy curve consists from segments which correspond to different total angular momenta of the system. Unlike the case of rotating trap segments are not straight lines, but are rather pieces of parabolas. Angular momentum again grows in steps. As well as in the case of the rotating trap, angular momentum takes values that are the multiples of the number of the particles in the outer shell of bosonic crystallite.

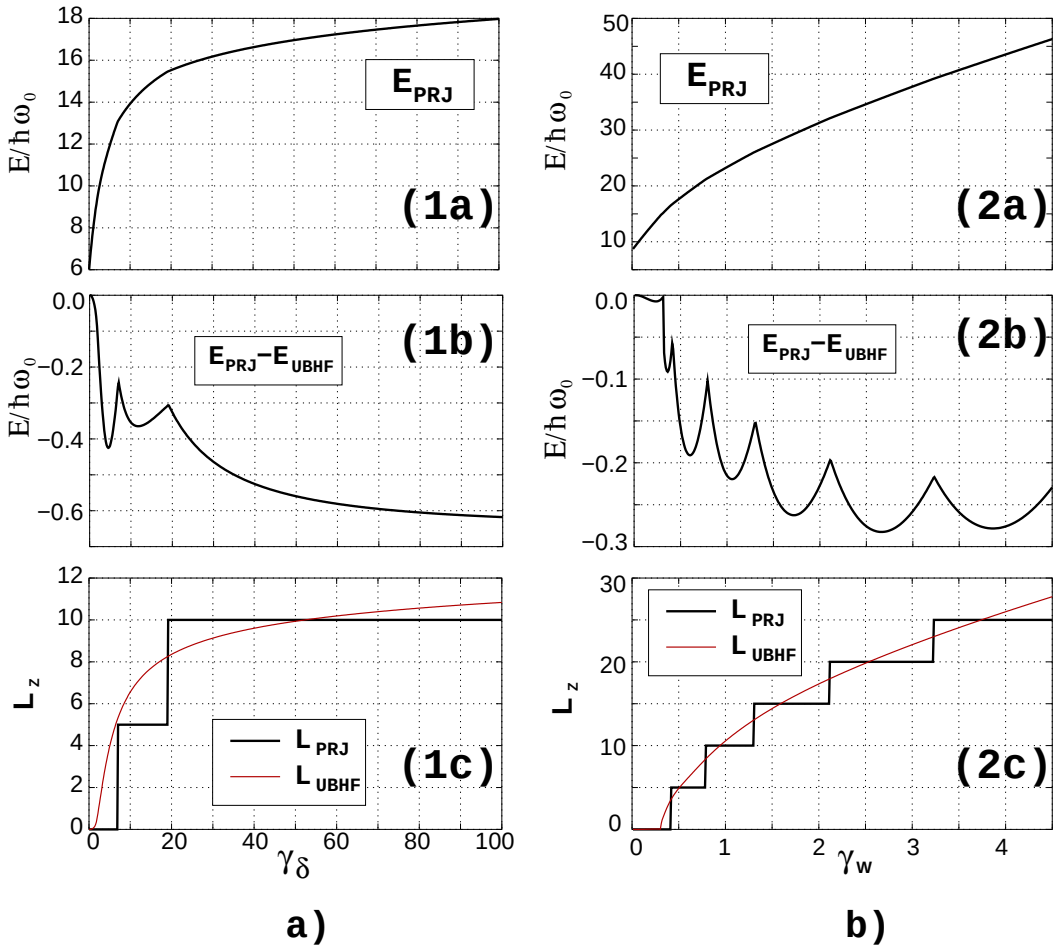

Figure 10: Six bosons in the rotating harmonic trap and in the magnetic field. Repulsion between bosons causes them to shift further from the center of the rotational symmetry of harmonic trap. At certain values of the repulsions strength (at fixed rotation frequency) some states with nonzero angular momenta (namely, the states that have angular momenta multiple to the number of particles in the outer shell of boson crystallite) become lower than state with $L_z = 0$. The meaning of the graphs in each row of this figure is the same as in the Fig.9. **1(a,b,c)** Neutral bosons in the rotating harmonic trap. Frequency of rotation of the trap $\Omega = 0.5\omega_0$. Note that in case of neutral bosons growth of total energy and angular momentum has tendency to saturation. **2(a,b,c)** Charged bosons in the harmonic trap in the external magnetic field. Cyclotron frequency for the magnetic field is equal to the trapping frequency $\omega_c = \omega_0$.

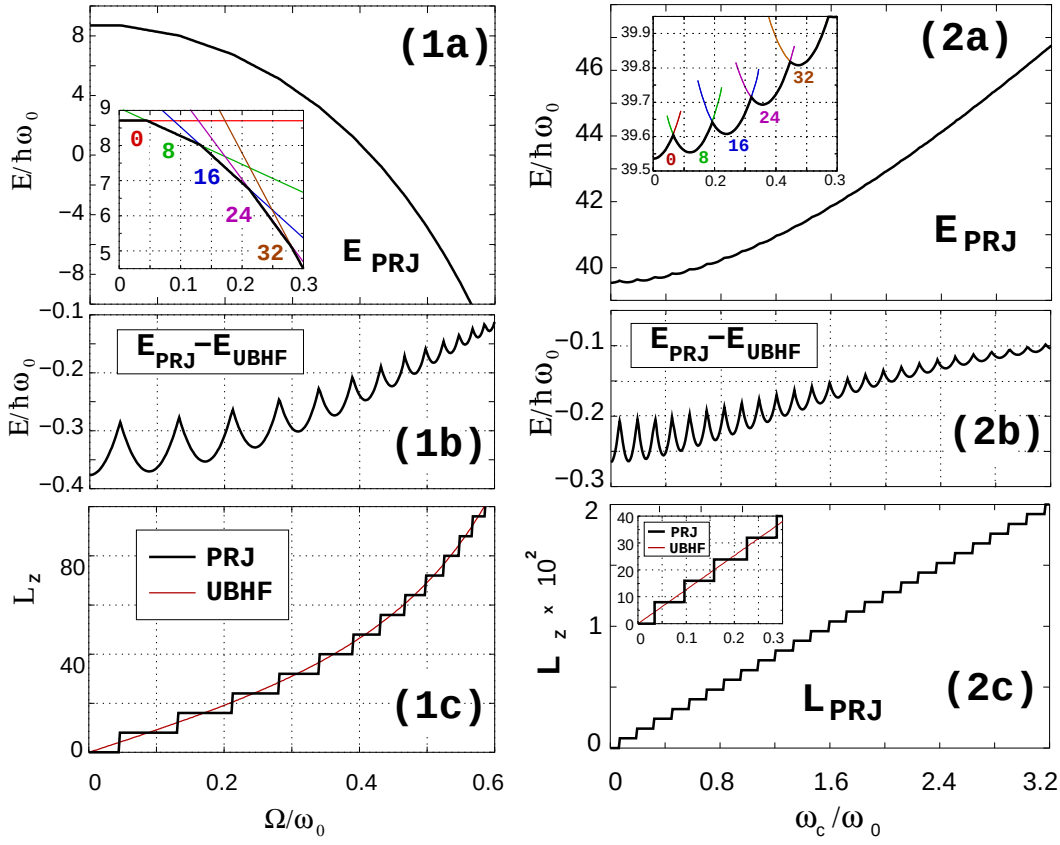

Figure 11: Eight bosons in the rotating ring-shaped trap and in the magnetic field. The meaning of the graphs in each row of this figure is the same as in the Fig.9. **1(a,b,c)** Neutral bosons in the rotating ring-shaped trap. **2(a,b,c)** Charged bosons in the ring trap in the magnetic field. The figures for the ring trap look very similar to the analogous figures for rotating frame. The only small difference between Fig.9 and this figure is that angular momentum grows with the frequency of rotation and strength of magnetic field faster.

For $n \gg 2$ the walls of the potential become very steep and cannot be destroyed by rotation at any frequency. If additionally $l_0/R_0 \to 0$ the ring becomes quasi-one dimensional. The problem of bosons trapped in a quasi-one dimensional potential has been considered often in previous theoretical studies (see e.g. Ref. [35]). We, however, think that the soft-wall potential (81) is more realistic, and in what follows we consider only this case.

As it can be seen from figures 9, 10 and 11, bosons in rotating harmonic trap and in rotating soft-walled ring trap behave similarly. For rotating traps (both harmonic and ring), the total energy diminishes with increasing rotation frequency (this is the effect of the centrifugal force); the energy curves in both cases consist from linear segments, each

one associated with a given angular momentum L. The angular momentum of the system is quantized and grows when the frequency of rotation increases. Quantization means that angular momentum grows in steps. At small frequencies the angular momentum is equal to zero and the system remains irrotational till some finite threshold frequency Ω^*. This behavior is analogous to the effect of superfluidity in condensates. When repulsion between atoms is increased, range of zero angular momentum shrinks and the system switches to new regimes (with nonzero total angular momentum). The energy curves for charged bosons in a magnetic field differ from the energy curves for rotating traps. In a magnetic field the energy of the system grows as the field increases and, instead of linear segments energy, the curve consists from pieces of parabolas, each piece corresponding to a different angular momentum. The energy curves for ring and harmonic traps for bosons in a magnetic field look similar.

The difference between the behavior of bosons in a ring and harmonic trap is that, unlike in the ring trap, where all particles are forced to be at the same distance from the center of the trap, in the harmonic trap particles can form crystallite structures with particles occupying positions at different distance from the center of the trap. This difference shows itself in the fact that for the ring trap, the angular momentum is always quantized in steps of the total number of the particles in the system, whereas for the harmonic trap, the quantization pattern is more complicated and defined by the specific symmetry of crystalline phase without direct connection to the total number of particles. As it is seen from Fig. 10, an increase of the strength of interaction at constant frequency of rotation causes changes in the total angular momentum of the system. This effect is a result of the growth of the size of the crystallite.

In the Fig. 12 we display the rotating Bose molecule and mean-field Gross-Pitaevskii ground-state energies of $N = 6$ strongly repelling (i.e., $\gamma_\delta = 50$) neutral bosons in a harmonic trap as a function of the reduced angular frequency of the trap (Figs 12(1a) and 12(1b)) and as a function of the repulsion strength (Figs. 12(2a) and 12(2b)). The Gross-Pitaevskii curve (thin red line) remains well above the rotating Bose molecule curve (thick green line)

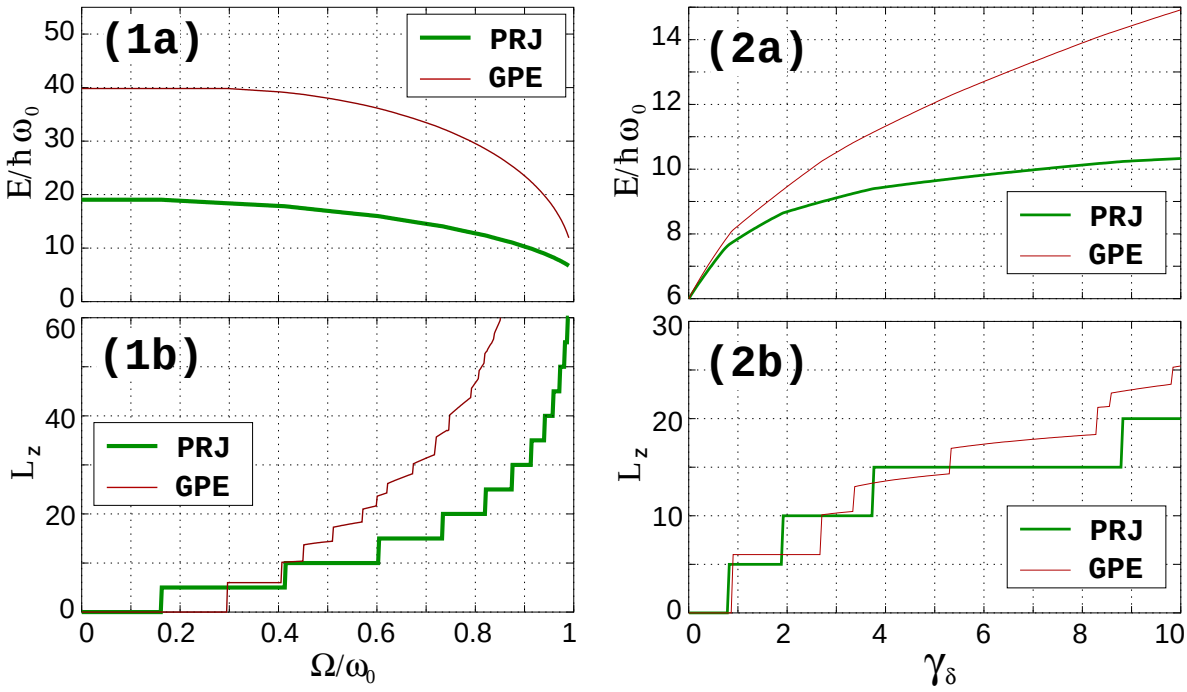

Figure 12: Properties of Gross-Pitaevskii solutions (thin solid red line) versus those of rotating Bose molecule wave functions (thick solid green line) for $N = 6$ neutral bosons in harmonic trap. Figures **(1a)** and **(1b)** show ground state energies and associated angular momenta as a function of the reduced rotational frequency Ω/ω_0 for the interaction strength $\gamma_\delta = 50$. Figures **(2a)** and **(2b)** show the same properties as a function of repulsion strength for fixed rotating frequency $\Omega/\omega_0 = 0.85$

in the whole range $0 \leq \Omega/\omega_0 \leq 1$ and $0 < \gamma_\delta \leq \infty$. The rotating Bose molecule ground-state angular momenta exhibit again the periodicity in steps of five units [Figs.12(1b) and 12(2b)]. As expected, the Gross-Pitaevskii total angular momenta are quantized [$L_z = 0$ (no-vortex) or $L_z = 6$ (one central vortex)] only for an initial range $0 \leq \Omega/\omega_0 \leq 0.42$. For $\Omega/\omega_0 \geq 0.42$, the Gross-Pitaevskii total angular momentum takes non-integer values and ceases to be a good quantum number, reflecting the broken-symmetry character of the associated mean field, with each kink signaling the appearance of a different vortex pattern of p-fold symmetry ($p = 1, 2, 3, 4, ...$) [36].

The energetic superiority of the RBM wave function over the GP solution demonstrated in Fig.12 was to be expected, since we considered the case of strongly repelling bosons. Unexpectedly, however, for a small number of neutral bosons the energetic advantage of the

RBM persists even for weakly repelling bosons, as illustrated in Fig. 12(2a). Indeed, Fig. 12 (2a) displays the rotating Bose molecule (thick solid green line) and Gross-Pitaevskii (thin solid line; online red) ground-state energies for $N = 6$ neutral bosons in a trap rotating with $\Omega/\omega_0 = 0.85$ as a function of the interaction parameter γ_δ. The surprising result in Fig.12(2a) is that the Gross-Pitaevskii curve remains above the rotating Bose molecule curve even for $\gamma_\delta \to 0$. Of course the RBM wave function is very close to that of a BEC without vortices when $\gamma_\delta \to 0$ (BECs *without* vortices are approximately feasible for small N). However, for small N, our results show that BECs *with vortices* (i.e., for $L_z \geq N$) are not the preferred many-body ground states; instead, formation of RBMs is favored. Note that the energy difference $E^{\rm GP} - E^{\rm PRJ}$ increases rapidly with increasing γ_δ, reflecting the fact that the RBM energies saturate (as is to be expected from general arguments), while the GP energies (even with vortices fully accounted for) exhibit an unphysical divergence as $\gamma_\delta \to \infty$; we have checked this trend up to values of $\gamma_\delta = 100$ (not shown). Of interest again is the fact that the RBM and GP ground-state angular momenta [Figs.12(1b) and 12(2b)] exhibit a different behavior.

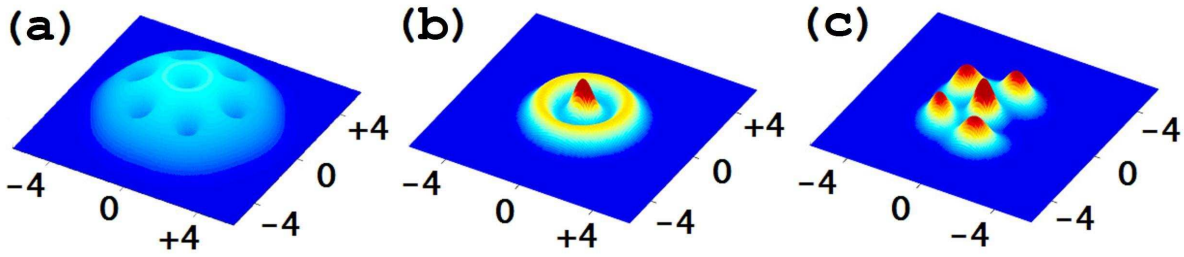

Figure 13: (a) Gross-Pitaevskii (BEC) single particle density at $\Omega/\omega_0 = 0.65$ having seven vortices with a six-fold symmetry (thus exhibiting breaking of the circular symmetry). (b) Rotating Bose molecule single particle density at $\Omega/\omega_0 = 0.65$ which does not break the circular symmetry. (c) Conditional probability density of the rotating Bose molecule at $\Omega/\omega_0 = 0.65$ revealing the intrinsic (1,5) crystalline pattern. The white dot denotes the observation point $\mathbf{r}_0$. Note the dramatic difference in spatial extent between the Gross-Pitaevski and rotating Bose molecule wave functions [compare (a) with (b) and (c). Lengths in units of l_0. The vertical scale is the same for (b) and (c), but different for (c).

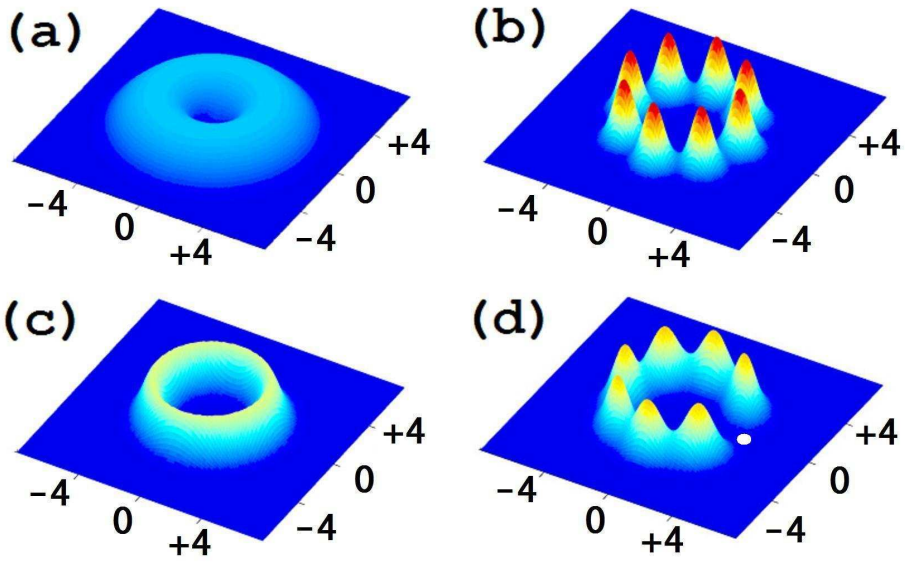

Figure 14: Single-particle densities and CPDs for $N = 8$ bosons in a rotating ring trap with $\Omega/\omega_0 = 0.2$ and $\gamma_\delta = 50$. Radius of the ring $R_0 = 3$. (a) Gross-Pitaevskii single particle density. (b) Unrestricted Bose-Hartree Fock single particle density exhibiting breaking of the circular symmetry. (c) rotating Bose molecule single particle density exhibiting circular symmetry. (d) conditional probability density for the rotating Bose molecule wave function [PRJ wave function, see Eq. (63)] revealing the hidden point-group symmetry in the intrinsic frame of reference. The observation point is denoted by a white dot. The rotating molecule ground-state angular momentum is $L_z = 16$. Lengths in units of l_0. The vertical scale is the same for (b), (c), and (d), but different for (a).

2.12 Summary.

In conclusion, we have introduced (and studied the ground-state properties of) a variational many-body wave function for repelling bosons in rotating traps that incorporates correlations beyond the Gross-Pitaevskii mean-field approximations. This variational wave function describes rotating boson molecules, i.e., localized bosons arranged in polygonal-ring-type patterns in their intrinsic frame of reference. For small numbers of neutral bosons, and in particular in the case of GP vortex formation, the RBM ground-state energies are lower than those associated with the corresponding Gross-Pitaevskii BEC solutions. Given the large differences between the properties of the RBM and BEC wave functions (which become more pronounced for larger interaction parameter γ_δ), and the recently demonstrated ability to experimentally control γ_δ [36, 37, 38, 4], we anticipate that our results could be

tested in experiments involving rotating optical lattices. Detection of RBMs could be based on a variety of approaches[1], such as the measurement of the spatial extent [contrast the RBM and BEC spatial extents in Figs.14(a)-14(b)], or the use of Hanbury Brown-Twiss-type experiments [39] to directly detect the intrinsic crystalline structure of the RBM.

[1] A more detailed discussion on possible detection approaches of strongly correlated bosonic states is given in N. Barberan et al. cond-matt/0603200

CHAPTER III

THERMOPOWER OF LUTTINGER LIQUID.

3.1 Electrons in a one-dimensional conductor.

Theory of metals is one of the most successful theories in condensed matter physics. Although interactions between electrons in the metal are strong, as well as the interactions between electrons and atoms of a crystal lattice, it is still possible to use relatively simple models to describe many phenomena. Bulk metals are usually described either within the approximation of a free Fermi gas or within the model of a Fermi liquid. The Fermi gas model is used for metals with weakly correlated electrons. In this model electrons are viewed as free particles. Fermi liquid theory describes metals with strongly correlated electrons. This theory is based on a conjecture of "electron" and "hole" quasiparticles that evolve from electrons and holes of a Fermi-gas upon adiabatically turning on interactions. These electron/hole quasiparticles are in one-to-one correspondence with bare electrons, have the same charge and obey Fermi-Dirac statistics.

One-dimensional metals are different. In one dimension the Fermi surface is just two points $\pm k_F$. In this case one can translate one end of the Fermi surface to the opposite end by adding a single wave vector $\pm 2k_F$. If the reciprocal vector of the crystal lattice is equal to $2k_F$, the system becomes unstable. This instability leads to modulation of the particles density, accompanied by displacements of the crystal lattice, and to opening of the gap in the single-electron density of states at the Fermi level so that the system becomes insulating. If the reciprocal crystal lattice is incommensurate to the vector $2k_F$ properties of the 1D Fermi gas are still very different from the properties of the Fermi gas in higher dimensions. There are several reasons for these differences.

At first, the elementary excitations in a 1D metal cannot be the same as in higher dimensions. This fact follows from conservation laws in one dimension. To excite an electron-hole pair with the total momentum q one needs to create an electron above the Fermi level with

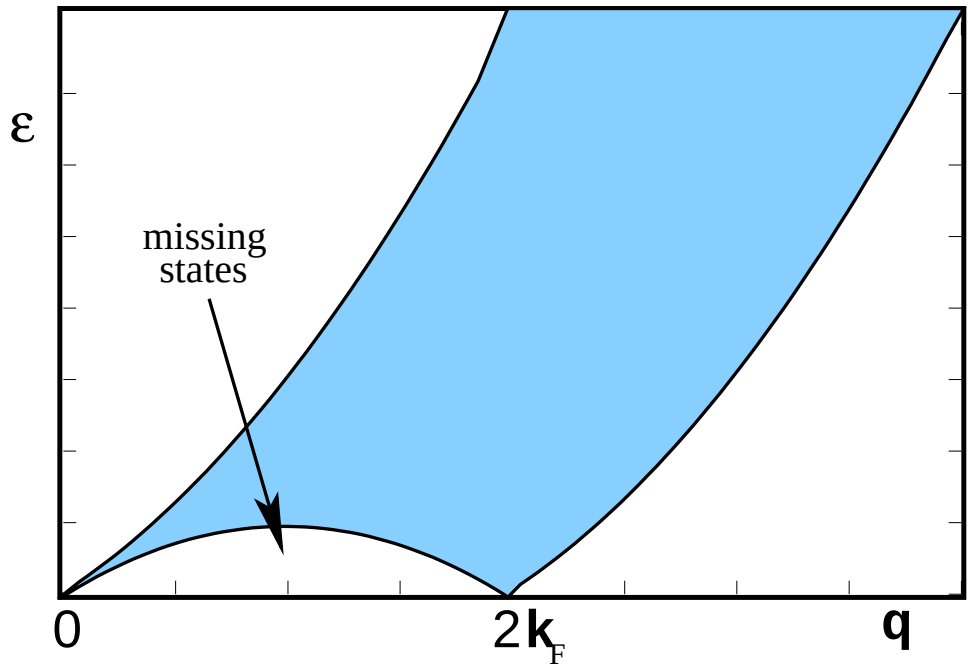

Figure 15: Spectrum of energies for electron-hole excitations. The distinctive feature of the resulting excitation diagram Fig. 15 is absence of the low-energy electron-hole pairs with wave numbers $0 < q < 2k_F$ (in higher dimensions this region is filled in). Because of the linear one-particle dispersion near the Fermi level, the pairs have narrow, quasiparticle-like dispersion near zero momentum: they can propagate coherently with the same group velocity. Any weak particle-hole interaction has a dramatic effect - it will bind the pair into a new particle - the bosonic excitation.

wave number k_e and a hole with wave number $k_h = k_e - q$. The energy of the electron relative to the Fermi level is $\varepsilon = k_e^2/2m - \varepsilon_F$, and the energy of the hole $\varepsilon = \varepsilon_F - k_h^2/2m$. The total energy, which is a sum of electron and hole energies can take on a range of values, depending on the value of the wave vector q of the pair. The distinctive feature of the resulting excitation diagram (Fig.15) is the absence of the low-energy electron-hole pairs with wave numbers $0 < q < 2k_F$ (in higher dimensions this region is filled in). The second reason for very special behavior of electrons in 1D is related to the statistics of the particles. Electrons are fermions and, therefore, they obey the Pauli principle, i.e. they cannot occupy the same location. For the case of a one-dimensional electrons this means that they are unable to pass each other to exchange places. Suppose that we excite one electron in the system, the excited electron will move till it collides with another electron. Since electrons move along the same line, as a result of the collision the first electron will

transfer its momentum to the second electron, and decelerate, while the second electron will accelerate. The second electron, in turn, will move till it collides with next electron on the line etc. Thus, the one-particle excitations in 1D quickly decay, turning into collective excitations, similar to sound waves in elastic media.

3.2 Realization of one-dimensional systems.

The real samples are three-dimensional. But if the size of a sample in some direction becomes comparable to the Fermi wavelength $L \sim \lambda_F$ of the electrons, then the motion of electrons along that direction becomes quantized. The spacing between energy levels of the discrete spectrum increases when the size of the sample becomes smaller. If the temperatures are very low and the size of the sample in some direction is sufficiently small, there will be no motion in that restricted direction and the system becomes effectively two-dimensional. If a sample has its two dimensions comparable to the Fermi wavelength, then the system becomes effectively one-dimensional.

There are several systems where the motion of electrons is restricted to one or two dimensions. One class of such systems is semiconductor heterostructures with modulated doping. Most popular of these are $GaAs/Al_xGa_{1-x}As$ heterostructures. Both materials $AlGaAs$ and $AlGaAs$ are semiconductors, but $AlGaAs$ semiconductor has a larger band gap than $GaAs$. When these two materials are connected together in one piece, the system becomes unstable and to restore the equilibrium some electrons should go from $AlGaAs$ to $GaAs$. The motion of electrons from $AlGaAs$ to $GaAs$ is stopped by electrostatic attraction by positively charged ionized donors in the $AlGaAs$. As a result of these processes, the band structure in both materials becomes distorted near the interface and forms a narrow and deep potential well for conducting electrons. Some finite number of the conducting electrons becomes trapped in this well between two semiconductors, forming a narrow conducting layer with relatively high concentration of carriers. The motion of the electrons in this layer is two-dimensional. To reduce scattering of conducting electrons in the layer the doped $AlGaAs$ is additionally separated from the $GaAs$ by an undoped $AlGaAs$ layer. The

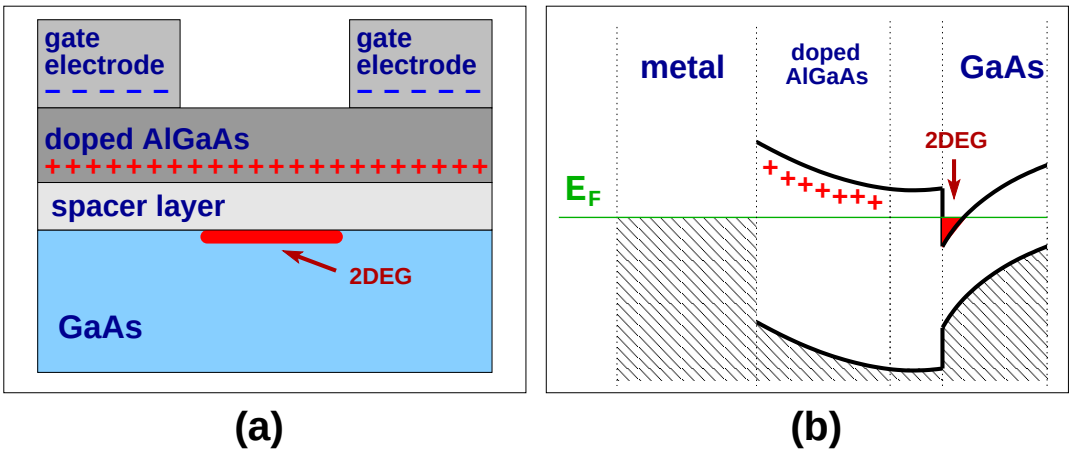

Figure 16: Two-dimensional electron gas. Fig.(a) shows a schematic cross sectional view of a gallium arsenide heterojunction, which is composed of layers of dissimilar semiconductor materials *GaAs* and *AlGaAs*. Doped *AlGaAs* is separated from the *GaAs* by the layer of undoped *AlGaAs*, the *spacer layer*, to reduce recombination scattering of the electrons of the 2DEG from the donors. The negatively charged split-gate electrodes are put on the top of the heterostructure to produce narrow quasi-one-dimensional conducting channels. Fig.(b) is the energy band diagram of this heterostructure. Due to exchange of the electrons between semiconductors, energy bands in both materials are distorted at the interface. The conduction electrons become trapped in the narrow potential well, producing a two-dimensional electron gas.

conductivity electrons in the layer between semiconductors have low effective mass, high mobility, large mean free path and large Fermi wavelength. The narrow quasi-one-dimensional conducting wire can be constructed out of a two-dimensional electron gas by constriction of motion within the conducting layer laterally using various techniques such as electron-beam lithography [40], ion-beam exposure [41], etching [42], split-gate technique [43, 44], etc. In the split-gate technique a pair of parallel electrodes (the gate) is attached on the top of the heterostructure (see Fig.16). A negative voltage applied to the gates depletes electrons in the two-dimensional layer under the electrodes, leaving the central part of the 2DEG undepleted. Varying the voltage of the gates will change the width of the 2D conducting channel. When the width of the 2DEG stripe becomes comparable to the Fermi wavelength, the the motion of the electrons in the lateral directions becomes quantized. For sufficiently high voltages of the gates motion of electrons in the lateral directions becomes impossible, i.e. electrons can move only in the direction parallel to the electrodes. Further increase of the

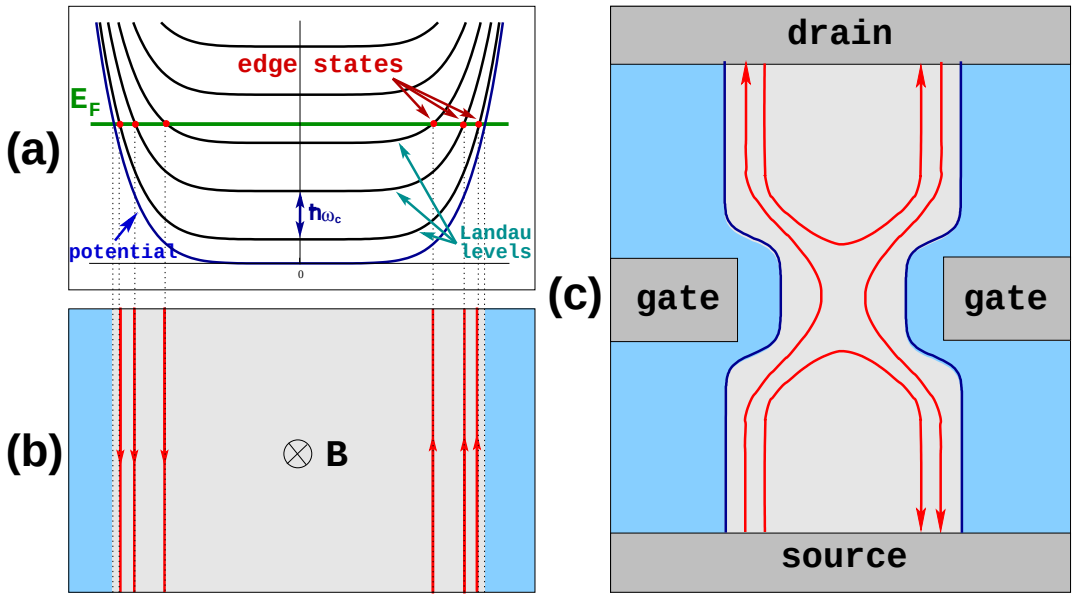

Figure 17: Quantum Hall edge states. Figure (a) shows the single-electron energy spectrum given by Eq.(85). The wave function with wavevector k in the x direction is localized about $y_0 = k\hbar/(m\omega_c)$. The red dots indicate edge states at the Fermi level. Figure (b) shows the top view of the sample. Red lines with arrows show positions of edge states in the sample and direction of the electron propagation. Electron-electron interactions modify the velocities of the electrons in the edge states, but not the direction of their motion. Figure (c) demonstrates a popular experimental setup. The opposite edge states can be brought together by electrostatically charged gates, which makes it possible to study tunneling of Quantum Hall quasiparticles between edges and backscattering processes in one-dimensional quantum wires.

voltage will pinch-off the conducting channel. Another class of systems that demonstrate quasi-one dimensional behavior of the electrons are the quantum Hall edge states. The quantum Hall edge states are produced by placing a two-dimensional electron gas into the strong magnetic field. The mechanism of formation of edge states can be easily understood for noninteracting electrons [45]. Consider a sample in the form of an infinite stripe along the axis x. The magnetic field B is taken in the z direction, perpendicular to the plane of the sample. The Hamiltonian of the particle in the noninteracting electron gas in the Landau gauge can be written in the form

$$H = \frac{1}{2m}\left(p_x + \frac{e}{c}By\right)^2 + \frac{1}{2m}p_y^2 + V(y) \tag{83}$$

where $V(y)$ is the confining potential of the stripe. For slow varying potentials $V(y)$, the

eigenfunctions of the Hamiltonian (83) can be approximately written as

$$\psi(x,y,t) = \frac{1}{2\pi} e^{i(kx - E_k t)} \Phi_n \left(y - \frac{k\hbar}{m\omega_c} \right) \tag{84}$$

where $\Phi_n(x)$ are the eigenfunctions of the harmonic oscillator, and $k = k_x$ is the momentum along the stripe in the x direction. Notice that the wave function (84) with the momentum k is localized near the point $y_0 = k\hbar/(m\omega_c)$. States with higher momenta k are confined closer to the edges of the sample. The functions (84) correspond to the energies

$$E_k = \hbar\omega_c \left(n + \frac{1}{2} \right) + V \left(\frac{k\hbar}{m\omega_c} \right). \tag{85}$$

The energy levels (85) are sketched in Fig.17. States with small momenta k are located near the middle of the sample and have energies far from the Fermi level. These states do not affect thermodynamic or transport properties of the system. On the other hand, as shown in Fig. 17 , near the boundaries of the sample, bulk Landau levels are pushed up by the confining potential and cross the Fermi level. States that correspond to the momenta $k = k_F$, such that $E_{k_F} = E_F$ are confined near the opposite edges of the sample, and are responsible for low-lying gapless excitation of the system. These states come in pairs - two states per each bulk Landau level. Each state carries a current. One can consider these states as one-dimensional chiral conducting channels. Since counter-propagating states are located near the opposite edges of the sample, the backscattering on the impurities and irregularities is weak. While a quantum wire, created by a split-gate technique, must be extremely clean, the quantum Hall edge states are relatively insensitive to disorder. This makes edge states an ideal system for the study of quantum transport in one dimension.

The third remarkable realization of one-dimensional quantum wires are *carbon nanotubes*. Carbon nanotubes are the large cylindrical carbon structures which belong to the family of fullerenes. The diameter of the carbon nanotubes is approximately 1nm and the length can be many times larger. There are different kinds of nanotubes. The simplest single-walled nanotube can be viewed as a one-atom-thick layer of graphite (called graphene) wrapped into a seamless cylinder. The graphene sheet can be wrapped into a cylinder in many different ways. The way the graphene sheet is wrapped is represented

by a pair of indices (n,m). Integers n and m are the numbers of primitive translation vectors of the honeycomb lattice of graphene. Depending on the combinations of numbers m and n, a carbon nanotube will have either semiconductor or metallic electronic structure. For a given (n,m) nanotube, if 2n + m=3q (where q is an integer), then the nanotube is metallic, otherwise the nanotube is a semiconductor. In particular, carbon nanotubes with $m = n$ are conductors. The current in the single-walled metallic nanotube is carried by a pair of one-dimensional subbands. Carbon nanotubes were discovered by Iijima in 1991 [46]. Experimentally, carbon nanotubes are produced by the carbon-arc technique [47], laser vaporisation of cobalt-nickel graphite targets [48], and chemical vapor deposition [49]. Nanotubes are very stiff structures, with very few defects and almost no phonons. These properties make them nearly ideal 1D conductors.

3.3 Model description of fermions in 1D. Bosonization.

There are many models of interacting fermions in one dimension. One of them is the very famous 1D Hubbard model. The Hamiltonian of the Hubbard model, written in second quantization notation, is

$$\hat{H} = -t \sum_{i\sigma} \left(a^{+}_{i,\sigma} a_{i+1,\sigma} + a^{+}_{i+1,\sigma} a_{i,\sigma}) \right) + U \sum_{i} n_{i\uparrow} n_{i\downarrow} \ . \tag{86}$$

in this model electrons hop between Wannier states of neighboring lattice sites. Operators $a^{+}_{i,\sigma}$ and $a_{i,\sigma}$ are creation and annihilation operators for electrons on the lattice site i with spin projection σ, and $n_{i\sigma} = a^{+}_{i,\sigma} a_{i,\sigma}$ is the electron density on the site i. The first term corresponds to the tight-binding model of the regular band theory, the coefficient t is called the "hopping rate". One can diagonalize the first term of the Hamiltonian (86) in the basis of plane waves and find the dispersion relation for electrons $E_k = -t\cos(k)$ for momentum $-\pi < k < +\pi$. The Fermi velocity is thus equal to $V_F = t\sin(k_F)$. The second term of Eq.(86) describes interaction between electrons. It says that electrons interact only if they occupy the same site. Parameter U in Eq.(86) is the energy of on-site interactions between electrons. The Hubbard model was first solved exactly by Lieb and Wu [50] using the *Bethe Ansatz* method. However, the wave functions they obtained are very complicated, and hardly can be used for calculation of anything useful. Only in the limiting cases of

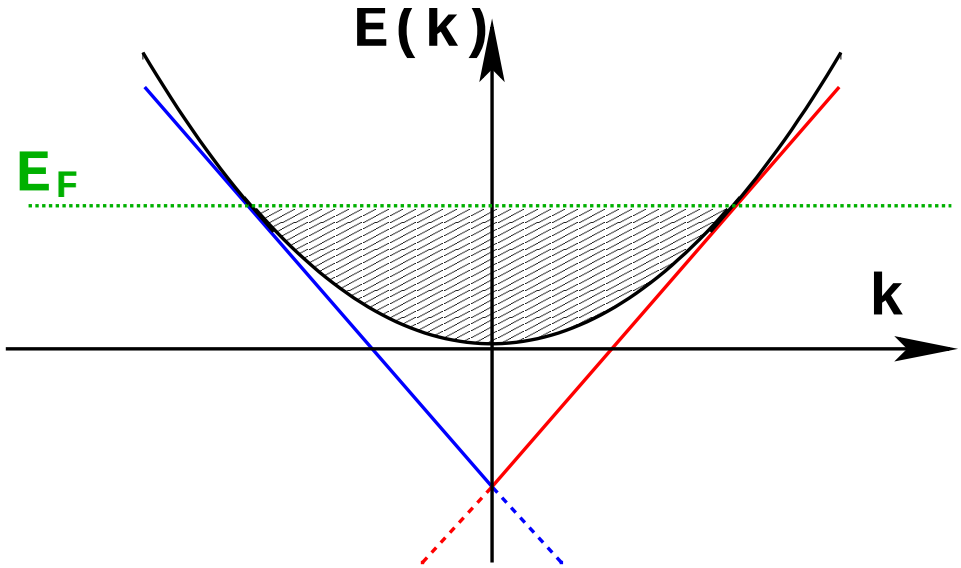

Figure 18: Single particle dispersion relation for Luttinger model. The dispersion relation of the Luttinger model consists of two branches, (shown in red and blue). Momentum in each of two branches can take any values from plus to minus infinity, which leads to appearance of unphysical states (dashed red and blue lines).

very large or very weak on-site repulsion, wave functions can be made simple enough for calculation of correlation functions and other quantities.

The Luttinger liquid model is another exactly solvable model, which describes interacting one-dimensional fermions. It was introduced in 1963 by Luttinger [51] and solved in 1965 by Mattis and Lieb [52]. Unlike the Bethe Ansatz solution for the Hubbard model, the solution of the Luttinger model is simple enough to allow calculation of different physical quantities. The initial solution by Mattis and Lieb was improved by Haldane [53], who found an elegant bosonic representation for fermionic operators. Bosonic treatment not only makes calculations simpler, but also clarifies physics of the phenomena under study. The Luttinger Liquid model is based on several approximations. In the Luttinger model the dispersion relation of fermions $\varepsilon(k)$ is linearized around the Fermi points $\pm k$, and, in addition, the Luttinger liquid considers unconstrained momentum $-\infty < k < +\infty$. These approximations are justified by the fact that we are interested in low-energy excitations of the system. These excitations cannot involve the states far away from the Fermi surface. The dispersion relation now contains two disconnected branches (see Fig 18). One of the

branches corresponds to right-moving electrons (red) and the other (blue) - to the left-moving electrons. Thus the Hamiltonian of the one-dimensional free electrons within the Luttinger model approximations can be written in the form

$$H_0 = V_F \sum_{mr} (r k_m - k_F) : C^+_{mr} C_{mr} : \tag{87}$$

where now C^+_{mr} and C_{mr} are the creation and annihilation operators of the electrons with momentum k_m (for a finite system of length L, momentum k is quantized, $k_m = 2\pi m/L$, $m = 0, \pm 1, \pm 2, \ldots$). Index $r = \pm 1$ labels two branches of the dispersion relation. Electrons on the branch $r = +1$ move with velocity V_F, and electrons on the branch $r = -1$ move with velocity $-V_F$. Double points $: \ldots :$ around operators denote normal ordering, i.e.

$$: \hat{A}\hat{B} \ldots \hat{Z} := \hat{A}\hat{B} \ldots \hat{Z} - \langle \hat{A}\hat{B} \ldots \hat{Z} \rangle_0 \ . \tag{88}$$

The normal ordered expressions of operators have zero expectation values in the ground state. The Fourier components of the particle density operators for right and left moving electrons ($q = 2\pi l/L$)

$$\rho_r(q) = \rho_{lr} = \sum_m : C^+_{m+l,r} C_{m,r} := \begin{cases} \sum\limits_m C^+_{m+l,r} C_{m,r}, & (l \neq 0) \\ N_r \equiv \sum\limits_m (n_{mr} - \langle n_{mr} \rangle_0), & (l = 0) \end{cases} \tag{89}$$

obey Bose type commutation relations (that can be checked by straightforward calculations using anticommutation properties of fermion operators).

$$\left[\rho_r(q), \rho_{r'}(q') \right] = \delta_{rr'} \delta_{qq'} \frac{rqL}{2\pi} \tag{90}$$

In addition to the relation (90), the noninteracting Hamiltonian (87) obeys the commutation relation

$$[H_0, \rho_r(q)] = V_F r q \rho_r(q) \tag{91}$$

this relation means that states created by operators $\rho_r(q)$ are the eigenstates of the Hamiltonian H_0 with energies $r V_F q$. One can use this property to express the Hamiltonian (87) in terms of the density operators

$$H_0 = \frac{\pi V_F}{L} \sum_{q,r} \rho_r(q) \rho_r(-q) \tag{92}$$

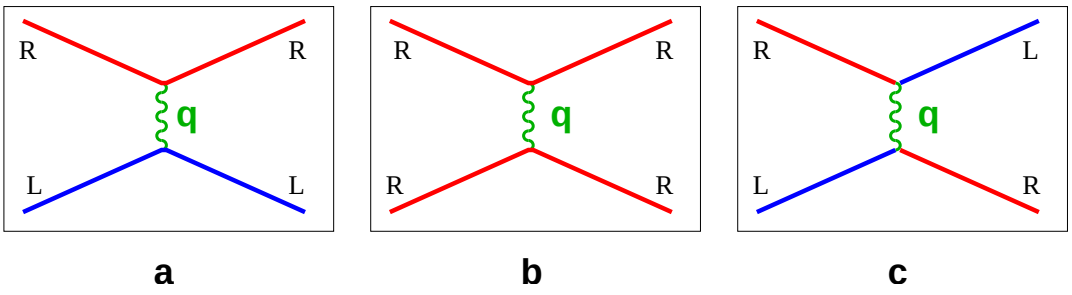

Figure 19: Types of interactions between electrons. The first two diagrams describe forward scattering processes, when electrons exchange small momentum $q \approx 0$ and after interaction continue their motion in the same directions. The third diagram describes backscattering process. In the last case $q \approx 2k_F$, and electrons change to the opposite direction of motion.

Both representations fermionic (87) and bosonic (92) are absolutely equivalent. While fermionic description becomes very complicated when interaction between particles are introduced, description of the system in terms of bosonic operators remains simple. To write the Hamiltonian which describes interaction between fermions we should take into account the processes of forward and backward scattering (see Fig.19). Forward scattering of electrons which belong to the same branch, i.e. processes of the type $(k_F, k_F) \to (k_F, k_F)$ are described by the term

$$H_{int}^{(a)} = \frac{1}{2L} \sum_{q,r} g^{(a)}(q) \rho_r(q) \rho_r(-q) \tag{93}$$

Forward scattering of electrons from different branches, i.e. processes $(k_F, -k_F) \to (k_F, -k_F)$ are described by the term

$$H_{int}^{(b)} = \frac{1}{2L} \sum_{q,r} g^{(b)}(q) \rho_r(q) \rho_{-r}(-q) \tag{94}$$

where $g^{(a)}(q)$ and $g^{(b)}(q)$ are the Fourier transforms of a real space interaction potential. Since forward scattering involves small momentum transfer, one can in many cases neglect q dependence of $g_{(a)}(q)$ and $g_{(b)}(q)$, and use a q independent parameters $g_{(a)} = g_{(a)}(0)$ and $g_{(b)} = g_{(b)}(0)$. There are also possible backward scattering processes, (see Fig. 19c) when electrons exchange branches, i.e. processes of the type $(k_F, -k_F) \to (-k_F, k_F)$. In the case of spinless electrons, the corresponding interaction term in the Hamiltonian can be written

as

$$H_{int}^{(c)} = \frac{1}{2L}\sum_{k_1,k_2}\sum_{q,r} g^{(c)}(q)\ C_r^+(k_1-2k_F-q)C_{-r}^+(k_2+2k_F+q)C_r(k_1)C_{-r}(k_2). \qquad (95)$$

Now, if we take into account relations $C_R^+(k_1-2k_F-q) = C_L^+(k_1-q)$ and $C_L^+(k_2+2k_F+q) = C_R^+(k_2+q)$, the equation (95) can be rewritten in the form

$$H_{int}^{(c)} = \frac{1}{2L}\sum_{k_1,k_2}\sum_{q,r} g^{(c)}(q)\ C_{-r}^+(k_1-q)C_r^+(k_2+q)C_r(k_1)C_{-r}(k_2). \qquad (96)$$

If we introduce ne variable $Q = q-(k_1-k_2)$, then (95) becomes

$$\begin{aligned} H_{int}^{(c)} &= \frac{1}{2L}\sum_{k_1,k_2}\sum_{Q,r}\tilde{g}^{(c)}(Q)\ C_r^+(k_1+Q)C_r(k_1)C_{-r}^+(k_2-Q)C_{-r}(k_2) = & (97)\\ &= \frac{1}{2L}\sum_{Q,r}\tilde{g}^{(c)}(Q)\ \rho_r(Q)\rho_{-r}(-Q) & (98)\end{aligned}$$

where $\tilde{g}^{(c)}(Q) = g^{(c)}(k_1-k_2+Q) \approx g^{(c)}(2k_F+Q)$. Comparing Eqs. (94) and (98), we see that the backward scattering term can be written in the same form as forward scattering terms and, therefore, does not constitute a new type of interaction. (Unfortunately, for electrons with spin, backward scattering cannot be rewritten in the same form as forward scattering, however, renormalization group techniques show that even in this case backward scattering is irrelevant for repulsive electron-electron interactions and therefore does not result in any new physics). Besides forward and backward scattering processes there is also a process called "Umklapp scattering", when two particles, which move in the same direction are scattered into the opposite direction. Umklapp scattering makes the Luttinger model unsolvable, but, similar to the backward scattering, renormalization group analysis shows that this process is an irrelevant perturbation (and does not affect the low-energy physics of the Luttinger Liquid). The total Luttinger Liquid Hamiltonian, which is the sum of the kinetic part H_0 and the interactions $H_{int}^{(a)}, H_{int}^{(b)}, H_{int}^{(c)}$, can be written as [53]

$$\begin{aligned} H_{LL} &= \frac{\pi V_F}{L}\sum_{q,r}\rho_r(q)\rho_r(-q) + \frac{1}{2L}\sum_{q,r}V_1(q)\rho_r(q)\rho_r(-q) + & (99)\\ &\quad + \frac{1}{2L}\sum_{q,r}V_2(q)\rho_r(q)\rho_{-r}(-q) & (100)\end{aligned}$$

where we introduced parameters $V_1(q) = g^{(a)}(q)$ and $V_2(q) = g^{(b)}(q) + \tilde{g}^{(c)}(q)$. Now if we define charge and current densities $\rho_N = \sum_r \rho_r$ and $\rho_J = \sum_r r\rho_r$, we will be able to rewrite

Eq. (99) in the form [53]

$$H_{LL} = \frac{\pi s}{2L} \sum_q \Big\{ \frac{1}{g} \rho_N(q)\rho_N(-q) + g\rho_J(q)\rho_J(-q) \Big\} \tag{101}$$

here $s = \sqrt{V_N V_J}$ and $g = \sqrt{V_N/V_J}$, with $V_N = V_F + (V_1(q) + V_2(q))/2\pi$ and $V_J = V_F + (V_1(q) - V_2(q))/2\pi$. Very often interaction between electrons is approximated by a delta function $U(x - x') = U_0\delta(x - x')$. In this case $V_1(q) = V_2(q) = U_0$

$$g = \left(1 + \frac{U_0}{\pi V_F}\right)^{-1/2} \qquad \text{and} \qquad s = V_F \left(1 + \frac{U_0}{\pi V_F}\right)^{1/2} = V_F/g \tag{102}$$

therefore, in the case of repulsive forces parameter $g < 1$ and for attractive forces $g > 1$. The sound velocity for the repelling electrons is higher than for noninteracting electrons.

The procedure of reexpression of the Hamiltonian of the fermionic system in terms of Bose operators is called *bosonization*. Details of the bosonization procedure for Luttinger model and the derivation of some other important formulas that were used in our calculations can be found in the work by Haldane [53] and in the review [54]. For example, annihilation and creation operators for bosonic excitations can be expressed in terms of densities

$$a_m^+ = \left(\frac{2\pi}{L|k_m|}\right)^{1/2} \sum_r \theta(rm)\rho_{mr}, \qquad a_m = \left(\frac{2\pi}{L|k_m|}\right)^{1/2} \sum_r \theta(rm)\rho_{-mr}. \tag{103}$$

One usually introduces the following pair of field operators

$$\Phi(x) = \frac{2\pi N}{L} x + i \sum_{m\neq 0} \sqrt{\frac{2\pi sg}{L\epsilon_m}} e^{-ik_m x - \alpha|k_m|/2} \left(a_m + a_{-m}^+\right) \mathrm{sign}(m) \tag{104}$$

$$\Pi(x) = -\frac{J}{2L} - \frac{1}{2} \sum_{m\neq 0} \sqrt{\frac{\epsilon_m}{2\pi sgL}} e^{-ik_m x - \alpha|k_m|/2} \left(a_m - a_{-m}^+\right) \mathrm{sign}(m) \tag{105}$$

where $N = N_R + N_L + k_F L/\pi$, and $J = N_R - N_L$. Field $\Phi(x)$ is related to the local charge density operator via relation $\partial\Phi(x)/\partial x = 2\pi(\rho(x) - \rho_0)$ where ρ_0 is the average density in the ground state with $N_R = N_L = 0$. Fields $\Phi(x)$ and $\Pi(x)$ are canonically conjugate

$$[\Pi(x), \Phi(x')] = \frac{i}{L} - i \sum_{n=-\infty}^{+\infty} \delta(x - x' + nL) \tag{106}$$

Fermion operators in the coordinate representation can be written as

$$\Psi_r(x) = \lim_{\alpha\to 0} \frac{1}{\sqrt{2\pi\alpha}} U_r^+ \exp\left\{ -\frac{i}{2} \left(r\Phi(x) + \Theta(x)\right) \right\} \tag{107}$$

where

$$\Theta(x) = -4\pi \int_0^x \Pi(x')\, dx' = \frac{2\pi J}{L} x + i \sum_{m\neq 0} \sqrt{\frac{2\pi s}{gL\epsilon_m}} e^{-ik_m x - \alpha|k_m|/2} \left(a_m - a_{-m}^+\right) \qquad (108)$$

Operators U_r and U_r^+, which are also called 'Klein factors', change the total number N_r of particles on a branch r by one. They are necessary because bosonic operators and any combination of bosonic operators conserve the total number of particles. One can interpret the expression for the fermion operator (107) in the following way: creating a particle at the point x introduces a peak of particle density $\rho(x) = \delta(x)$, and, since density is related to phase Φ, the peak of density means a step kink of the phase $\Phi(x) = 2\pi\theta(x)$. To create this kink one should shift all phases at the points $x' > x$ by the value $\delta\Phi = 2\pi$. The displacement of phases is achieved by the shift operator $\exp(2\pi i \int_{-\infty}^{x} \Pi(x')\, dx')$. In order to satisfy anticommutation relation one should also multiply the shift operator by the factor $\exp(-ir\Phi(x))$, and one gets the final expression (107) for the fermion operator.

In terms of fields $\Phi(x)$ and $\Pi(x)$ the Hamiltonian of the Luttinger Liquid is

$$H_{LL} = \frac{1}{2} \int_0^L dx \Big\{ 4\pi s g \Pi^2 + \frac{s}{4\pi g} (\nabla\Phi)^2 \Big\} \qquad (109)$$

this Hamiltonian is mathematically equivalent to the Hamiltonian of an elastic string. The field $\Phi(x)$ is called a "displacement field", and it corresponds to the shift of electrons due to a charge density wave. The elementary excitations described by the Eq.(109) are the collective sound-like density fluctuations, which propagate with the sound velocity $s = V_F/g$. These collective excitations are the only low-energy excitations in the system: there is no single quasiparticle excitations similar to the excitations in the Fermi liquid.

3.4 Transport properties of 1D quantum wires.

The fundamental problem of electron transport is response of the system to an external applied electric voltage and temperature difference. This problem can be solved in different ways, depending on specific properties of the system.

Let us first consider a one-dimensional ballistic quantum wire with free *spinless* fermions. In a typical transport experiment a one-dimensional quantum wire is connected to higher-dimensional Fermi liquid reservoirs, which we call leads, or electrodes. Suppose that a small

voltage $V = (\mu_L - \mu_R)/(-e)$ is applied between right and left leads. Experimentally it is also possible to heat up one lead to create a temperature difference $\Delta T = T_L - T_R$ between the leads. The current through a such wire can be found using the Landauer formula [55]

$$I = e \int dE\ \rho(E) v(E) \tau(E) \left[f_L(E) - f_R(E) \right] \ , \tag{110}$$

where $\rho(E) = (2\pi\hbar v(E))^{-1}$ is the one-dimensional density of states, and $v(E)$ is the velocity of electrons with energy E in the wire. The product of density of states and velocity along the wire is just a constant $\rho(E)v(E) = 1/h$, which can be moved out of the integral sign. $\tau(E)$ is the transmission probability for the particles with energy E. Functions $f_R(E)$ and $f_L(E)$ are the Fermi distributions for the electrons in the right and left lead $f_i(E) = 1/(\exp((E - \mu_i)/T_i) + 1)$. Assuming that voltage and temperature difference are small (i. e. $|\Delta T| \ll T$ and $|eV| \ll \mu$), one can expand the distribution functions in the leads and write

$$f_i(E) = f^0(E) + \frac{\partial f^0(E)}{\partial E}(\mu_i - \mu) + \frac{\partial f^0(E)}{\partial E}\frac{(T_i - T)}{T}(E - \mu) \tag{111}$$

where $f^0(E)$ is the Fermi distribution of electrons in the leads when voltage and temperature differences are zero. Substituting this expansion into the Landauer formula (110) we get

$$I = \frac{e^2 V}{h} \int dE\ \tau(E) \frac{\partial f^0(E)}{\partial E} + \frac{e\Delta T}{hT} \int dE\ \tau(E)(E - \mu) \frac{\partial f^0(E)}{\partial E} \tag{112}$$

For the low temperatures ($T \ll \mu$) derivative of the Fermi distribution is a sharp peak, centered at the Fermi energy. One can use this fact to simplify the integrals in Eq.(112). In general, when calculating integrals containing derivatives of a Fermi distribution, the following approximate relation can be used

$$\int_{-\infty}^{+\infty} F(E) f'(E)\ dE \approx -F(\mu) - \frac{\pi^2 T^2}{6} F''(\mu) \tag{113}$$

This relation can be proved by replacing the function $F(E)$ by its Taylor expansion (to the third term) near the point $E = \mu$ and calculating exactly the resulting integrals. The total current through the wire takes simple form

$$I = -\frac{e^2 \tau(\mu)}{h} V - \frac{e\pi^2 T \tau'(\mu)}{3h} \Delta T \tag{114}$$

The conductance of the system, the ratio of the current through the system versus the voltage which induced this current (in the limit when temperatures of the right and left leads are the same), can be written as

$$G = \frac{e^2}{h}\tau(\mu) \tag{115}$$

This formula says that even in the perfect ballistic contact with no scattering ($\tau(\mu) = 1$), conductance is not infinite. If there are several noninteracting one-dimensional quantum channels then the conductance of the system is the sum of conductances of individual channels. By setting the current (114) through the junction to zero we can obtain thermopower of the contact

$$S \approx -\frac{\pi^2}{3}\frac{T}{e}\frac{\tau'(\mu)}{\tau(\mu)} = -\frac{\pi^2}{3}\frac{T}{e}\frac{\partial \ln G(E)}{\partial E}\bigg|_{E\to\mu} \tag{116}$$

Thermopower expresses the ability of a system of charged particles to generate an electromotive force when a temperature gradient is applied across the system. Equation (116) is the so called Mott's formula for thermopower. This formula is also true for noninteracting electrons in higher dimensions with diffusive motion of the particles [56]. While for noninteracting particles formulas for low dimensional systems look similar to formulas in higher dimensions, when interaction are turned on, low dimensional systems start to exhibit some new phenomena, which cannot be found in higher-dimensional systems. One of the most interesting examples which demonstrates importance of interactions in low-dimensional systems is charge transport through an impurity. Within a Luttinger Liquid model Kane and Fisher showed [57, 58] that in the case of repulsive interactions the current in a one-dimensional system is strongly suppressed, compared to a non-interacting situation. Even a weak impurity leads to zero conductance of Luttinger liquid at zero temperature. For finite temperatures conductance of the Luttinger Liquid wire scales as $G(T) \propto T^{2(1/g-1)}$, where g is the correlational parameter of the Luttinger Liquid. Notice that for a wire with noninteracting electrons conductance does not depend on temperatures for small temperatures. The major suppression of the current in the Luttinger Liquid by an impurity can be explained by the orthogonality catastrophy. Namely, since the potential of the typical impurity is very sharp and high, the charged collective excitations that normally

are responsible for current in a Luttinger Liquid cannot easily pass through the barrier. The current through the potential barrier (impurity) is transmitted by the single electrons. Therefore, during a single tunneling process one electron near the barrier should be removed and, when the tunneling is over, this electron should be absorbed back into the Luttinger Liquid on the other side of the barrier. Removal of an electron from a Luttinger Liquid or addition of an electron to a Luttinger Liquid requires a modification of wave functions of all other electrons in the system. For a long wire the resulting effect is dramatic, and this is the reason why conductance of a one-dimensional system is so sensitive to interaction between electrons. Thermopower is also strongly affected by the interaction between electrons. However, it turns out [59, 60] that thermopower is affected less than conductance, that is, it remains a linear function of the temperature as in the case of noninteracting electrons. It has been shown in the [60] via a phenomenological model that for a Luttinger Liquid connected to leads of noninteracting electrons the thermopower can still be represented by a Mott-like formula with an additional interaction-dependent renormalization factor. Although the assumptions made in the Ref. [60] are reasonable and the model gives a simple and qualitatively correct description of charge transport in Luttinger Liquid wires, there was no consistent quantitative theory of thermoelectric effects in Luttinger Liquids. This chapter of the Thesis presents results of the study [61] of the thermopower of the infinite Luttinger liquid of spinless electrons. We consider two different systems: i) infinite Luttinger liquid with an impurity, and ii) infinite Luttinger liquid without impurity, but with nonlinear electron spectrum.

3.5 Dispersion induced thermopower.

For an ideal impurity-free Luttinger liquid thermopower is zero. This is a direct consequence of the linear spectrum of electrons in the Luttinger model. Nonlinear corrections to the electron spectrum in the energy region $\epsilon \sim E_F$ will induce a finite thermopower. When the corrections are small, they can be treated by the perturbation theory. We will take into account only quadratic corrections to the linearized electron spectrum at $\epsilon \sim E_F$ (in the

following formulas we use a system of units with $\hbar = k_B = 1$)

$$E_r(k) = v_F r(k - k_F) + A(k - k_F)^2, \qquad A = (v_F/2)(\partial v_F/\partial E_F) \tag{117}$$

where nonlinearity parameter A is assumed to be small $A \ll v_F/p_F$.

According to Eq.(101), in the case of the perfect linear spectrum for electrons ($A = 0$), the Hamiltonian of the spinless Luttinger liquid in coordinate representation is

$$H_0 = \frac{\pi s}{2} \int\limits_{-\infty}^{+\infty} dx \left[g\rho_J(x)\rho_J(x) + \frac{1}{g}\rho_N(x)\rho_N(x) \right] \tag{118}$$

Here $s = v_F/g$ is the velocity of plasmons and $g^{-1} = \sqrt{1 + U_0/\pi v_F}$ is the correlational parameter for spinless electrons. The density operators $\rho_{N(J)}$ obey commutation relations $[\rho_N(x), \rho_J(x)] = -(i/2\pi)\partial_x \delta(x - x')$. The nonlinearity in the dispersion relation of the electrons leads to unharmonic bosonic term that describes the interaction between plasmons

$$H_A = A\frac{\pi^2}{12} \int\limits_{-\infty}^{+\infty} dx \left[\rho_N^3(x) + 3\rho_N \rho_J^2(x) \right] + H.c. \tag{119}$$

It is useful to reexpress densities $\rho_N(x)$ and $\rho_J(x)$ in terms of the bosonic fields $\Phi(x)$ and $\Pi(x) = (4\pi sg)^{-1}\partial_t \Phi(x)$, obeying canonical commutation relations

$$[\Pi(x), \Phi(x')] = -i\delta(x - x') \tag{120}$$

as a result, the total Hamiltonian of our model, which is the sum of Hamiltonians (118) and (119) takes the form

$$H = H_0 + H_A = \frac{1}{8\pi sg} \int\limits_{-\infty}^{+\infty} dx \left[(\partial_t \Phi)^2 + s^2(\partial_x \Phi)^2 \right] + \tag{121}$$

$$+ \frac{A}{96\pi} \int\limits_{-\infty}^{+\infty} dx \left[(\partial_x \Phi)^3 + \frac{3}{(sg)^2}(\partial_x \Phi)(\partial_t \Phi)^2 + H.c. \right]$$

In the linear response approximation the average direct current

$$J(x) = \int dx' \sigma^{(1)}(x, x') E(x') + \frac{1}{T} \int dx' \sigma^{(2)}(x, x') \nabla T(x') \tag{122}$$

is determined by two kinetic coefficients $\sigma^{(1),(2)}$, which can be expressed via current-current or current - heat flux correlation functions using Kubo formulas

$$\sigma^{(1)}(x,x') = \int_0^\infty dt \int_0^\beta d\lambda \ \langle j(-i\lambda,x)\ j(t,x')\rangle \tag{123}$$

$$\sigma^{(2)}(x,x') = \int_0^\infty dt \int_0^\beta d\lambda \ \langle q(-i\lambda,x)\ j(t,x')\rangle \tag{124}$$

where $\beta = 1/T$ is the inverse temperature, $j = -(e/2\pi)\partial_t\Phi$ is the charge current operator, and $q(x)$ is the energy current operator, which is defined by energy conservation equation $\partial_t h(x) + \partial_x q(x) = 0$ with the Hamiltonian density $h(x)$ given as $H_0 = \int dx h(x)$. It is easy to find that in terms of the density operators the energy current can be written as

$$q(x) = \frac{\pi s^2}{2}\rho_J(x)\rho_N(x) + H.c. = -\frac{s}{8\pi g}\partial_t\Phi\partial_x\Phi + H.c. \tag{125}$$

In a homogeneous system the kinetic coefficients do not depend on coordinate, therefore thermopower coefficient S is given by the ratio of two transport coefficients

$$S|_{J=0} = -\frac{\sigma^{(2)}}{T\sigma^{(1)}} \tag{126}$$

Since the electron dispersion at the Fermi energies is weak ($p_F(\partial v_F/\partial E_F) \ll 1$), we can evaluate the thermopower coefficient perturbatively. To the lowest order in perturbation theory with respect to nonlinearity coefficient (A), one gets

$$\sigma^{(1)}(x,x') \approx \int_0^\infty dt \int_0^\beta d\lambda \ \langle \hat{T}_c\ j(-i\lambda,x)j(t,x')\rangle_0 \tag{127}$$

$$\sigma^{(2)}(x,x') \approx \pi e s^3 g \int_0^\infty dt \int_0^\beta d\lambda \ \langle \hat{T}_c\ q(-i\lambda,x)j(t,x')S_1(-i\beta,0)\rangle_0 \tag{128}$$

where

$$S_1(-i\beta,0) = \int_C \hat{H}_A(\tau')d\tau' \tag{129}$$

Time-dependent operator $\hat{H}_A(\tau')$ in the Eq. (129) is the non-harmonic part (119) of the Hamiltonian in the interaction representation. The thermal average $\langle\ldots\rangle_0$ is taken with respect to unperturbed Hamiltonian H_0, and the symbol $\hat{T}_c$ denotes the ordering of operators along the contour C in the complex plane (see Fig.20). The calculation of coefficients G_V

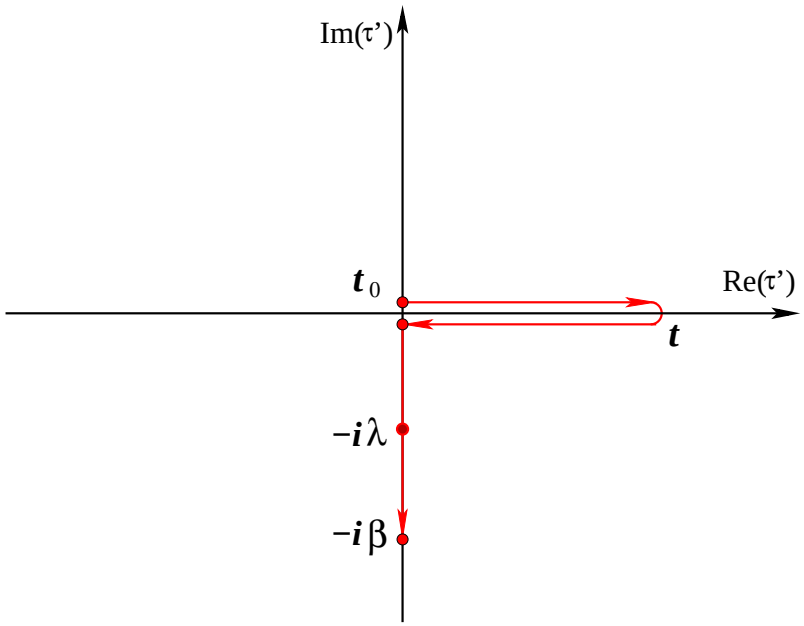

Figure 20: The integration contour C in the complex time plane. To find necessary kinetic coefficient we need to calculate so-called contour-ordered Green functions (see Eqs.(127) (128),(129)). Contour C starts at the point t_0, passes through t once and then returns back to t_0 and then goes along imaginary axis through the points $-i\lambda$ to the point $-i\beta$. The contour defines the procedure of the time ordering in the Green function. The detailed explanation of this shape of the contour can be found in the Ref. [62]

and $G_{\Delta T}$ is straightforward, although quite lengthy, and it is outlined in the Appendix D. However the functional dependence of the thermopower on correlation parameter g can be determined even without explicit calculations.

Let us consider the canonical transformation

$$\Phi(x,t) = \sqrt{g}\chi \ , \qquad \Pi_\phi = \frac{1}{\sqrt{g}}\Pi_\chi. \tag{130}$$

This transformation allows us to eliminate the factor g in the harmonic part of the Luttinger liquid Hamiltonian, Eq.(121). The current operators j and q in the correlation functions in Kubo formulas (127) and (128) can be reexpressed in terms of the current operators $j^{(0)} = -(e/2\pi)\partial_t\chi$ and $q^{(0)} = -(s/4\pi)\partial_x\chi\partial_t\chi$ as follows:

$$j = -\frac{e}{2\pi}\partial_t\Phi = \sqrt{g}j^{(0)} \ , \qquad q = -\frac{s}{4\pi}\partial_x\Phi\partial_t\Phi = q^{(0)} \tag{131}$$

Using these equations one can easily find the structure of transport coefficients

$$\sigma^{(1)}(x,x') \approx g\int_0^\infty dt\int_0^\beta d\lambda\ \langle\hat{T}_c j^{(0)}(-i\lambda,x)j^{(0)}(t,x')\rangle_0 = \frac{ge^2}{2\pi} \tag{132}$$

$$\sigma^{(2)}(x,x') \approx \sqrt{g}\int_0^\infty dt\int_0^\beta d\lambda\ \langle\hat{T}_c q^{(0)}(-i\lambda,x)j^{(0)}(t,x')S_1(-i\beta,0)\rangle_0 = \\ = AT(g^2+C_1)W(s,T) \tag{133}$$

where C_1 is a numerical constant (its value is determined by straightforward perturbational analysis: see Appendix D). $W(s,T)$ is some function of the plasmon velocity s and the temperature of the system$T$. The thermopower coefficient can be written in the form

$$S(T,g) = -\frac{2\pi T(g^2+C_1)W(s,T)}{ge^2}A \tag{134}$$

Notice that the function $W(s,T)$ can not depend explicitly on either Fermi velocity or on the correlational parameter g. The exact form of of this dependence (up to a constant) can be found by considering the limiting case of noninteracting electrons, i.e. the limit $g=1$. For noninteracting electrons dispersion-induced thermopower is known [63]

$$S_F(T) = -\frac{\pi}{3}\frac{T}{ev_F}\frac{\partial v_F}{\partial E_F} \tag{135}$$

Comparing equations (135) and (134) we can find that

$$W(s,T) = \frac{\pi}{3}\frac{e}{s^2}\frac{1}{(1+C_1)} \tag{136}$$

Thus, by making use of dimensional analysis supplemented with scaling arguments, one can get (up to a numerical constant) the expression for the dispersion induced thermopower:

$$S(T,g) = -\frac{\pi^2}{3}\frac{g(g^2+C_1)}{1+C_1}\frac{T}{ev_F}\frac{\partial v_F}{\partial E_F} \tag{137}$$

In the Appendix D it is shown, by a direct calculation of the correlation functions in perturbation theory, that numerical constant $C_1=1$, and our final result for the dispersion-induced thermopower is

$$S(T,g) = \frac{1}{2}g(g^2+1)S_F(T) \tag{138}$$

As follows from the Eq.(138), the repulsive electron-electron interaction ($g < 1$) suppresses the thermopower of a homogeneous Luttinger liquid. For very strong repulsion strength ($g \ll 1$) thermopower changes approximately linearly with parameter g: $S(T, g) \sim gS_F$.

3.6 Luttinger liquid with an impurity.

In the previous section we considered thermopower of the Luttinger liquid due to nonlinearities in the dispersion relation. The thermopower of a Luttinger liquid can be induced also by the backscattering of the electrons from impurities in the wire. In this section we consider an infinite Luttinger liquid with a single impurity. We assume that the impurity is neutral and nonmagnetic. Due to the neutrality of the impurity its potential is short-range.

Conductance G_V of an infinite Luttinger liquid with impurity was calculated for the first time in the Ref. [57], where it has been shown that G_V scales with the temperature as the power-law function with the exponent that depends strongly on coupling constant. It is natural to assume an analogous behavior of the thermo-electric coefficient $G_{\Delta T}$. Thus, from purely dimensional considerations , one could expect a linear temerature behavior of "impurity induced" thermopower $S^{(i)}_{LL}(T, g)$ even for strongly interacting systems. However, unlike the case of dispersion-induced thermopower, the exact form of dependence of $S^{(i)}_{LL}(T, g)$ on the dimensionless parameter g can not be obtained from dimensional considerations.

Renormalization group analysis of the system shows that for repulsive interaction potential the impurity potential that causes backscattering of the electrons is a relevant perturbation, and thus at low temperatures, studying low-energy properties of the system it is good approximation to replace the single Luttinger liquid, which is infinite in both directions by a pair of semi-infinite Luttinger liquids connected via a weak link (junction). The charge transport can in this case be evaluated perturbatively by making use of the tunneling Hamiltonian method.

3.6.1 Tunneling Hamiltonian method

The tunneling Hamiltonian method is used to describe the tunneling processes between two conducting media like normal metals, superconductors etc. The method is based on the assumption of weakness of the link between the media, when one can consider only

single-particle tunneling and neglect all other types of processes. Calculation of tunneling current starts from replacement of the original Hamiltonian of the system by the effective Hamiltonian

$$H = H_R + H_L + H_T \tag{139}$$

where H_R and H_L are the Hamiltonians of the left and right media and H_T is the tunneling Hamiltonian, which describes transition of the electrons between these media.

In our specific problem of Luttinger liquid with impurity H_R and H_L are the Hamiltonians of the right and left semi-infinite Luttinger liquids, and Hamiltonian H_T can be written in the form

$$H_T = \int_{-\infty}^{0} dx_1 \int_{0}^{+\infty} dx_2 \left(\langle x_2|\hat{T}|x_1\rangle \psi_2^\dagger(x_2)\psi_1(x_1) + \langle x_1|\hat{T}|x_2\rangle \psi_1^\dagger(x_1)\psi_2(x_2) \right) \tag{140}$$

where $\psi_m(\psi_m^\dagger)$ is the electron annihilation (creation) operator, index m labels two identical semi-infinite segments of the LL-wire, $\langle x_2|\hat{T}|x_1\rangle$ is the tunneling matrix element in the coordinate representation, i.e. the amplitude for the process of electron tunneling from the point x_1 to the point x_2. In general amplitudes $\langle x_2|\hat{T}|x_1\rangle$ are nonlocal, but if the range of the potential of the impurity is very small, then expression (140) can be significantly simplified.

In the Luttinger liquid one can introduce the "slow" annihilation and creation operators of two types – for right and left moving electrons: $\psi_m(x) = e^{ip_F x}\Psi_{m,R}(x) + e^{-ip_F x}\Psi_{m,L}(x)$. Then in the first approximation, for a point-like neutral impurity $\langle x_2|\hat{T}|x_1\rangle = \lambda_0\delta(x_2 - x_1)$ and the tunneling Hamiltonian (140) of the contact is reduced to the expression

$$H_T = \sum_{r_1,r_2} \left(\lambda_0 \Psi_{2,r_2}^\dagger(0)\Psi_{1,r_1}(0) + h.c. \right) \quad , \tag{141}$$

It turns out, however, that Eq.(141) does not allow one to evaluate effects related to temperature difference between two semi-infinite Luttinger liquids. To obtain temperature induced effects we have to take into account the finite size of the barrier. We can do it by modifying the tunneling Hamiltonian. The modified Hamiltonian comprises the extra-terms with the

derivatives of the field operators

$$\begin{aligned} H_t &= \sum_{r_1,r_2} \left(\lambda_0 \Psi^\dagger_{2,r_2}(0) \Psi_{1,r_1}(0) + h.c. \right) + \\ &+ \sum_{r_1,r_2} \left(-i\hbar\lambda_1 \left(r_1 \Psi^\dagger_{2,r_2}(0) \partial_x \Psi_{1,r_1}(0) - r_2 \partial_x \Psi^\dagger_{2,r_2}(0) \Psi_{1,r_1}(0) \right) + h.c \right). \end{aligned} \tag{142}$$

Here $|\lambda_1|$ is a small additional parameter ($|\lambda_1| p_F \sim |\lambda_0|$).

Tunneling Hamiltonian can be written in the momentum representation

$$\begin{aligned} H_T &= \sum_{p_1,p_2} \left[T_{p_1,p_2} c^\dagger_{1,p_1} c_{2,p_2} + T^*_{p_1,p_2} c^\dagger_{2,p_2} c_{1,p_1} \right] = \\ &= \sum_{r_1,r_2} \sum_{q_1,q_2} \left[T_{r_1,r_2}(q_1,q_2) C^\dagger_{1,r_1}(q_1) C_{2,r_2}(q_2) + T^*_{r_1,r_2}(q_1,q_2) C^\dagger_{2,r_2}(q_2) C_{1,r_1}(q_1) \right] \end{aligned} \tag{143}$$

where $T_{p_1,p_2} = \langle p_1 | \hat{T} | p_2 \rangle$ is the tunneling amplitude, operators c_{n,p_n} $c^\dagger_{n,p_n}$ are annihilation and creation operators for electrons in the momentum representation and operators $C_{n,r_n}(p_n)$ and $C^\dagger_{n,r_n}(p_n)$ are the Fourier transforms of the fields $\Psi^\dagger_{n,r_n}(x)$ and $\Psi_{n,r_n}(x)$ (see Eq. (107)). Notice that form (142) of the tunneling Hamiltonian corresponds to the tunneling amplitude which depends upon the momentum of the tunneling electron

$$T_{p_1,p_2} = T_{r_1,r_2}(q_1,q_2) = \lambda_0 + \lambda_1 r_1 q_1 + \lambda_1 r_2 q_2 \tag{144}$$

where $q_m = (p_m - r_m p_F)$ is the momentum of the electron toward the Fermi level. Finite size of the impurity leads to the tunneling amplitude which depends on the momentum of tunneling electrons.

We assume that tunneling amplitude is so small that the tunneling rate of electrons through the barrier to the leading order can be obtained from the Fermi's "golden rule". For noninteracting electrons current through the junction can be written in the form

$$J = 2\pi e \sum_{p_1,p_2} |T_{p_1,p_2}|^2 \delta(E_1 - E_2 - eV) \left[f(E_1) - f(E_2) \right] \tag{145}$$

where $f(E) = 1/[e^{\beta E} + 1]$. Formula (145) assumes rigid relation between momentum and energy. When interactions between electrons are taken into account such rigid relation becomes wrong. Interactions between particles lead to smearing of dispersion relation. The

smearing of dispersion relation for particles is described by the spectral density function $A(k, E)$. Spectral density is proportional to a probability that electron with a momentum k has energy E. For noninteracting particles spectral density is just a Dirac delta function. For example, for 1D noninteracting free electrons spectral density is

$$A^{(0)}(k, E) = 2\pi\delta\left(E - \frac{\hbar^2 k^2}{2m}\right) \tag{146}$$

interactions will smear the delta peak over some range of energies. Spectral density is related to the imaginaly part of Fourier transform of retarded electron Green function:

$$A(k, \omega) = -\frac{1}{\pi}\mathrm{Im}[G^R(k, \omega)] \tag{147}$$

and obeys integral relations

$$\frac{1}{2\pi}\int dE A(k, E) = 1 \qquad \text{and} \qquad \frac{1}{2\pi}\int \frac{dk}{2\pi} A(k, E) = \rho(E) \tag{148}$$

The first of the Eqs.(148) is a normalization relation and the second is a definition of density of states $\rho(E)$, which is a probability for an electron to have energy E. Using the spectral densities, we can write expression for the tunneling current of interacting electrons

$$J = 2\pi e \sum_{p_1,p_2} |\hat{T}_{p_1,p_2}|^2 \int \frac{E_1}{2\pi} A(p_1, E_1) \int \frac{E_2}{2\pi} A(p_2, E_2)\delta(E_1 - E_2 - eV)\,[f(E_1) - f(E_2)] \tag{149}$$

3.6.2 Thermopower of the Luttinger liquid with an impurity.

In this section we show how to evaluate analytically the current induced by the temperature difference $J_{\Delta T}$, and determine the dependence of the thermopower of a Luttinger liquid on the interaction strength. We start with a general expression (149) for the tunnel current in a system of interacting electrons

$$J = 2\pi e \int_{-\infty}^{+\infty} dp_1 \int_{-\infty}^{+\infty} dp_2\ |\hat{T}_{p_1,p_2}|^2 \int_{-\infty}^{+\infty} d\varepsilon A_{T_1}(p_1, \varepsilon) A_{T_2}(p_2, \varepsilon + eV)\,[f_{T_2}(\varepsilon + eV) - f_{T_1}(\varepsilon)] \tag{150}$$

where $f_T(\epsilon) = 1/[\exp(\varepsilon/T) + 1]$ is the Fermi-Dirac distribution function and $A_T(p, \varepsilon)$ is the electron spectral density, and $\hat{T}_{p_1,p_2}$ is the bare tunneling amplitude. We assume that tunneling amplitude depends on the momentum of the electrons

$$|\hat{T}_{p_1,p_2}|^2 = |\hat{T}_{r_1,r_2}(q_1, q_2)|^2 = \delta_{r_1,r_2}\left(t_S^2 + \frac{\partial t_S^2}{\partial E_F} V_F(r_1 q_1 + r_2 q_2)\right) + \tag{151}$$
$$+\delta_{r_1,-r_2}\left(t_R^2 + \frac{\partial t_R^2}{\partial E_F} V_F(r_1 q_1 + r_2 q_2)\right)$$

Here $p_m = r_m p_F + q_m$, $m = 1, 2$ and $r_m = \pm 1$. First term in the Eq.(151) describes straightforward tunneling processes when electron after tunneling continues its motion in the same direction. The second term describes processes of reversing scattering when electron after interaction with impurity barrier changes its direction of motion. In the first case momentum does not change significantly $p_1 - p_2 \approx 0$, whereas in the second case particle is reflected to the opposite branch r of the dispersion relation and $p_1 - p_2 \approx \pm 2k_F$.

In the linear response approximation the tunnel current is a sum of two currents, $J = J_V(T) + J_{\Delta T}(T)$: one induced by the voltage drop V across the junction and the other induced by the temperature difference ΔT between two segments of the wire, i. e.

$$J_V = 2\pi e^2 V \sum_{r_1,r_2} \int_{-\infty}^{+\infty} dq_1 \int_{-\infty}^{+\infty} dq_2 \int_{-\infty}^{+\infty} d\varepsilon \; |\hat{T}_{r_1,r_2}(q_1,q_2)|^2 A_T(r_1,q_1,\varepsilon) A_T(r_2,q_2,\varepsilon) \frac{\partial f(\varepsilon)}{\partial \varepsilon} \tag{152}$$

$$J_{\Delta T} = 2\pi e \Delta T \sum_{r_1,r_2} \int_{-\infty}^{+\infty} dq_1 \int_{-\infty}^{+\infty} dq_2 \int_{-\infty}^{+\infty} d\varepsilon \; |\hat{T}_{r_1,r_2}(q_1,q_2)|^2 A_T(r_1,q_1,\varepsilon) A_T(r_2,q_2,\varepsilon) \frac{\partial f(\varepsilon)}{\partial T} \tag{153}$$

Where now the spectral functions $A_T(r, q, \varepsilon)$ of the electrons are taken at a mean temperature $T = (T_1 + T_2)/2$ and the derivatives of the distribution function are given by the formulas

$$\frac{\partial f(\varepsilon)}{\partial \varepsilon} = -\frac{1}{4T} \frac{1}{\cosh^2(\varepsilon/2T)} , \qquad \frac{\partial f(\varepsilon)}{\partial T} = \frac{\varepsilon}{4T^2} \frac{1}{\cosh^2(\varepsilon/2T)} \tag{154}$$

To evaluate the kinetic coefficients G_V and $G_{\Delta T}$, one needs to know the exact analytic expression for the spectral function $A_T(r, q, \varepsilon)$ at a finite temperature.

$$A_{T_m}(r_m, q, \omega) = -\frac{1}{\pi} \mathrm{Im}[G^R_{m,r_m}(q,\omega)] \tag{155}$$

where $G^R_r(q,\omega)$ is an imaginary part of Fourier transform of retarded Green's function:

$$G^R_{m,r_m}(x,t) = -i\Theta_H(t) \left\langle \left\{ \Psi_{m,r_m}(x,t), \Psi^\dagger_{m,r_m} \right\}_+ \right\rangle = \tag{156}$$

$$= \Theta_H(t) \left[G^>_{m,r_m}(x,t) - G^<_{m,r_m}(x,t) \right] \tag{157}$$

To calculate these Green's functions we will use a bosonization technique, described in the previous chapters. Namely, we represent fermion operators $\Psi_r(x,t)$ as an exponential of the boson fields $\Phi(x,t)$ and $\Theta(x,t)$ then using formula

$$\Psi_{m,r_m}(x) = \lim_{\alpha\to 0} \frac{1}{\sqrt{2\pi\alpha}} U^+_{m,r_m} \exp\left\{-\frac{i}{2}\left(r_m\Phi_m(x) + \Theta_m(x)\right)\right\} \tag{158}$$

and relation

$$\langle e^{i\phi(t)} e^{-i\phi}\rangle = e^{\langle\phi(t)\phi\rangle - \langle\phi\phi\rangle} = e^{\langle\langle\phi(t)\phi\rangle\rangle} \tag{159}$$

If we completely neglect tunneling through the impurity, we will have two semi-infinite Luttinger liquids with an open boundary, which reflects all electrons. To describe an open boundary we can use a method of reflections, i.e., assuming that the impurity is located at the point $x = 0$, we describe the perfect reflection from the boundary by imposing on a fermion field condition

$$\Psi_{m,r_m}(x) = -\Psi_{m,r_m}(-x). \tag{160}$$

The boson field that yield this boundary condition in the momentum representation take the form (see Appendix E)

$$\Theta_m(x) = i\int\limits_{-\infty}^{+\infty} dp \sqrt{\frac{2s}{g\epsilon_p}}\left(b_p - b_p^\dagger\right)\cos\left(\frac{\epsilon_p}{s}x\right) \tag{161}$$

$$\Phi_m(x) = i\int\limits_{-\infty}^{+\infty} dp \sqrt{\frac{2sg}{\epsilon_p}}\left(b_p + b_p^\dagger\right)\sin\left(\frac{\epsilon_p}{s}x\right) \tag{162}$$

where b_p and $b_p^\dagger$ are the standard bosonic annihilation and creation operators that obey commutation relations $[b_p, b_{p'}^\dagger] = \delta_{p,p'}$, and $\epsilon_p = s|p|$ is the energy of the bosonic excitations with momentum p. With the help of Eqs. (161), (162) and Eq.(158) it is straightforward to evaluate the fermion Green's functions. In particular, for $iG^>$ one gets in the vicinity of the contact ($x \sim 0$) the following expression

$$\langle\Psi_{m,r_m}(x,t)\Psi^\dagger_{m,r_m}\rangle \simeq \frac{1}{2\pi a}\left[\frac{1}{(1+i\frac{v_F\chi}{a})}\frac{\pi T_m\chi}{\sinh(\pi T_m\chi)}\right]^{\frac{1}{2}(\frac{1}{g}+r_m)} \times \\ \times\left[\frac{1}{(1+i\frac{v_F\eta}{a})}\frac{\pi T_m\eta}{\sinh(\pi T_m\eta)}\right]^{\frac{1}{2}(\frac{1}{g}-r_m)}, \tag{163}$$

where $\chi = t - x/s$ and $\eta = t + x/s$.

The next step is to calculate the Fourier transform of the Green's functions. It is helpful now to introduce new variables $X_\pm = \pi T(t \pm x/s)$ and $\Omega_\pm = (\omega \pm ks)/2$, and the dimensionless temperature $\bar{T} = \pi T a/v_F$. In terms of these variables the Fourier transform of $iG^>$ has the form

$$iG^>_{m,r_m}(\Omega_+,\Omega_-) = \frac{\bar{T}^{\frac{1}{g}-1}}{8\pi^2 gT}\exp\left(-i\frac{\pi}{2}\frac{1}{g}\right)\int_{-\infty}^{\infty}dX_+\int_{-\infty}^{\infty}dX_-\exp\left[\frac{i}{\pi T}(\Omega_+X_- + \Omega_-X_+)\right]\times$$
$$\times\left[\frac{1}{X_- - i\bar{T}}\frac{X_-}{\sinh X_-}\right]^{\frac{1}{2}(\frac{1}{g}+r_m)}\left[\frac{1}{X_+ - i\bar{T}}\frac{X_+}{\sinh X_+}\right]^{\frac{1}{2}(\frac{1}{g}-r_m)} . \qquad (164)$$

The spectral density $A(\omega,q)$ is expressed through $G^>(\omega,q)$ by the standard relation

$$A_{m,r_m}(\Omega_+,\Omega_-) = \frac{1}{2\pi}\mathrm{Im}\left[iG^>_{m,r_m}(\Omega_+,\Omega_-) + iG^>_{m,r_m}(-\Omega_+,-\Omega_-)\right] . \qquad (165)$$

Since we are interested in the limit $\bar{T} \ll 1$ the integrals in Eq.(164) can be taken analytically. After some algebra we get the analytic expression for the spectral density function of a spinless Luttinger Liquid with an open boundary, at finite temperatures $T \ll E_F$,

$$A_{m,r_m}(\Omega_+,\Omega_-) = \frac{1}{(2\pi)^3 gT}\bar{T}^{\frac{1}{g}-1}\cosh\left(\frac{\Omega_+ + \Omega_-}{2T}\right)\times$$
$$\times\int_{-\infty}^{\infty}dX_-\cos\left(\frac{\Omega_+X_-}{\pi T}\right)\left(\frac{1}{\cosh X_-}\right)^{\frac{1}{2}(\frac{1}{g}+r_m)}\times$$
$$\times\int_{-\infty}^{\infty}dX_+\cos\left(\frac{\Omega_-X_+}{\pi T}\right)\left(\frac{1}{\cosh X_+}\right)^{\frac{1}{2}(\frac{1}{g}-r_m)} = \qquad (166)$$
$$= \begin{cases} \frac{1}{(2\pi)^3 gT}(2\bar{T})^{\frac{1}{g}-1}\cosh\left(\frac{\Omega_+ + \Omega_-}{2T}\right)\frac{\left|\Gamma\left(\frac{1}{4}\left[\frac{1}{g}+r_m\right]+\frac{i}{2\pi}\beta\Omega_+\right)\right|^2}{\Gamma\left(\frac{1}{2}\left[\frac{1}{g}+r_m\right]\right)}\frac{\left|\Gamma\left(\frac{1}{4}\left[\frac{1}{g}-r_m\right]+\frac{i}{2\pi}\beta\Omega_-\right)\right|^2}{\Gamma\left(\frac{1}{2}\left[\frac{1}{g}-r_m\right]\right)} , & \text{if } g<1. \\ \delta(\omega - r_m v_F k) , & \text{if } g = 1. \end{cases}$$

Substituting Eq.(166) into Eqs. (152) and (153) and performing the integration over the momenta and energy (see Appendix F) one gets the desired kinetic coefficients (here we restore the normal dimensionality)

$$G_V = \frac{e^2}{2\pi\hbar}t_0^2 R_g^{(j)}(T) \quad , \quad G_{\Delta T} = \frac{\pi^2}{3}\frac{e}{\hbar}k_B^2 T\frac{\partial t_0^2}{\partial E_F}R_g^{(j)}(T) , \qquad (167)$$

where the renormalization coefficients $R_g^{(j)}(T)$ ($j = 1, 2$) are given by

$$R_g^{(j)}(T) = \frac{2j+1}{2}B\left(\frac{2j+1}{2},\frac{1}{g}\right)\left(\pi\frac{k_B T a}{\hbar v_F}\right)^{2(\frac{1}{g}-1)} . \qquad (168)$$

Here $B(x,y) = \Gamma(x)\Gamma(y)/\Gamma(x+y)$ is the Beta function and the effective transmission probability $t_0^2 \ll 1$ at the Fermi energy is defined as

$$t_0^2 = \left(\frac{2\pi}{\hbar v_F}\right)^2 \sum_{r_1,r_2} (t_S^2 \delta_{r_1,r_2} + t_R^2 \delta_{r_1,-r_2}) \, . \tag{169}$$

The expression for the conductance given in Eq.(167) coincides with the known result [57, 64]. One can see from Eqs.(167) and (168) that the thermoelectric cross-coefficient $G_{\Delta T}$ is renormalized by the interaction in analogy with the conductance. Consequently, the influence of the interaction on the thermopower is far less dramatic than that on the transport coefficients. The thermopower of a LL is still a linear function of temperature [59, 60] as is the thermopower of a system of noninteracting electrons. The electron-electron interaction in a Luttinger liquid model leads only to a temperature independent multiplicative renormalization of the thermopower S_0 of the free electrons

$$S_L^{(i)}(T,g) = \frac{3g}{2+g} S_0(T) \, . \tag{170}$$

For an infinite LL the renormalization factor decreases with increase of the interelectron interaction, and for strongly interacting particles $S_L^{(i)}(g \ll 1) \simeq (3/2) g S_0$.

3.7 Summary.

We have evaluated the thermopower of an infinite spinless LL induced by (i) the dispersion of the electron spectrum near the Fermi energy, and by (ii) the backscattering of the electrons by an impurity. We showed that the thermopower treated by perturbation theory (with respect to the nonlinearity of the electronic spectrum and the bare electron tunneling amplitude), is described by the Fermi liquid formulas renormalized by interaction-dependent factors.

We found that for an *infinite* Luttinger in the case of dispersion induced thermopower Eq.(138) as well as in the case of the impurity induced thermopower Eq.(170), renormalization coefficient decreases with repulsion strength V_0, (since the correlation parameter is equal to $g^{-1} = \sqrt{1 + V_0/\pi\hbar v_F}$ for spinless electrons). We should emphasise again that Eqs.(138) and (170) stand for an infinite LL. In real experiments, however, the Luttinger Liquid wire (e.g. a carbon nanotube [65]) is connected to 3D or 2D metallic leads where

the electrons can be regarded as noninteracting particles. It is known that the transport properties of a Luttinger Liquid wire connected to (noninteracting) electron reservoir differ from the transport properties calculated for an infinite LL, even for adiabatic contacts. The best known example of such a behavior is the conductance G_L of an impurity-free LL wire. For an infinite LL, formally $G_L = gG_0$ (G_0 is the conductance quantum, $G_0 = e^2/h$ for spinless electrons), while for a LL wire connected to leads, $G_L = G_0$ (the so called "no renormalization theorem" for the conductance of a Luttinger liquid [66, 67, 68]). Note that the heat conductance G_T is also different for the above two situations (see Ref. [69, 70]).

To estimate the thermopower of a finite LL wire adiabatically connected to leads of noninteracting electrons we will follow the approach proposed in Ref. [71]. In the case of weak tunneling through the impurity, the voltage drop across the impurity and the one measured between the leads are different quantities. This fact is evident in the limit of strong interaction $g^2 \sim \hbar v_F/e^2 \ll 1$ when the Coulomb blockade is pronounced; the shift of the chemical potentials of the leads $\Delta\mu_L = eU$ can not change significantly the voltage drop V across the impurity (placed in the middle of a sufficiently long LL wire). In a previous study it has been shown that $V = g^2U$ for arbitrary interaction strength [71]. Therefore, to relate (at least qualitatively) the thermopower $S_L^{(i)}(T, g)$ evaluated above to the thermopower $S_W^{(i)}(T, g)$ of a LL wire adiabatically connected to leads of noninteracting electrons, we have to replace first the voltage V in our formulae by g^2U. Since this substitution affects only the voltage induced current, it influences the thermopower $S_W^{(i)}(T, g) \simeq S_L^{(i)}(T, g)/g^2$ and now $S_W^{(i)}(T, g) \sim S_0(T)/g \gg S_0(T)$ for strongly interacting particles. We see that in a real situation, when the voltage drop is measured between the leads the electron-electron interaction in the wire enhances the impurity-induced thermopower. It supports our claim [60] based on estimation of the thermopower in a phenomenological model of charge and heat transport in a LL.

Finally, we may inquire about the effect of the leads on the dispersion-induced thermopower. In the absence of electron backscattering the leads keep the conductance of a LL wire unrenormalized [66, 67, 68], i.e. $G_L = e^2/h$. Therefore, the dispersion-induced thermopower of a finite LL wire $S_W^{(d)}(T, g) = gS_L^{(d)}(T, g)$ is suppressed even stronger by the

interelectron interaction than the above calculated quantity $S_L^{(d)}$. For strongly interacting ($g \ll 1$) particles $S_W^{(d)}(T,g) \sim g^2 S_F(T) \ll S_F(T)$ (S_F is the corresponding Fermi-liquid thermopower, Eq.(138)). Thus, one could expect that in experiments involving wires of strongly correlated electrons the measured thermopower would be associated mostly with imperfections in the wire (impurities, barriers at the boundaries between the 1D wire and the leads, etc.).

CHAPTER IV

FORCE AND MAGNETIZATION OSCILLATIONS IN S/N/S AND S/2DEG/S JUNCTIONS.

Small superconductor – normal metal – superconductor (S/N/S) junctions can be formed either straightforwardly by attaching separately fabricated metallic nanowires to the bulk superconducting leads, or by using a scanning tunneling microscope in which the tip of the scanning tunneling microscope is pushed into the surface and then slowly retracted. Formation and mechanical properties of such metallic nanojunctions (formed with a scanning tunneling microscope) were predicted in numerical simulations long ago [72] (see also Fig.21), and they have been the subject of subsequent research endeavors [73]. It has been shown that for normal junctions (i.e. when both tip, surface and the narrow part of the junction are in the normal state) the oscillatory behavior of the elongation force is correlated with a quantized staircase behavior of the electrical conductance [74, 75, 76, 77]. However, the influence of superconductivity on nanomechanical properties of such nanowires has not been explored yet, they are the subject of this part of the Thesis. In this chapter we consider superconductivity-induced effects of magnetization and force oscillation in small S/N/S, and superconductivity-induced magnetization oscillations in the superconductor – two-dimensional electron gas – superconductor (S/2DEG/S) junctions.

4.1 Model of the nanowire junction between two superconductors.

We assume that both the tip and the surface of the junction are made from the same material and that the magnitude of the superconductivity order parameter is the same, but phases of the order parameter in the tip and the surface can be different and can be controlled. Furthermore, we additionally simplify our model by modeling the normal part of the S/N/S junction by a cylinder of length L and cross-section area $S = V/L$. The

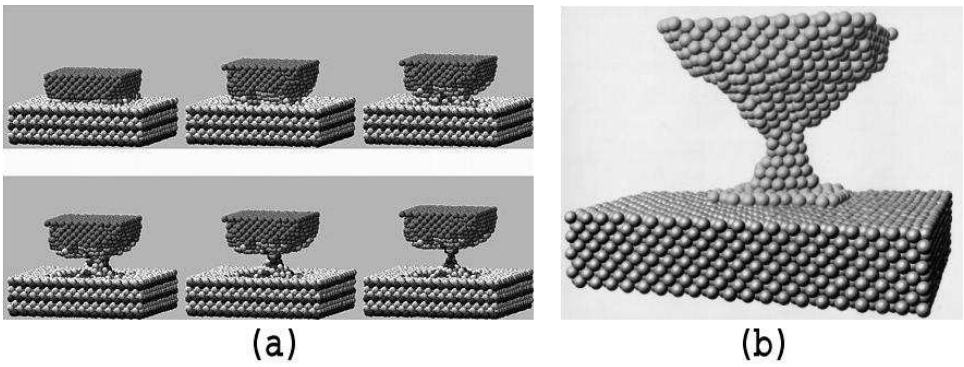

Figure 21: Nanocontact formation in the scanning tunneling microscope experiment. These pictures are from the Ref. [72]. I want to thank David Luedtke for giving me these results. The contact is formed by pushing the sharp tip into the surface being studied by the scanning tunneling microscope and then, after some time, slowly pulling it back. Fig.(a) shows different stages of contact formation process, and Fig.(b) gives a close look at the atomic structure of the created nanocontact.

diameter of the narrow part of the junction can be made as thin as few atoms. As a result, the motion of the electrons in the narrow part, in the directions perpendicular to the axis of the junction becomes quantized. At low temperatures only a few transverse modes are occupied and can conduct current, all the other higher modes are empty. The motion of electrons in each open channel is effectively one-dimensional.

The junction can be stretched or compressed by applying force F (see Fig. 22). We assume that the volume of the junction remains constant during elongation process [72]. Therefore, the elongation of the wire decreases the area of cross-section of the narrowest part of the contact. The number of the open channels (i.e. occupied transverse modes) is proportional to the area of cross section and therefore also decreases with elongation of the wire. We assume that the connection between narrow part of the junction and the leads is adiabatic (i.e. potentials in the points of connection are sufficiently smooth and do not cause transition of electrons from one open channel to another). Adiabatic boundaries between tip and surface and nanowire make the open conducting channels independent from each other so that any property (like conductance force or magnetization) of the total junction is the sum of the properties of independent open channels. For example, in the case when bulk leads are not superconducting, each transverse mode has the same conductance $G_1 = 2e/h$,

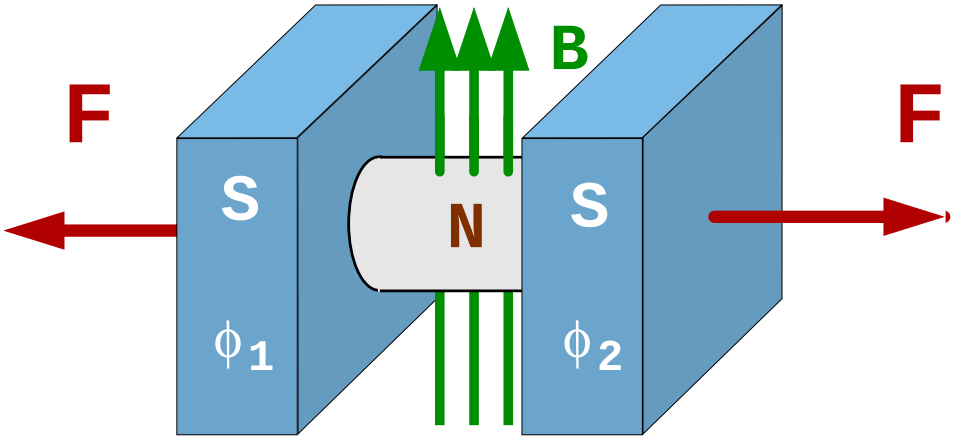

Figure 22: Model of the nanoscopic junction created in the STM experiment. The real junction is modeled by two bulk superconductors connected via cylindrical nanoscopic junction. Since the diameter of the junction in its cylindrical part is comparable to the Fermi wavelength, the motion of the electrons in this part in perpendicular directions is quantized. Moreover, due to the phenomenon of Andreev reflection, motion of the electrons in the direction along the axis of the contact is quantized. The superconducting leads of our small junction can have different phases of the order parameter. When we discuss the magnetic properties of such a junction, we assume that the magnetic field is acting only on the normal part of the junction and is zero near superconductors.

so that the total conductance of the contact with $N_\perp$ open transverse modes is equal to $G_N = 2eN_\perp/h$. When the junction is stretched the number of channels in the junction decreases one by one, leading to the staircase behavior of conductance and to peaks of force [74]. Transition of the bulk parts of the contact into a superconducting state should change the spectrum of quasiparticles in these parts of the system, which in turn will affect the properties of each channel and of the whole junction. In the next section we estimate the magnitude of the effects related to superconductivity.

4.2 Estimates of magnitude of the force due to superconductivity.

In normal metals the cohesive force in an atomic-scale contact can be estimated as $F_n \sim \varepsilon_F/\lambda_F$, where ε_F and λ_F are the Fermi energy and wavelength. The onset of superconductivity introduces a new energy scale, i.e. the superconducting gap $\Delta \ll \varepsilon_F$, and a new length scale, i.e. the superconductivity coherence length $\xi_0 = \hbar v_F/\pi\Delta$. On first sight, the resulting superconductivity-induced forces are expected to be of the order of $F_{sc} \sim \Delta/\xi_0$,

and when added to the aforementioned normal-metal forces (F_n , which are of the order of several nN), they are estimated to be below the atomic force microscopy (AFM) detection limit [78]. However, in the superconducting regime, under certain conditions all the transverse channels ($N_\perp$) supported by the junction will contribute coherently to the free energy, and when $N_\perp \gg 1$ the above consideration may result in a gross underestimation of F_{sc}.

4.3 Quasiparticle excitations in the superconductors. Andreev reflection.

According to BCS theory of superconductivity, quasiparticles of Fermi liquid at low temperatures (if there is attractive interaction between them) form bound pairs, so-called 'Cooper pairs'. Cooper pairs obey Bose statistics and at low temperatures condense, forming a quantum fluid. Condensation of pairs leads to opening of the energy gap in the spectrum of quasi-particle excitations (see Fig. 23). The value of the gap corresponds to the minimum energy (per particle) needed to break the Cooper pair.

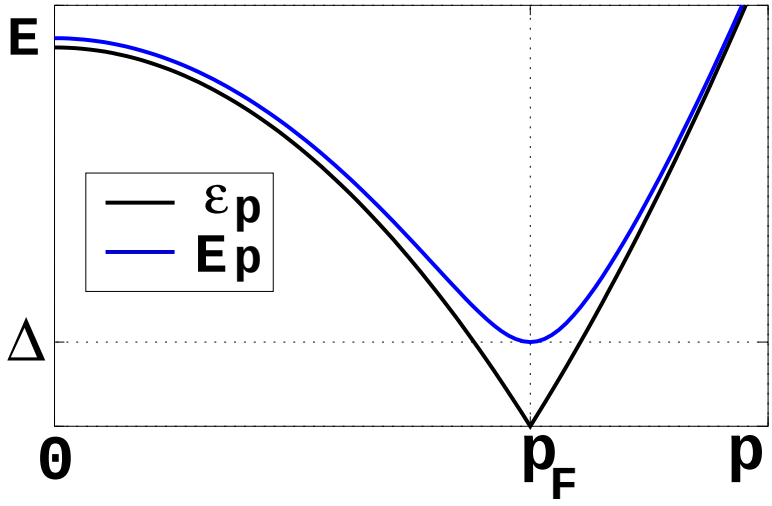

Figure 23: Dispersion relation for elementary excitations in normal metal and in superconductor. Black curve shows dispersion relation in the normal state $\Delta = 0$. Blue curve shows dispersion relation for superconductor. Energy spectrum for excitations in superconductor "bogolons" has a gap Δ. Bogolons are created when a Cooper pair is torn apart. The gap in the spectrum of bogolons is equal to half of the minimum energy necessary to break a Cooper pair. There is no electron-like or hole-like quasiparticles with energies $E < \Delta$ in superconductor.

When a superconductor is brought into contact with a normal metal, many interesting

quantum phenomena can be observed. One such phenomena is the Andreev reflection, named after Andreev who first noticed that an electron is reflected at the N/S interface in an unusual way. The difference between normal and Andreev reflection is demonstrated in Fig. 24. In the Andreev reflection an electron is transformed into a hole with almost the same momentum, but with opposite group velocity. The reasons for such strange behavior are the following. From one side, an electron with energy $|E| < \Delta$ in the normal part of the N/S contact that approaches the interface cannot penetrate into superconductor since there are no single-particle excitations with such energy in the superconductor. On the other hand, there is no mechanism for normal scattering process at the interface which is able to reverse the momentum of the electron and bounce it back. The solution of this problem suggested by Andreev is that an electron is reflected as a hole, moving with the same momentum, but with opposite velocity. Transformation of the electron into the hole at the interface during Andreev reflection is accompanied by the creation of a Cooper pair on the side of the superconductor, so that total charge in the system is conserved. Andreev reflection is a very nonlocal process. Formation of the Cooper pair that is to be injected into the superconductor starts already in the normal metal. On the other hand, electrons and holes penetrate inside the superconductor over the distances of the order of coherence length $\xi = \hbar v_F/\Delta$, which is greater than any microscopic lengthscale. In other words, Andreev reflection is a proximity effect.

A system in which a normal conductor is sandwiched between two superconductors is called a metallic Josephson junction. Properties of the bulk S/N/S junctions are somewhat different from the properties of regular Josephson junctions, where two superconductors are separated by a thin insulating film. The interference of the incident electron waves and those reflected from N/S interfaces as hole waves produces in a normal part of the junction a set of discrete Andreev-Kulik (AK) states [79], that are responsible for a nondissipative equilibrium current through the system (Josephson current).

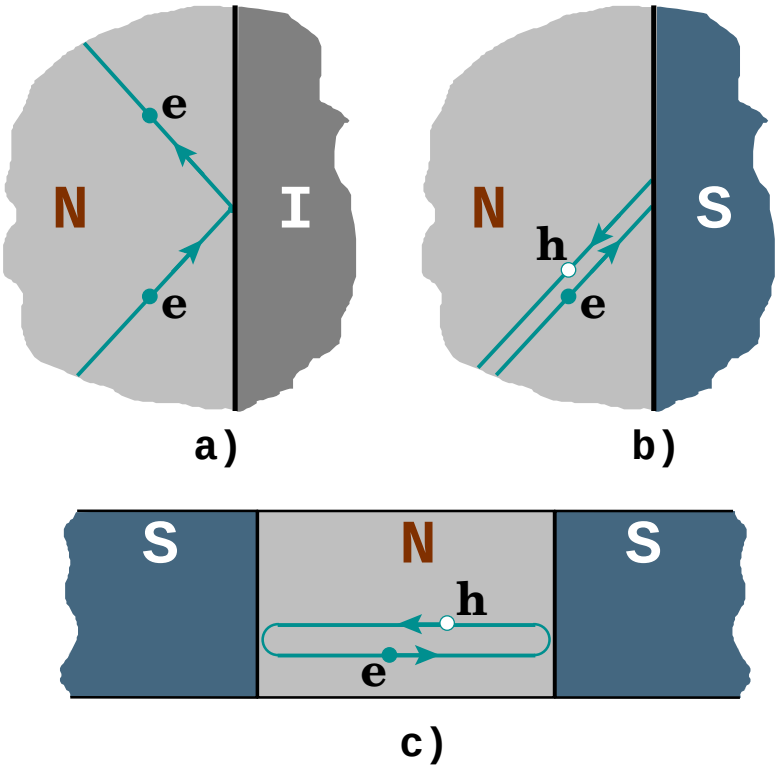

Figure 24: Normal reflection versus Andreev reflection. Formation of Andreev levels in the S/N/S junction. Fig.(a) shows normal specular reflection and Fig.(b) shows Andreev reflection. In the normal side in Andreev reflection an electron incident on the NS surface is reflected as a hole. The total charge in the system is conserved because as a result of Andreev reflection a Cooper pair with the total charge $2e$ is absorbed in the superconductor. Fig.(c) demonstrates the principle of formation of an Andreev level in the normal part of S/N/S junction: an electron is reflected as a hole on the first surface and then the hole is reflected back into the electron on the second surface.

4.4 One -dimensional model for transverse modes. Bogolubov - de Gennes equation.

Since the motion of the electrons in each transverse mode of the contact is effectively one-dimensional and modes in an adiabatic junction are independent from each other, we model each transverse mode as a one-dimensional metal. We totally neglect interactions between electrons inside the normal part of the junction [1].

To find the spectrum of Andreev levels we use the Bogolubov-de Gennes equation [82],

[1] We could as well have used the Luttinger Liquid model to describe one-dimensional transverse channels between superconductors (see e.g. Refs. [80] and [81]). It turns out, however, that for adiabatic constrictions both models produce the same final result.

which is a Schrödinger equation for a two-component wave function $\Psi = \begin{pmatrix} \chi \\ \eta \end{pmatrix}$ of quasiparticles, with components χ and η satisfying normalization condition $|\chi|^2 + |\eta|^2 = 1$:

$$\begin{pmatrix} H_0(\mathbf{r}) & \Delta(\mathbf{r}) \\ \Delta^*(\mathbf{r}) & -H_0^*(\mathbf{r}) \end{pmatrix} \begin{pmatrix} \chi(\mathbf{r}) \\ \eta(\mathbf{r}) \end{pmatrix} = E \begin{pmatrix} \chi(\mathbf{r}) \\ \eta(\mathbf{r}) \end{pmatrix} \tag{171}$$

In this equation $H_0(\mathbf{r}) = (1/2m)[\hat{\mathbf{p}} - (e/c)\mathbf{A}]^2 + V(\mathbf{x}) - \mu$ is the Hamiltonian of the system in the normal state, $\Delta(\mathbf{r})$ is the complex order parameter of superconductivity, and μ is the Fermi energy.

Let us first consider normal and superconducting states of the uniform one-dimensional conducting channel in the case of zero external magnetic field. Equation (171) is an eigenvalue problem. Eigenfunctions of this eigenvalue problem are the elementary excitations of the system. And the eigenvalues are the energies of these elementary excitations. In the uniform system ($V(x) = 0$ for all x) in the absence of superconductivity, the spectrum of eigenvalues of Eq.(171) is continuous from $-\infty$ to $+\infty$ without gaps. For a given energy E there are four eigenfunctions

$$\Psi_e = \begin{pmatrix} 1 \\ 0 \end{pmatrix} e^{\pm i p_e x} \qquad \text{and} \qquad \Psi_h = \begin{pmatrix} 0 \\ 1 \end{pmatrix} e^{\pm i p_h x} \tag{172}$$

where wave vectors p_e and p_h are given by the formulas

$$p_e = p_F \sqrt{1 + E/\mu} \qquad \text{and} \qquad p_h = p_F \sqrt{1 - E/\mu} \tag{173}$$

Functions Ψ_e in the (172) correspond to electrons and functions Ψ_h describe a hole.

In the superconducting state the order parameter Δ is not zero, and the matrix of Bogolubov-de Gennes equation is not diagonal and the functions Ψ_e and Ψ_h are not the eigenvectors. This means that electrons and holes are not the elementary excitations of the system in superconducting the state. For a superconductor with order parameter $\Delta(x) = \Delta e^{i\phi}$, eigenfunctions of the Bogolubov - de Gennes equation can be written in the form

$$\Psi_{qe} = \begin{pmatrix} v e^{i\phi/2} \\ u e^{-i\phi/2} \end{pmatrix} e^{\pm i q_{qe} x} \qquad \text{and} \qquad \Psi_{qh} = \begin{pmatrix} u e^{i\phi/2} \\ v e^{-i\phi/2} \end{pmatrix} e^{\pm i q_{qh} x} \tag{174}$$

where

$$u = \sqrt{\frac{1}{2}\left(1 + \frac{\sqrt{E^2 - \Delta^2}}{E}\right)} \qquad \text{and} \qquad v = \sqrt{\frac{1}{2}\left(1 - \frac{\sqrt{E^2 - \Delta^2}}{E}\right)} \tag{175}$$

Comparing the wave functions Ψ_{qe} and Ψ_{qh} with the wave functions Ψ_e and Ψ_h given by Eq.(172) we see that elementary excitations of the superconductor are the coherent combinations of the electron-like and the hole-like excitations. Elementary excitations Eq.(174) are called "bogolons". Electric charge of the bogolons is not an integer multiple of the electron charge e, but equals $Q = e(u^2 - v^2)$. Energy of the bogolons is related to their quasi-momentum according to the dispersion relation

$$E_p = \sqrt{\varepsilon_p^2 + \Delta^2} \tag{176}$$

where $\varepsilon_p = \pm\left(\frac{p^2}{2m} - \epsilon_F\right)$ is the energy of an electron or hole with momentum p. This dispersion relation is shown on the Fig. 23.

Now let us consider a one-dimensional conductor in the S/N/S state. We can solve the Bogolubov-de Gennes equation for every region separately and then we will join the solutions at the interfaces between the regions. Let us assume that there is no conventional specular reflection at the N/S interfaces, that is potential $V(x)$ is zero everywhere. We also assume that the absolute value of the order parameter is the same on both ends of the contact, since the tip and the surface of the scanning tunneling microscope are made from the same material and are at the same temperature, namely, we assume that the order parameter across the system is

$$\Delta(x) = \begin{cases} \Delta \exp(i\phi_1), & \text{for } x < -d \\ 0, & \text{for } -d < x < d \\ \Delta \exp(i\phi_2), & \text{for } x > d \end{cases} \tag{177}$$

For the normal part of our system the Bogolubov-de Gegennes solution can be written in general form as

$$\Psi_N = C_R \begin{pmatrix} 1 \\ 0 \end{pmatrix} e^{ip_e x} + C_L \begin{pmatrix} 1 \\ 0 \end{pmatrix} e^{-ip_e x} + D_R \begin{pmatrix} 0 \\ 1 \end{pmatrix} e^{-ip_h x} + D_L \begin{pmatrix} 0 \\ 1 \end{pmatrix} e^{ip_h x} \tag{178}$$

where the first two terms describe electrons moving in opposite directions and the last two

terms describe holes. For the left superconductor wave function we can write

$$\Psi_{S1} = A_R^{in}\begin{pmatrix} ue^{i\phi_1} \\ v \end{pmatrix} e^{iq_1^e} + B_R^{in}\begin{pmatrix} ve^{i\phi_1} \\ u \end{pmatrix} e^{-iq_1^h} + A_L^{out}\begin{pmatrix} ue^{i\phi_1} \\ v \end{pmatrix} e^{-iq_1^e} + B_L^{out}\begin{pmatrix} ve^{i\phi_1} \\ u \end{pmatrix} e^{iq_1^h} \quad (179)$$

whereas for the right superconductor it should be

$$\Psi_{S2} = F_R^{out}\begin{pmatrix} ue^{i\phi_2} \\ v \end{pmatrix} e^{iq_2^e} + G_R^{out}\begin{pmatrix} ve^{i\phi_2} \\ u \end{pmatrix} e^{-iq_2^h} + F_L^{in}\begin{pmatrix} ue^{i\phi_2} \\ v \end{pmatrix} e^{-iq_2^e} + G_L^{in}\begin{pmatrix} ve^{i\phi_2} \\ u \end{pmatrix} e^{iq_2^h} \quad (180)$$

where parameters A, B, C, D, F, G should be found by matching solutions (178,179,180) at the interfaces. Components u and v in the Eqs.(178,179,180) are given by the Eqs.(175), and the wave vectors p_e and p_h are given by the Eqs.(173). Wave vectors for the quasiparticles in the left and right superconductor are

$$q^e = k_F\sqrt{1 + \frac{\sqrt{E^2 - \Delta^2}}{\mu}} \approx k_F + \frac{i}{\mu}\sqrt{\Delta^2 - E^2} \quad (181)$$

$$q^h = k_F\sqrt{1 - \frac{\sqrt{E^2 - \Delta^2}}{\mu}} \approx k_F - \frac{i}{\mu}\sqrt{\Delta^2 - E^2} \quad (182)$$

Since $E < \Delta$ wave vectors q^e and q^h are not real, but contain some imaginary part. The imaginary part means that the wave functions of the quasiparticles Ψ_{s1} and Ψ_{s2} is decaying in the superconductors away from the normal region because quasiparticles below the gap cannot exist; they form Cooper pairs and disappear.

The normal part of the junction is the source of the quasipasticles. At low temperatures Cooper pairs are being broken mostly at the interfaces to the superconducting sections and there are no other sources of bogolons with $E < \Delta$ in the system. Thus, the amplitudes $A_L^{out}, B_L^{out}, F_R^{out}, G_R^{out}$ of particles going inside normal part should be zero. For the remaining parameters A, B, C, D, F, G we have four boundary conditions - two on each interface, namely:

$$\Psi_{S1}(-d) = \Psi_N(-d) \qquad \left.\frac{d\Psi_{S1}}{dx}\right|_{x=-d} = \left.\frac{d\Psi_N}{dx}\right|_{x=-d} \quad (183)$$

at the first interface, and

$$\Psi_N(-d) = \Psi_{S2}(-d) \qquad \left.\frac{d\Psi_N}{dx}\right|_{x=-d} = \left.\frac{d\Psi_{S2}}{dx}\right|_{x=-d} \quad (184)$$

at the second interface. As a result we get a homogeneous system of eight equations with eight unknowns. From the requirement of zero determinant of this system we get an equation for energies

$$(v^2 e^{i\phi - ik_h L} - u^2 e^{-ik_e L})(v^2 e^{i\phi + ik_e L} - u^2 e^{ik_h L}) = 0 \tag{185}$$

where $\phi = \phi_2 - \phi_1$ phase difference across the junction and $L = 2d$ is the length of the normal part. After some algebraic manipulations with equation (185) we reproduce the well known Andreev-Kulik spectrum [79]

$$\left(2 \arccos \frac{E}{\Delta} - 2\frac{E}{\Delta_L}\right) = \pm\phi + 2\pi n \qquad n = 0, \pm 1, \pm 2, \ldots \tag{186}$$

where $\Delta_L = \hbar v_F / L$.

Spectrum (186) consists from two families of levels. The first family corresponds to the plus sign in the Eq.(186) , and the other to the minus sign. At zero phase difference these two families of levels are degenerate. When the phase difference is changed, the levels of the first set increase their energies whereas the levels of the second set decrease. The first set of levels is responsible for Josephson current in the right direction, and levels of the second set - for the Josephson current in left direction. At nonzero phase difference ϕ there is some imbalance between population of these families of levels so that the total current through the junction is nonzero.

Equation (186) describes a clean junction. For the the junction with impurities it is replaced by the equation

$$\left(2 \arccos \frac{E}{\Delta} - 2\frac{E}{\Delta_L}\right) = \pm\alpha + 2\pi n \qquad n = 0, \pm 1, \pm 2, \ldots \tag{187}$$

where

$$\cos\alpha = R + D\cos\varphi \qquad \text{and} \qquad R = 1 - D. \tag{188}$$

parameter D is the transparency of the impurity. This spectrum was previously used to calculate Josephson current through the S/N/S junctions [83, 84]. We use the spectrum (186) to find superconductivity- induced force and magnetization. Equation (186) is a transcendental equation for energies E of Andreev levels. Before we can use this equation

in our calculations, it should be simplified and written in a more explicit form. Luckily, such simplification is possible in cases of short ($L \ll \xi$) and long junctions ($L \gg \xi$). For a short junction, the discrete spectrum of Andreev levels is

$$E_0 \simeq \Delta W(\varphi) \left(1 - \frac{L\sqrt{D}}{\xi_0} \left|\sin\frac{\varphi}{2}\right|\right) \ , \tag{189}$$

where $W(\varphi) = \sqrt{1 - D\sin^2\frac{\varphi}{2}}$. In this case, the discrete spectrum has only a single, twice-degenerate level. For the long junction energy levels are very dense, and if we consider only the first few Andreev levels near the Fermi energy, then for such levels $E \ll \Delta$ and spectrum (186) is approximated by

$$E_L^{\pm} = \pi\Delta_L \left(\pm\frac{\alpha}{2\pi} + \frac{1}{2} + n\right) \tag{190}$$

where phase α defined by Eq.(188). Knowing the energy spectrum of electrons in each transverse mode of the junction we are ready to calculate the forces in the junction.

4.5 Force in S/N/S junctions.

We assume that the junction is in the state of thermodynamical equilibrium. The superconducting bulk parts of the system (tip and surface) are big and can exchange electrons with macroscopic superconducting reservoirs which can be regarded as infinite. As is well known from thermodynamics, the force equals the spatial derivative of the thermodynamical potential Ω, i.e.

$$F = -\partial\Omega/\partial L. \tag{191}$$

There are two contributions to the Andreev force $F_A = F_\perp + F_L$, where $F_\perp$ is related to the dependence of the number of quantized transverse channels, $N_\perp$, on the degree of elongation, and F_L originates from the dependence of the Andreev bound states on the length of the junction.

Let us denote a grand-canonical thermodynamic potential of the single channel by $\Omega_n(\varphi, L)$. The total grand canonical potential of the whole junction is simply the sum $\Omega(\varphi, L) = \sum_n \Omega_n(\varphi, L)$ To simplify the physical picture, to make further considerations

more intuitive we use semiconductor model of our semiconductor-normal-semiconductor structure [85, 86]. In this model superconductor is modeled with a semiconductor with a gap 2Δ. Electron-like and hole like bogolons are replaced by electrons and holes. Energies of electrons with $k > k_F$ are positive, whereas energies of holes with the same wave vectors is negative, and vice versa for $k < k_F$. Probability of an electron excitation is f, whereas probability of a hole excitation is $(1-f)$. Such model is simply a new way of representation of the same concepts.

4.5.1 Short junctions.

Let us consider first the superconductivity-induced force oscillations in short junctions. Since the Andreev states in the short junctions are independent of the mode index [87], total thermodynamic potential of the junction is equal to the thermodynamical potential of a single mode times the number of modes in the junction, $\Omega_s(\varphi, L) \approx N_\perp(L)\Omega_A(\varphi, L)$ where $\Omega_A(\varphi, L)$ corresponds to a single-channel S/N/S junction. In a cylindrical geometry number of transverse modes is given by the expression $N_\perp(L) \simeq \pi V/\lambda_F^2 L$, where V is the volume of the normal part of the junction. In general, both bound (superscript (b) below) and scattering Andreev states contribute to $\Omega_A(\varphi, L)$; for our purpose only the bound states are important (see below), and thus $F_A^{(b)} = F_\perp^{(b)} + F_L^{(b)}$, where

$$F_\perp^{(b)} = \frac{N_\perp}{L}\Omega_A^{(b)}(\varphi, L), \qquad F_L^{(b)} = -N_\perp \frac{\partial \Omega_A^{(b)}(\varphi, L)}{\partial L}. \tag{192}$$

Withing the semiconductor model, thermodynamical potential Ω_A of the single channel in the short junction can be calculated simply as the thermodynamic potential for a two-level system $(E^{(+)}, E^{(-)}) = (E_0, -E_0)$, where energy E_0 is given Eq. (189). Straightforward calculation yields

$$F_\perp^{(b)} \simeq -2N_\perp \frac{T}{L} \ln\left\{\frac{\cosh^2\left(W(\varphi)\Delta/2T\right)}{\cosh^2(\Delta/2T)}\right\}, \tag{193}$$

$$F_L^{(b)} \simeq 2N_\perp \frac{\Delta}{\xi_0} W(\varphi)\sqrt{D\sin^2\frac{\varphi}{2}}\tanh\left(\frac{\Delta}{2T}W(\varphi)\right). \tag{194}$$

where $W(\varphi) = \sqrt{1 - D\sin^2\frac{\varphi}{2}}$. For low transparency junctions ($D \ll 1$) force $F_\perp^{(b)}$ may be approximated as

$$F_\perp^{(b)} \simeq \frac{N_\perp \Delta}{L} D\sin^2\frac{\varphi}{2}\tanh\left(\frac{\Delta}{2T}\right) \sim \frac{N_\perp \Delta}{L} D\ , \tag{195}$$

and since $F_L^{(b)} \sim N_\perp(\Delta/\xi_0)\sqrt{D}$ it is evident that $|F_\perp^{(b)}| \gg |F_L^{(b)}|$, provided that $D \gg (L/\xi_0)^2$. In contrast, when $D \ll (L/\xi_0)^2 \ll 1$ the $F_L^{(b)}$ contribution dominates.

For point contacts (i.e. extremely short junctions) the Andreev force can be calculated (when $D \gg (L/\xi_0)^2$) by taking the limit $L/\xi_0 \to 0$ for the Andreev bound states Eq.(189). In this case, continuum states do not affect the free energy (see e.g. Ref.[88]) and, therefore, they do not contribute to the force. In contrast, for low transparency junctions the L/ξ_0-corrections to the bound state energies determine the force oscillations. To this order the continuum states do contribute to the free energy and they can change the dependence of the AF on the phase difference. Thus, Eq.(194) can be considered as an estimate of the AF in a short junction. the contribution of the continuum states ($F_A^{(c)}$) is extremely small, i.e. $F_A^{(c)}(D \ll 1) \ll (L/\xi_0)^3(\varepsilon_F/\lambda_F)$.

The phase-dependent force in a superconducting quantum point contact (QPC) ($D = 1$) is related to the quantized Josephson current J_s (see Ref.[87])

$$J_s = \frac{e}{\hbar}\left(-L\frac{\partial F_A^{(b)}}{\partial\varphi}\right) = N_\perp\frac{e\Delta}{\hbar}\sin\frac{\varphi}{2}. \tag{196}$$

The force oscillations (portrayed by the dependence of the force on the contact size) are determined by two distinct contributions: (i) a large phase-independent term (operative also in normal-metal NWs) of the order of $N_\perp\varepsilon_F/\lambda_F$ originating from incoherent contributions of all the conducting electrons to the thermodynamic potential [76, 77, 89], and (ii) a coherent SC-induced force (Eqs.(193) and (194)). It is the latter, phase-dependent, term that is directly related to the quantized Josephson current.

The amplitude of the Andreev force oscillations may be readily estimated as follows: for $D \sim 1$ and $L \ll \xi_0$ the amplitude of the Andreev force is of the order of $F_A^{(b)} \sim N_\perp\Delta/L \sim L\varepsilon_F/\xi_0\lambda_F \sim (L/\xi_0)\,[nN]$; in the ballistic regime for a non-transition metal $\xi_0 \sim 10^{-5} - 10^{-4}cm$. Using state-of-the-art instrumentation such forces (e.g. $10^{-2} - 10^{-1}nN$), can be measured [90].

4.5.2 Long junction.

In long junctions spectrum of Andreev levels is approximated by Eq.(190). Since this spectrum does not depend on the superconducting gap Δ, for low temperatures ($T \ll$

Δ) all the thermodynamic properties of a long ballistic junction are essentially material independent. Evaluation of the Josephson current in this case is equivalent to the calculation of the persistent current for chiral fermions on a ring [91].

We will consider only clean long junctions, so that $\alpha = \phi$. The corresponding phase-dependent part of the thermodynamic potential $\Omega_A(\phi)$ for the Andreev-Kulik spectrum (190) can be evaluated as follows. The thermodynamic potential of the particles in the Andreev state $(n, \pm)$ is

$$\Omega_n^s = -T \ln \left(1 + e^{-\beta E_n^{\pm}}\right) = -T \ln \left\{1 + \exp\left(-\beta\pi\Delta_L \left(s\frac{\phi}{2\pi} + n + \frac{1}{2}\right)\right)\right\} \tag{197}$$

where number $s = \pm 1$ indexes families of Andreev levels. Thermodynamical potential Ω_A of a single transverse mode is equal to the sum of thermodynamical potentials of all Andreev levels

$$\Omega_A = \sum_{s=\pm} \sum_n \Omega_n^s \tag{198}$$

Summation over index n can be performed using Poisson formula

$$\sum_{n=-\infty}^{+\infty} \Omega_n^{\pm} = 2\mathrm{Re} \sum_{k=1}^{\infty} \int_{-\infty}^{+\infty} \Omega^{\pm}(x) e^{2\pi i k x} dx + \int_{-\infty}^{+\infty} \Omega^{\pm}(x) dx \tag{199}$$

where $\Omega^{\pm}(n)$ is the same as $\Omega_n^{\pm}$, except that index n is a continuous variable. The last integral in right hand side of the equation (199) is diverging. The divergence is a consequence of the simplifications made to the Andreev spectrum in the limit $L \gg \xi$. Namely, spectrum (190) corresponds to the infinite gap in the dispersion relation of quasiparticles. For $|n| \gg 1$ this approximation is not valid. Moreover we assume that spectrum of levels is infinite in both directions and that separation between levels is constant at all energies. These assumptions are also not good if $|n| \gg 1$. To fix the problem with divergence in the (199) we should subtract from (198) a thermodynamic potential of the normal (and therefore gapless) system. Spectrum of normal system is continuous and, as it is easily to see, its contribution to the thermodynamic potential equals exactly to the diverging integral in the formula (199). The remaining integrals in the Poisson formula are finite and describe only effects related to the superconductivity of the tip and surface. The straightforward

evaluation of the integrals in Eq. (199) yields for superconductivity induced thermodynamic potential $\tilde{\Omega}_A(\phi)$ relation

$$\tilde{\Omega}_A(\phi) = 4T \sum_{k=1}^{\infty} \frac{(-1)^k}{k} \frac{\cos k\phi}{\sinh(2\pi T k/\Delta_L)} \ . \tag{200}$$

Force oscillations, induced by the Andreev-Kulik level structure in a single-channel long S/N/S junction, according to formula (191), can be found by simply taking the derivative of (200). In the limit of high ($T \geq \Delta_L$) and low ($T \ll \Delta_L$) temperatures, superconductivity-induced force in one transverse mode can be written as ($|\varphi| \leq \pi$)

$$\tilde{F}_A \simeq \begin{cases} \frac{\Delta_L}{2\pi L}\left(\varphi^2 - \frac{\pi^2}{3}\right) \ , & T \ll \Delta_L \\ \\ -16\pi \frac{T^2}{L\Delta_L} \exp\left(-\frac{2\pi T}{\Delta_L}\right) \cos\varphi \ , & T \geq \Delta_L \ . \end{cases} \tag{201}$$

We focus here only on the phase-dependent part of the thermodynamic potential, $\tilde{\Omega}_A(\varphi)$, and the resulting Andreev (or, equivalently, Casimir [81]) force $\tilde{F}_A$, since, as aforementioned, the force in superconducting junctions (Eq.(201)) is added to a much larger phase-independent term ($\sim \varepsilon_F/\lambda_F$) that dominates the cohesive force in metallic NWs. In a multi-channel junction the thermodynamic potential is the sum over transverse channels (ln)

$$\tilde{\Omega} = \sum_{ln} \tilde{\Omega}_A^{(ln)}(\varphi), \tag{202}$$

where $\tilde{\Omega}_A^{(ln)}(\varphi)$ is given by Eq.(200) with $\Delta_L^{(ln)} = \hbar v_F^{(ln)}/L$ substituted for Δ_L. For a long junction the Fermi velocity enters explicitly the expression for a single channel supercurrent, and the total current in a multichannel junction strongly depends on the junction geometry [92]. As mentioned earlier, we model the normal part of a long S/N/S junction by a cylinder of length L and cross-section area $S = V/L$. The Schrödinger equation of motion of electrons in the cylindrical coordinates (ρ, ϕ, z) is

$$-\frac{\hbar^2}{2m}\left[\frac{\partial^2}{\partial\rho^2} + \frac{1}{\rho}\frac{\partial}{\partial\rho} + \frac{1}{\rho^2}\frac{\partial^2}{\partial\phi^2} + \frac{\partial^2}{\partial z^2}\right]\Psi = E\Psi \tag{203}$$

If we write $\Psi(\rho, \phi, z) = R(\rho)\Phi(\phi)Z(z)$ we can reduce the partial differential equation (203)

to a system of ordinary differential equations for the functions $R(\rho)$, $\Phi(\phi)$ and $Z(z)$:

$$\begin{cases} \frac{1}{Z(z)}\frac{d^2Z}{dz^2} = -k_z^2 \\ \frac{1}{\Phi(\phi)}\frac{d^2\Phi}{d\phi^2} = -l^2 \\ \frac{\rho^2}{R(\rho)}\frac{d^2R}{d\rho^2} + \frac{\rho}{R(\rho)}\frac{dR}{d\rho} - l^2 + \rho^2(\frac{2mE}{\hbar^2} - k_z^2) = 0 \end{cases} \tag{204}$$

where k_z and l are some constants. Due to periodic condition $\Phi(\phi + 2\pi) = \Phi(\phi)$ parameter l should be integer. Parameter k_z is the longitudinal wave vector of electrons, and l is the angular momentum of motion around z axis. Solutions of the system (204) are

$$\begin{cases} Z(z) = A_1 e^{+ik_z z} + B_1 e^{-ik_z z} \\ \Phi(\phi) = A_2 e^{+il\phi} + B_2 e^{-il\phi} \\ R(\rho) = A_3 J_l(\rho\xi) + B_3 N_l(\rho\xi)\ , \qquad \text{where } \ \xi = \sqrt{\frac{2mE}{\hbar^2} - k_z^2} \end{cases} \tag{205}$$

where J_l and N_l are Bessel and Neumann functions of l-th order. Since wave function should be finite everywhere inside the cylinder we have to take $B_3 = 0$ since $N_l \to \infty$ when $\rho \to 0$. Assuming hard-wall boundary conditions for electrons at the lateral surface of the cylinder, wave function should satisfy boundary condition $\Psi(R, \phi, z) = 0$, which in turn means that

$$R(R) = A_3 J_l\left(R\sqrt{\frac{2mE}{\hbar^2} - k_z^2}\right) = 0. \tag{206}$$

Equation (206) gives energy eigenstates of the electrons in the cylindrical contact, it can be rewritten in the explicit form

$$E_{ln} = \frac{\hbar^2\gamma_{ln}^2}{2mR^2} + \frac{\hbar^2 k_z^2}{2m} \tag{207}$$

where γ_{ln} are the Bessel function zeroes: $J_l(\gamma_{ln}) = 0$. We can use equation (207) to find the longitudinal velocities of electrons at the Fermi-level in different conducting channels. Setting in the Eq.(207) $E_{ln} = \varepsilon_F$ and rewriting kinetic term associated with motion along the axis of the cylinder as $E_z = mv_F^2/2$, we find that the longitudinal velocity of electrons at the Fermi surface in the $(ln)-$th channel is

$$v_F^{(ln)}(L) = \sqrt{2\left(\varepsilon_F - \frac{\hbar^2\pi L}{2mV}\gamma_{ln}^2\right)/m}. \tag{208}$$

The dependencies of the Andreev force on the phase difference (φ) and on the length (L) of the nanowire are displayed, respectively, in Figs. 25 and 26, where we show $\Delta F(\varphi) =$

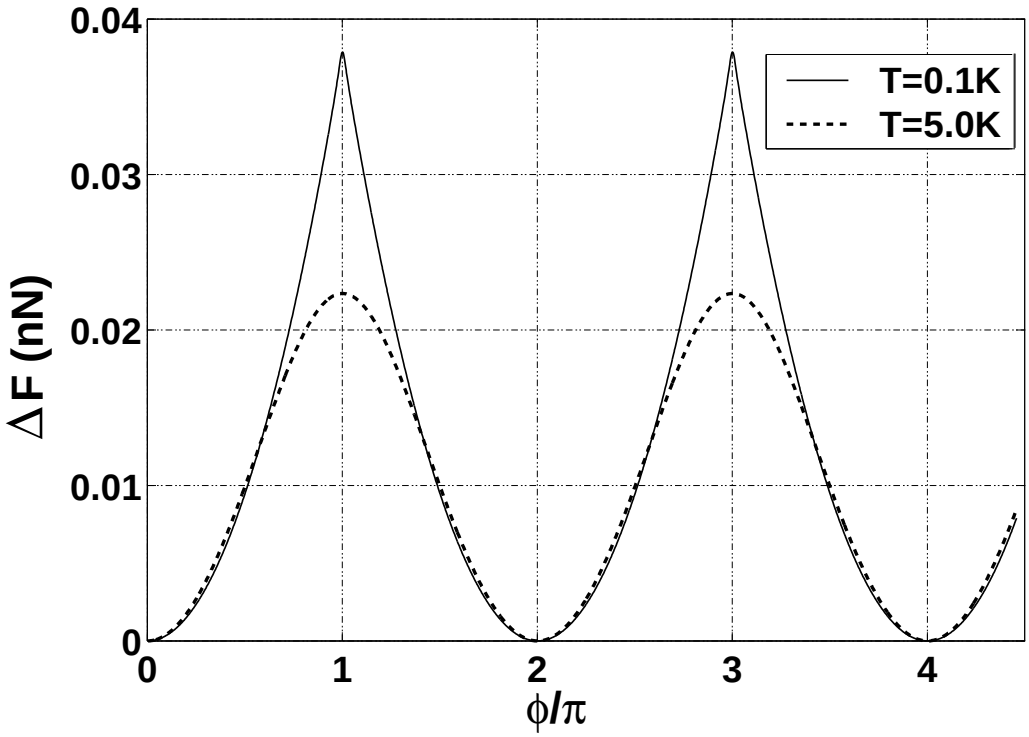

Figure 25: Force ΔF in the nanowire S/N/S junction as a function of phase difference φ. We use the physical parameters for Pb, i.e. $\varepsilon_F = 1.5 \times 10^{-11} erg$, and $v_F = 1.83 \times 10^8 cm/s$. The volume $V = 5 \times 10^{-15} cm^3$, and the length of the junction $L = 10^{-4} cm$. Results are shown for two temperatures, both below $T_c(Pb) = 7.18K$. The force was calculated as follows: first, using Eq.(198), the grand canonical potential was found for each transverse mode (each with a different $\Delta_L^{ln} = \hbar v_F^{ln}/L$, see Eq.(208)). The total potential is the sum over all the transverse modes (Eq.(202)), and its derivative with respect to L was evaluated numerically.

$F_A(\varphi) - F_A(0)$. From Fig. 26 we observe that the force is enhanced at special values of the phase difference $\varphi_r = \pi(2r+1)$, $(r = 0, \pm 1, \pm 2, ...)$. At $\varphi = \varphi_r$ one of the AK bound states coincides with the Fermi energy and, most significantly, this state is $4N_\perp$-fold degenerate [93], thus amplifying its contribution. Direct observation of the superconductivity-induced nanomechanical effect predicted here may be obtained through : (i) generation of a nanowire of length L via separation of an antiferromagnetic tip-surface contact, using a superconducting material (e.g. Pb) at $T < T_c$, followed by (ii) measurement of the force required to maintain the nanowire length (L) as a function of variations of the phase-difference across the S/N/S junction (as seen from Fig. 26 this force maximizes at $\varphi = \pi$).

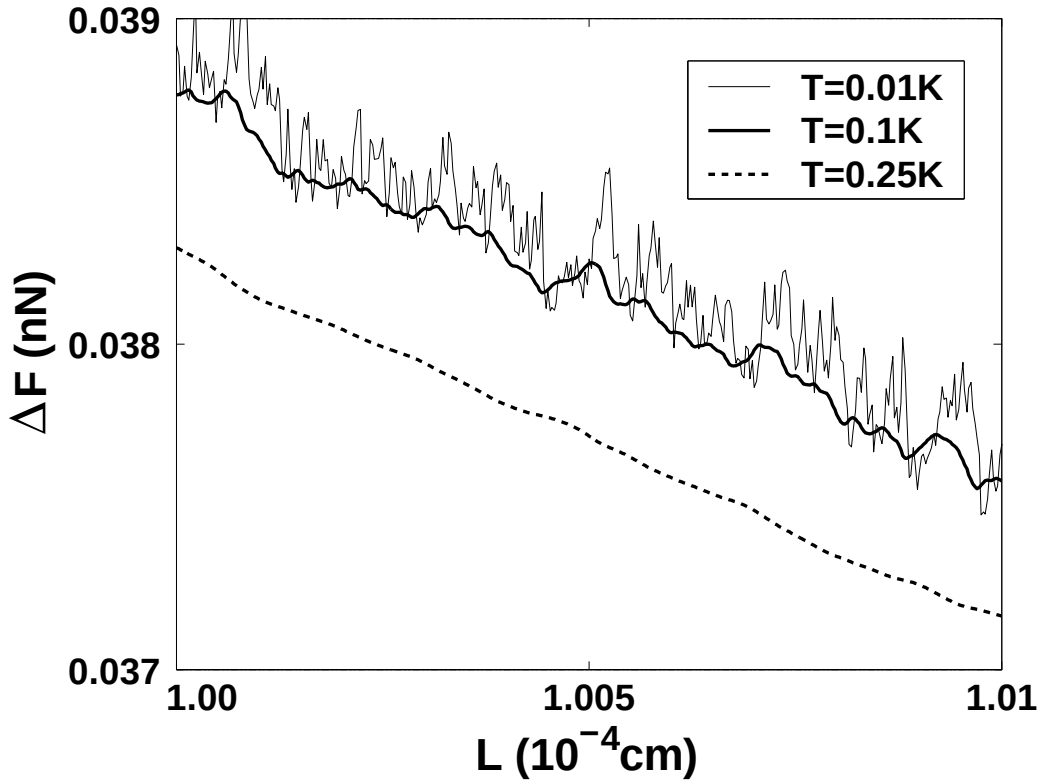

Figure 26: Force in S/N/S junction as a function of length of the junction calculated for different temperatures. The parameters of the junction and the method of calculation are as in Fig.25.

The variation of the elongation force (for $\varphi = \pi$) with the NW length is shown in Fig. 26. We note first that even though the number of open channels is very large for the NW junction shown in Fig. 26, the magnitude of the forces is significantly smaller than in the case of short junctions (see previous subsection) [2]. The aperiodic variations of the Andreev force originating from the change in the number of open channels upon elongation, are particularly pronounced at lower temperatures. Note however, that such aperiodic variations occur also for normal metal NW [76, 77] and consequently separation of the superconductivity-induced contribution may be difficult.

[2]For a long junction ($L \gg \xi_0$) with only a very small number of channels ($N_\perp \sim 1$), the force is negligibly small $\tilde{F}_A \sim \hbar v_F/L^2 \sim (\varepsilon_F/\lambda_F)(\lambda_F/L)^2$. On the other hand, for a relatively short (i.e. $L \sim 0.1\xi_0 \sim 10$ nm) ballistic NW, the SC-induced contribution to the force can become quite large. For such a NW with a diameter $2R = L$ we estimate (using the Sharvin expression $k_F^2/4\pi$, where $k_F(Pb) \sim 10^8$ cm^{-1}) that the number of channels is ~ 1500. From Eqs. (4) and (5) we obtain an AF (evaluated at $\varphi = \pi$) of 10^{-1}nN for $T = 0.1$K, and half this force for $T = 6$K.

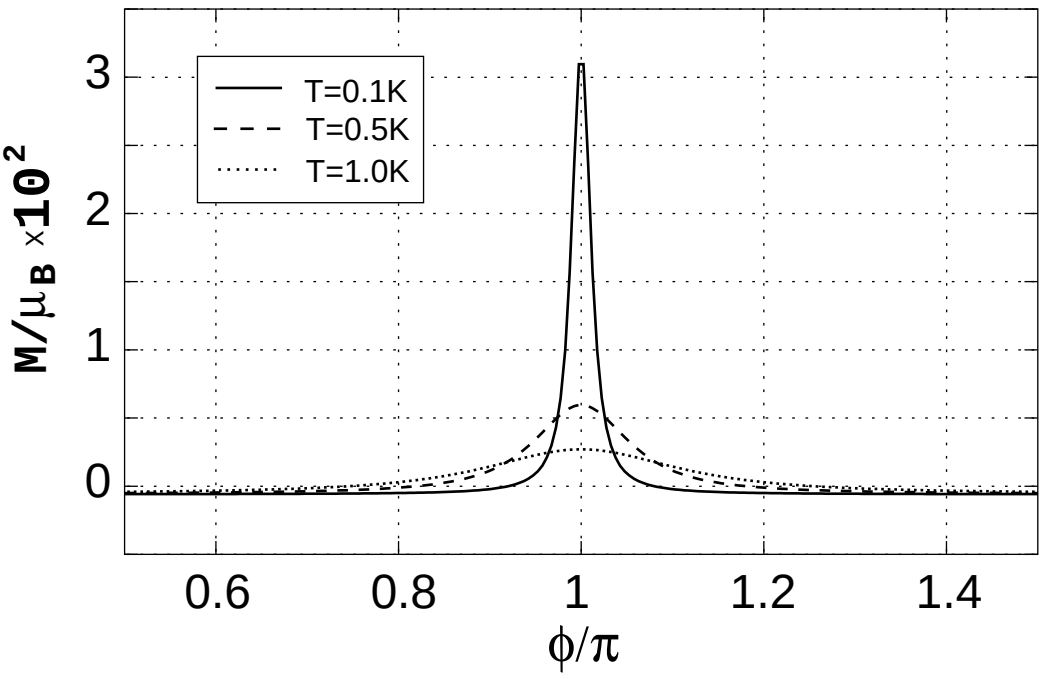

Figure 27: Magnetization of the junction in a magnetic field of 5 Oe, plotted versus the phase difference ϕ for several temperatures. The parameters of the junction are as in Fig.26. Notice that away from the resonance magnetization can become negative. This at first glance strange result is simply a consequence of our regularization procedure when we dropped the second divergent term in the equation (199). The more delicate regularization (see later) shows that there is an additional phase independent term which is equal to Pauli paramegnetizm of the sample in the normal state. In other words, this figure demonstrates only phase dependent part of magnetization.

4.6 Magnetization of S/N/S junctions in magnetic field.

Superconductivity of the bulk parts of the nanocontact influences not only its mechanical properties, but also its magnetic properties. In this section we consider a multichannel superconducting long junction in a weak magnetic field $\mu_B B \ll \Delta$ (where μ_B is the Bohr magneton), applied locally (i.e. only to the normal metal nanowire part of the S/N/S junction).

$$B(x) = \begin{cases} B, \text{ if } |x| < L/2 \\ 0, \text{ otherwize} \end{cases} .$$

These requirements are important to guarantee that the field does not create currents (or, equivalently, phase gradients) along S/N interfaces. When the magnetic field influences

both the normal and the superconducting parts of a S/N/S junction the supercurrent may be suppressed even for weak fields. Under such circumstances the AK level structure may be globally destroyed (see e.g. [94]) We totally neglect all magnetic effects due to spatial motion of electrons in the junction. The only significant influence on the Andreev-Kulik levels is through the Zeeman coupling of the electron spin $\mathbf{s}$ to the magnetic field, $H_Z = g\mu_B \mathbf{s}\cdot\mathbf{B}$ (g is the g-factor). The thermodynamic potential $\delta\Omega_A(\varphi, B) \equiv \Omega_A(\varphi, B) - \Omega_A(0, 0)$ takes the form (see. Eq.(200))

$$\delta\Omega_A(\varphi, B) = -4T \sum_{k=1}^{\infty} \frac{(-1)^k}{k} \frac{(1 - \cos k\varphi \cos k\chi)}{\sinh(2\pi kT/\Delta_L)}, \tag{209}$$

where $\chi \equiv \Delta_Z/\Delta_L$ and $\Delta_Z = g\mu_B B$ is the Zeeman energy splitting. Note that the influence of the Zeeman interaction on the thermodynamics of the S/N/S junction is equivalent to the influence of a gate voltage on the thermodynamic properties of quantum rings [91]. The magnetization $M_A = -\partial\delta\Omega_A(\varphi, B)/\partial B$ at low ($T \ll \Delta_L$) and high ($T > \Delta_L$) temperatures is given for a single channel junction as

$$M_A \simeq \begin{cases} -g\mu_B \left(\frac{\chi}{\pi}\right) \ , \quad T = 0 \ ; \ |\chi| \leq \pi, \ \ |\phi| \ll \pi \\ \\ -8g\mu_B \frac{T}{\Delta_L} e^{-\frac{2\pi T}{\Delta_L}} \cos\varphi \sin(\chi) \, , \ T \geq \Delta_L \ . \end{cases} \tag{210}$$

Note, that the superconductivity-induced magnetization M_A, can be of the order of several μ_B (if $g \gg 1$) even for a single-channel junction, and withing certain range of phases it is insensitive to the superconducting phase difference at low temperatures.

For a multichannel quantum junction at low temperatures the dependence of $M_A(\varphi)$ exhibits typical resonant behavior at the resonant phases φ_r, as shown in Fig. 27. This is a manifestation of the effect of "giant oscillations", known previously for conductance oscillations [95]. At these phases Andreev states of energies $E_A = \pm g\mu_B B$ become $2N_\perp$-fold degenerate [95], leading to giant enhancement of thermodynamic and kinetic characteristics of ballistic junctions in magnetic fields.

Since at resonance the coherent contribution ($\propto N_\perp$) of all transverse modes dominates the magnetization, we predict at low temperatures ($T \ll \Delta_Z$): (i) a giant response ($\propto N_\perp$) of an S/N/S junction to a magnetic field, and (ii) a step-like behavior of the magnetization as

a function of the wire diameter. At other values of the phase difference, different transverse channels contribute to $\delta\Omega_A$ with different periods (i.e. in general, incoherently), resulting in a complex structure of the magnetic oscillations.

In the most cases a supercurrent is suppressed by the Zeeman interaction [96]. A magnetic field would also suppress the predicted Andreev force $\delta F_A(\varphi, B) = -\partial\delta\Omega_A(\varphi, B)/\partial L$. At low temperatures ($T \ll \Delta_L$) the force (which is periodic both in the phase, φ, and in the dimensionless Zeeman energy splitting $\chi = \Delta_Z/\Delta_L$) can be written for a single-channel junction as ($|\varphi|, |\chi| \leq \pi$): $\delta F_A \simeq (\Delta_L/2\pi L)\left[(\varphi)^2 - (\chi)^2\right]$.

4.7 Magnetization of Superconductor – 2D Electron Gas – Superconductor (S/2DEG/S) contact.

In this section we consider another class of systems, which are theoretically very similar to the systems of nanoscopic S/N/S junctions considered in the previous section. We discuss mesoscopic magnetic effects in the superconductor- two-dimensional electron gas - superconductor (S/2DEG/S) structure schematically represented on the Fig.28. Such systems have been recently realized experimentally [97, 98]. Like in a three-dimensional contact, the small size of the system in its narrowest part leads to quantization of the transverse motion of electrons. For a narrow rectangular strip of a two-dimensional electron gas bridging two bulk superconductors, motion of electrons in the direction perpendicular to the surface of the 2D gas is forbidden completely, i.e. electrons are confined to zero point oscillations in that direction, whereas motion within the plane of the 2D gas, along surfaces of superconductor, is allowed but is quantized.

We assume that the properties of the 2DEG/S interface are very similar to the properties of N/S interface, namely, the electrons and holes from the two-dimensional electron gas part of the constriction, whose energies are lower than the gap in the spectrum of superconductors, cannot move into the superconductor, but are Andreev reflected. As in the case of three-dimensional S/N/S junctions we assume that electrons from different transverse modes do not mix, so that we can describe each mode within a simplified one-dimensional Bogolubov - de Gennes model. We assume that the left and right superconductors have

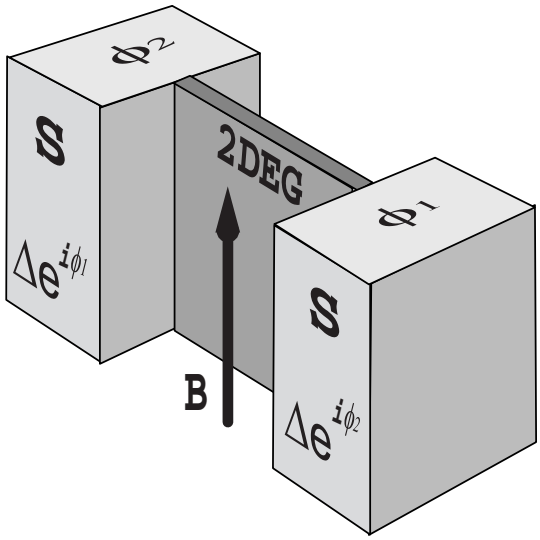

Figure 28: Scheme of the S/2DEG/S junction. Two superconductors with different phases of the order parameter connected via two-dimensional electron gas (2DEG). Magnetic field is applied locally between superconductors parallel to the plane of 2DEG and is negligibly weak near S/N interfaces. A similar system was considered in the paper [99] where effects of Zeeman splitting and spin-orbit interactions on the Josephson current was studied.

uniform order parameters of the same magnitude Δ but different phases ϕ_1 and ϕ_2 and that the order parameter inside the two-dimensional electron gas is zero.

There are, however several important differences between S/N/S and S/2DEG/S cases. First, the effective mass of electrons m_s in the superconductors can differ very much from the effective mass m_n in the two-dimensional electron gas. Second, we assume that the S/2DEG/S junction is clean and, therefore, function $U(x)$, which determines the external potential, is zero everywhere except at the interfaces. At the interfaces ($x = \pm L/2$) the difference in material structure of the superconductor and semiconductor always leads to formation of potential barriers, which can significantly affect the properties of the system and it would be incorrect to ignore them. We model these potential barriers by Dirac delta-functions of equal strength W.

$$U(x) = W(\delta(x + L/2) + \delta(x - L/2)). \tag{211}$$

Like for a 3D S/N/S contact, we assume that the magnetic field is weak ($g\mu_B B(x) \ll \Delta$, where μ_B is the Bohr magneton and g is the Lande g-factor) and acts only on the nonsuperconducting part of the junction (see Eq.209). To avoid any orbital magnetic effects

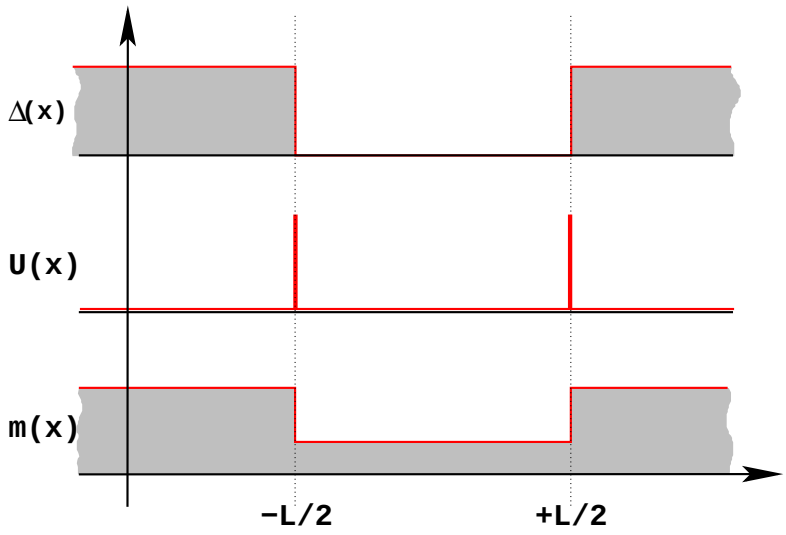

Figure 29: Model of S/2DEG/S system. As well as for three-dimensions S/N/S system, we assume that order parameter is equal to zero in 2DEG part. In the bulk superconductors order parameter is non-zero constant. We assume that absolute value of the order parameter is the same in the left and right superconductors, but phases can be different. Due to different electronic structure of superconductor and two-dimensional electron gas, effective mass of electrons in these media can be different. Effective mass of electrons in superconductors m_s is approximately equal to the free electron mass m_e, whereas in typical 2DEG it is two orders of magnitude less than m_e, for example, in heterostructure made from $InAs$ the effective mass is only $m_{2D} = 0.023m_e$. At the interface between superconductor and 2DEG one can expect presence of some potential barriers due to chemical reactions between two materials or due to features of fabrication of the contact. Potential barriers at the interfaces may also form due to difference in structure of electronic bands. We model such barriers at the interfaces by delta function potentials.

we direct the magnetic field parallel to the surface of the 2DEG.

The Andreev-Kulik levels are obtained by matching solutions of the Bogolubov - de Gennes equation for the uniform regions at the S/2DED interfaces. The result of the matching procedure for the system with barriers and with different masses of electrons in two-dimensional gas and superconductor is very cumbersome. To simplify it we will use the Andreev approximation [100, 101]. Namely, in the lowest nonvanishing order in $\max(\Delta, E)/\epsilon_F$ we make the approximation of replacing wave vectors of electrons and holes inside S and 2D parts of the junction with the Fermi wave vectors: $k_e \approx k_h \approx k_F^{(n)}$ and $q_e \approx q_h \approx k_F^{(s)}$, where $k_F^{(s)}/k_F^{(n)} = \sqrt{m_s/m_n}$. On the other hand if we have a difference of wave vectors then we should take $k_e - k_h \approx m_n\epsilon/(\hbar^2 k_F^{(n)})$ and $q_e - q_h \approx m_s\Delta/(\hbar^2 k_F^{(s)})$. In a

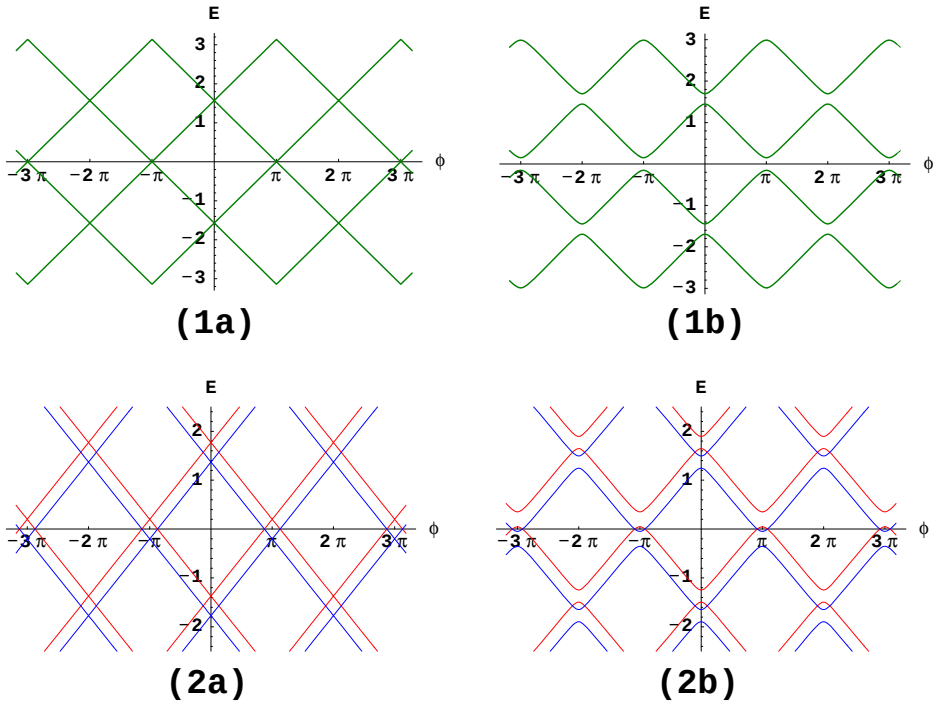

Figure 30: Andreev levels in a one-dimensional transverse mode in S/2DEG/S junction. Figure (1a) shows a spectrum of Andreev levels for long clean S/N/S junction with equal masses of electrons in the normal part and in superconductors as a function of phase difference. Figure (1b) shows Andreev levels for Josephson junction when effective masses of electrons in superconducting and in normal parts are different or when there are barriers at the interfaces. It turns out that the effect of barriers at the interfaces on the Andreev spectrum is the same as effect of different masses. Figures (2a) and (2b) show the effect of magnetic field on Andreev spectrum. Magnetic field splits levels. Red lines correspond to the levels with magnetic moment along magnetic field and blue lines - to levels with magnetic moment against the field. For a single mode magnetization is maximal when the Fermi energy is between red and blue levels.

long junction ($L \gg \xi_0 = \hbar v_F/\Delta$) the bound state energies close to the Fermi level, $\epsilon \ll \Delta$, are

$$\epsilon_{n,\sigma}^{(\pm)}(\phi) = \pi\omega_L \left(\pm\frac{\Theta}{2\pi} + n \right) + \frac{\sigma}{2} g\mu_B B, \tag{212}$$

where the new phase Θ is defined as

$$\begin{aligned} \Theta &\approx \pi - \arccos\left(\frac{R_1\cos(\phi) + R_2\cos(2Lk_F) + R_3\sin(2Lk_F)}{D_Z} \right) \\ D_Z &= \left(m_s(m_n+m_s) + 4m_n^2 Z^2\right)^2 \qquad R_1 = 4m_n m_s^3 \\ R_2 &= -\left((m_n-m_s)^2 m_s^2 + 8m_n^2(m_n-3m_s)m_s Z^2 + 16 m_n^4 Z^4\right) \end{aligned}$$

$$R_3 \;=\; 8m_n m_s Z\left((m_n - m_s)m_s + 4m_n^2 Z^2\right).$$

Here $Z = Wm/(\hbar k_F)$ is the parameter, which describes the barrier strength and $\omega_L = \hbar v_F/L$ is the energy level spacing. If the effective masses of the charge carriers in the superconducting leads and in the two-dimensional electron gas are equal, we reproduce the results obtained in Refs.[102, 103, 104]. Eq.(212) describes two sets ($\pm$) of discrete levels, labeled by integer indices $n = 0, \pm 1, \pm 2, \ldots$ and an additional index $\sigma = \pm 1$, which characterizes the splitting of the energy levels in the magnetic field. Since the scattering properties of the the interfaces are assumed to be spin-independent, spin is conserved in both Andreev and normal reflection. The magnetization of each populated Andreev-Kulik level, according to Eq.(212), is $g\mu_B/2$. Mesoscopic harmonic factors $\sin / \cos(2Lk_F)$ in Eq.(213) are associated with the interference of the incident and *normally* reflected quasiparticle waves. They appear due to strong change in the quasi-momentum of the quasiparticle at the interface in normal reflection. In a transparent S/N/S junction ($Z = 0$) with equal effective masses these oscillations are absent since in a pure Andreev reflection momentum is approximately conserved and the result (212) reduces to the Kulik spectrum (186). For a transparent S/N/S junction in zero magnetic field B Andreev-Kulik levels from two different sets ($\pm\phi$) intersect at $\phi_r = \pi + 2\pi r$ ($r = 0, \pm 1, \pm 2, \ldots$). At these special points the levels are four-fold degenerate for a single channel junction. The situation changes if the junction is not transparent. Even if the barriers are very small, levels do not intersect, they oscillate periodically with the phase difference, approaching each other at the points $\phi = \pi k$ ($k = 0, \pm 1, \pm 2$). Every Andreev level is now two-fold degenerate. In the external magnetic field Andreev-Kulik levels split and become non-degenerate. Magnetization produced by the Andreev state $n\sigma(\pm)$ of the transverse mode l is

$$M_{l,\sigma}^{(\pm)}(n) = -\frac{\mu\sigma}{1 + \exp\left(-\beta\epsilon_{l,n,\sigma}^{(\pm)}(\phi)\right)}. \tag{213}$$

Subscript l, which enters this formula, implies that transverse modes are different. The total magnetization of a *single* transverse mode is given by a sum over all Andreev states. It is useful to combine the levels with opposite directions of magnetic moment in pairs, $M_l^{(\pm)}(n) = M_{l,+1}^{(\pm)}(n) + M_{l,-1}^{(\pm)}(n)$ and then sum up pair contributions $M_l^{(\pm)}(n)$ over the

index n using the Poisson summation formula

$$\sum_{n=-\infty}^{+\infty} M_l^{(\pm)}(n) = \int_{-\infty}^{\infty} M_l^{(\pm)}(\nu)d\nu + 2\mathrm{Re}\sum_{k=1}^{+\infty}\int_{-\infty}^{\infty} M_l^{(\pm)}(\nu)e^{2\pi ik\nu}d\nu. \tag{214}$$

Such ordering guarantees convergence of the first and the second term in (214). The total magnetization of the single transverse mode is [105]

$$M_l = \frac{g^2\mu_B^2 B}{\pi\omega_L} + \frac{4Tg\mu_B}{\omega_L}\sum_{k=1}^{\infty}\frac{\cos(k\Theta)\sin(k\chi)}{\sinh\left(2\pi kT/\omega_L\right)}, \tag{215}$$

where $\chi = g\mu_B B/\omega_L$. The first term in Eq.(215) does not depend on the phase difference or the temperature. This term describes Pauli magnetization of the junction. It remains the same even if the tip and the surface become nonsuperconducting. It is the second term which gives oscillations of magnetization. At high temperatures ($T \gg \omega_L$) when the Fermi distribution is smeared over many Andreev levels the amplitude of these oscillations is small in comparison with the first term in (215). The sum in Eq. (215) can be truncated at $k = 1$ so that magnetization of each transverse mode oscillates as $A\cos(\Theta)$ with the amplitude $A = (4g^2\mu^2 BT/\omega_L^2)\exp\left(-2\pi T/\omega_L\right)$.

In the opposite limiting case, at low temperatures ($T < g\mu_B B$), only a small number of states near the Fermi energy contribute to the magnetization. Andreev levels can be shifted by changing the phase difference ϕ between superconductors. At certain values of the phase difference some Andreev states approach very close to the Fermi energy. At these phase differences the magnetization of the junction is maximal.

Taking into account only one pair of states which is the closest (at the given $\phi = \phi_r$) to the Fermi energy and neglecting the contribution of the other states we can approximate the previous formula by a simple expression

$$M_l^{(osc)} \approx +\frac{g\mu_B}{\exp\left(\frac{\omega_L}{2T}\Theta - \frac{g\mu_B}{2T}B\right)+1} - \frac{g\mu_B}{\exp\left(\frac{\omega_L}{2T}\Theta + \frac{g\mu_B}{2T}B\right)+1} \tag{216}$$

where angle Θ is defined by Eq.(213). The same result can be achieved if we use the Euler-Maclaurin summation formula to approximate Eq. (215) in the vicinity of the points $\phi_r = \pi(1+2r)$.

Like in the case of 3D contacts, in order to get the total magnetization of the system we have to sum up contributions of all open transverse modes (channels). The channel is open

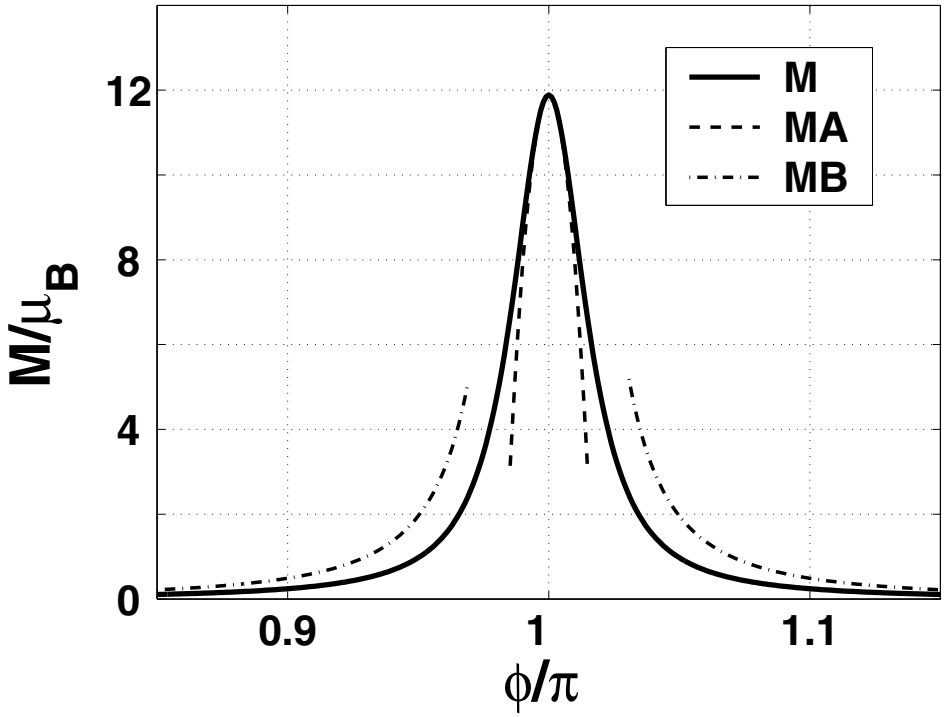

Figure 31: Magnetization of the transparent ($Z = 0$) S/2DEG/S junction with harmonic lateral confining potential in magnetic field $B = 10\,Oe$ as a function of phase difference plotted together with its asymptotes MA (Eq. 220) and MB (Eq. 221). For the demonstration we choose the materials with the same effective masses We assume that superconductors are made from niobium, therefore the Fermi energy is $\epsilon_F(Nb) = 8.52 \times 10^{-12} erg$, effective masses $m^S_{eff} = m^N_{eff}$, length of the 2DEG part of the junction is $L = 10^{-4} cm$, and width $d = 6 \times 10^{-5} cm$. Results are shown for temperature $T = 0.1K$, which is much below the critical temperature of niobium $T_c(Nb) = 9.2K$. Notice that resonance peaks are extremely narrow, their width $\delta\phi \sim g\mu_B B/\omega_L$ is approximately equal to the phase change necessary to shift the spectrum of Andreev levels on the value of Zeeman splitting.

if the energy of its lowest longitudinal mode is smaller than the Fermi energy of the superconducting leads it is connected to. Since barriers at the S/2DEG interfaces are assumed small, the motion in the longitudinal direction is almost unperturbed (the realistic case for junctions fabricated in $InGaAs$ heterostructures with Nb electrodes [97]). Confinement in the lateral direction is usually produced by the electrostatic potential generated by gate electrodes etched on the surface of the heterostructure.

We provide results for two simple models of the confining potential: *i*) hard wall potential and *ii*) parabolic potential. For more accurate description one needs to solve Schrödinger and Poisson equations consistently as described in works [106] and [107].

For hard wall boundary conditions, we can write velocity of electrons and holes with energies near the Fermi energy in the lth channel in the form

$$v_l = \sqrt{\frac{2}{m_n}\left(\epsilon_F - \frac{1}{2m_n}\left(\frac{\hbar\pi l}{d}\right)^2\right)}. \tag{217}$$

The velocities of quasiparticles in a multichannel junction with parabolic confinement $U(y) = m\Omega_\perp^2 y^2/2$ are

$$v_l = \sqrt{\frac{2}{m_e}\left(\epsilon_F - \hbar\Omega_\perp\left(l + \frac{1}{2}\right)\right)}, \tag{218}$$

where lateral frequency $\Omega_\perp = \sqrt{8\epsilon_F/(m_n d^2)}$ is chosen such that $U(y = \pm d/2) = \epsilon_F$.

The separation between Andreev levels $\omega = \omega_l = \hbar v_F^{(l)}/L$ is different for different transverse modes. If the 2DEG junction is wide, the number of the transverse modes is large, we can replace the summation over the modes by integration and write the magnetization of the S/2DEG/S junction as

$$M \approx N_\perp g\mu_B \int_0^1 D(\xi, \alpha, \beta)\lambda(\xi)d\xi \ . \tag{219}$$

Here function $D(\xi, \alpha, \beta) = f(\alpha\xi - \beta) - f(\alpha\xi + \beta)$ is the difference between occupation of two states with opposite momenta, $f(\eta) = 1/(e^\eta + 1)$ is the Fermi distribution and $\alpha = \hbar v_F\Theta/(2LT)$, $\beta = g\mu_B B/(2T)$. Weight function $\lambda(\xi)$ is equal to 2ξ for a "soft wall" potential and to $\xi/\sqrt{1-\xi^2}$ for "hard wall" potential.

The integral in the right hand side of the Eq. (219) unfortunately cannot be calculated analytically, but we can find an asymptotic behavior of magnetization at several different values of the phase difference ϕ. In the vicinity of the resonance points ϕ_r where $\Theta \ll LT/(\hbar v_F)$, magnetization is the highest, and is approximately equal to

$$M \approx N_\perp g\mu_B \tanh\left(g\mu_B B/4T\right)\left[1 - \frac{C_1}{12}\left(\frac{\Theta\hbar v_F}{LT}\right)^2 \mathrm{sech}^2\left(g\mu_B B/4T\right)\right] \tag{220}$$

The constant C_1 is equal to 1/2 in the 'hard walls' potential and to 2/3 in the 'soft walls' potential. On the other hand, if the phase is far away from the resonance ($\Theta \gg LT/(\hbar v_F)$) magnetization slowly approaches to

$$M \approx C_2 N_\perp g^2\mu_B^2 BT\left(\frac{2L}{\hbar v_F\Theta}\right)^2 \ln 2 \tag{221}$$

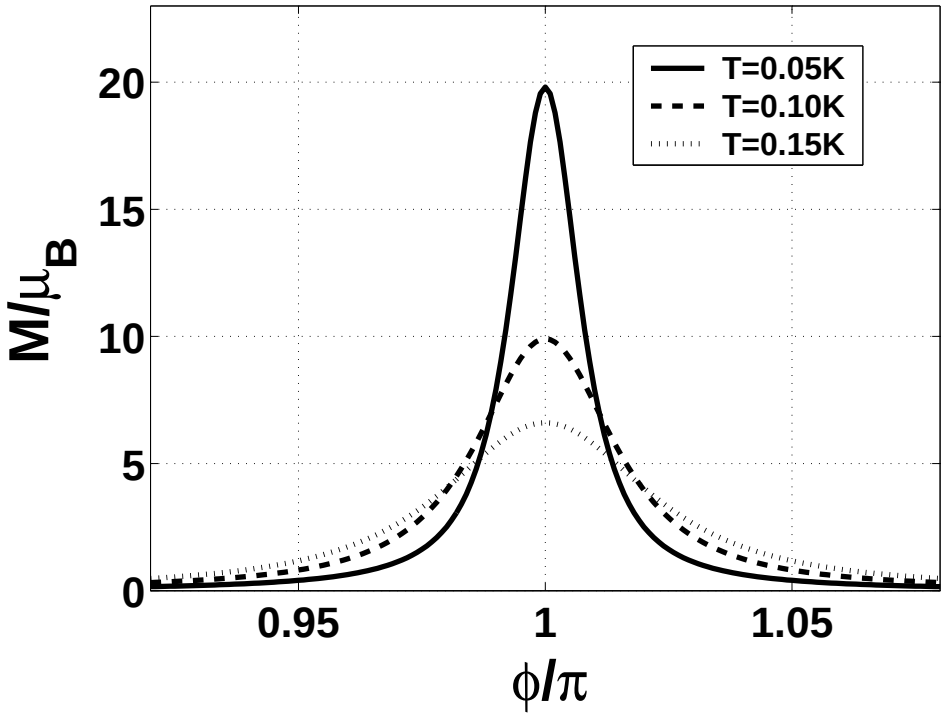

Figure 32: Magnetization of the transparent S/2DEG/S junction in a magnetic field $B = 10Oe$ at several temperatures plotted versus phase difference. Width of the junction $d = 5 \times 10^{-5} cm$. All other parameters of the junction are as in Fig.31

In Fig.31 we show the result of numerical calculation for the total magnetization as a function of the phase difference and compare this numerical result with the asymptotic behavior in Eqs.(220) and (221). Fig. 32 shows behavior of the magnetization at several different temperatures. Higher temperatures lead to smearing of the Fermi distribution and the resonance peaks become smaller and broader. Since in the transparent clean junction condition for resonance $\phi = \phi_r$ is the same for all transverse modes, magnetization at the resonances is proportional to the number of transverse modes. This effect is analogous to giant oscillations of conductance considered in Ref. [108]. Therefore, the wider the junction, the larger heights of the peaks at the resonances. This behavior is illustrated in Fig. 33. On the other hand, if we vary length of the junction, it will affect only width of the peaks, whereas height of the peaks will remain unchanged (see Fig. 34).

If the junction is not transparent, electrons and holes incident on the surface may be

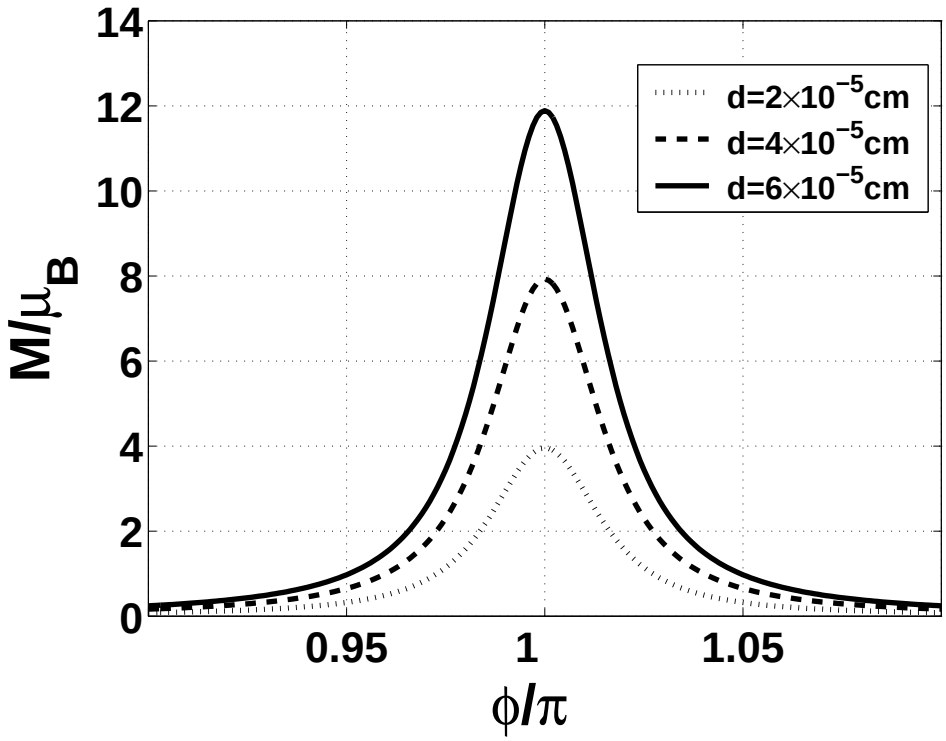

Figure 33: Magnetization as a function of the width of 2DEG part of transparent S/2DEG/S junction. Length of the junction $L = 10^{-4}cm$. Temperature $T = 0.1K$. Strength of the magnetic field and all other parameters are the same as for Fig.31.

reflected normally from a S/2DEG interface. This processes modifies the spectrum of Andreev levels. Andreev levels do not intersect and do not cross the Fermi energy at any value of the phase ϕ. As a consequence, the amplitude of the magnetization peaks decreases. Difference in the effective masses of the 2DEG and superconductors has similar effect on magnetization as the presence of barriers at the interfaces. Namely, due to mismatch of the Fermi velocities, some of electrons are being normally reflected the 2DEG/S surface. The larger the difference between effective masses, the larger the fraction of all incident electrons that are reflected from the interfaces normally.

In the clean S/2DEG/S or S/N/S junction every Andreev reflected electron, picks up an additional phase $\delta\phi = \pm\phi_{1,2} + \arccos(E/\Delta)$ at the interface, whereas normal electrons do not pick up such phase. Reflected electron-hole wave function is a mixture of Andreev and normally reflected electrons and holes. Resonance conditions for this mixture are different

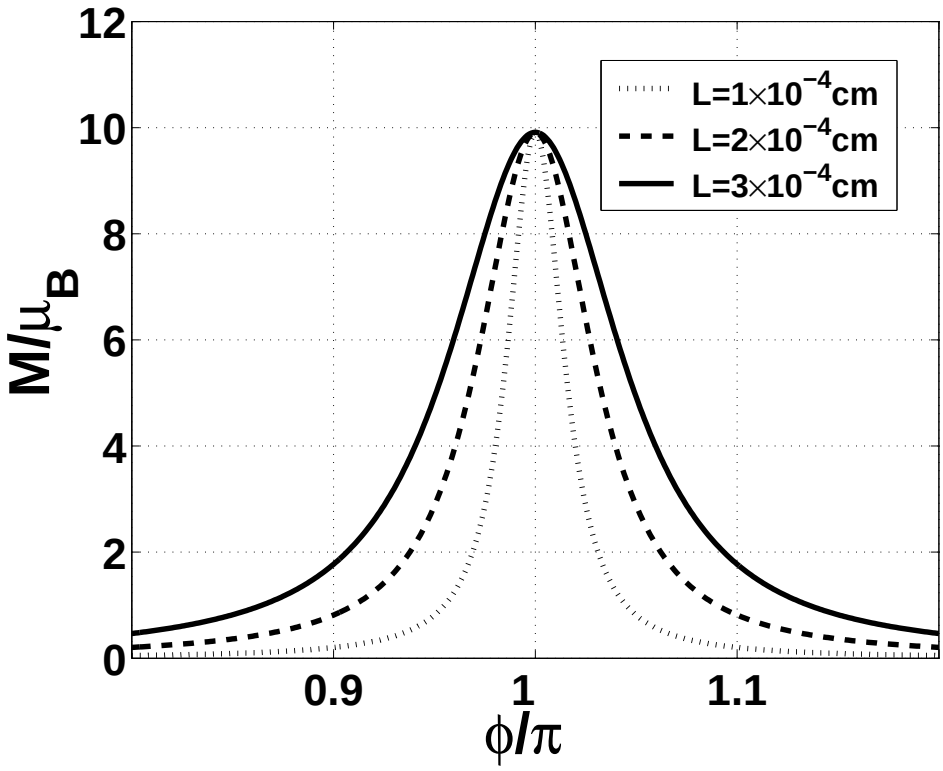

Figure 34: Magnetization of the transparent S/2DEG/S junction versus phase difference ϕ for different lengths of the 2DEG part. Width of the junction is $d = 5{\times}10^{-5}cm$, temperature $T = 0.1K$ and magnetic field $B = 10Oe$.

from resonance conditions for wave functions in the clean S/2DEG/S junction, where only Andreev reflection can occur. Resonance conditions in the junction with barriers or with different effective masses depend not only on the phase difference, but also on the length of the junction. Although it is always possible to achieve resonance for one channel, since different transverse channels have different longitudinal velocities, it is difficult to satisfy resonance conditions for many channels at once. Resonant peaks for magnetization of each single channel are very narrow; the majority of the channels are off resonance even for small barriers or slightly different materials. As a result total magnetization of the junction in both cases of barriers and different masses is strongly suppressed. Therefore, for observation of strong resonance we recommend the use of materials with close effective masses.

Magnetization, as well as superconducting current in a S/2DEG/S junction, is a result of difference in the population of different Andreev levels. Josephson current through the

junction is possible only when energy levels of two sets ($dE_n/d\phi > 0$ and $dE_n/d\phi < 0$) are unequally populated. Similarly, magnetization of the S/2DEG/S junction is a result of different population of the states with opposite directions of magnetic moments. Magnetization is more sensitive to the barriers and mass differences than Josephson current. The explanation to this high sensitivity is the following. Since we are constrained to use weak external magnetic fields to avoid destruction of superconductivity, Zeeman splitting of Andreev levels is small ($\mu_B B = \Delta_Z \ll \omega_L$); in this situation impurities, barriers or mass difference that modify the spectrum of Andreev levels can move them away from the region ($\sim T$) where gradient of the Fermi distribution is high. Even small shift Δ_b of energy levels from the Fermi level may result in the situation $T \ll \Delta_Z \ll \Delta_b$ when both levels with opposite direction of magnetic moment are almost equally populated, giving together small magnetization $M_l \ll \mu_B$. This situation does not happen with levels that belong to different sets. These levels are well separated $\sim \Delta_L$ and small change $\Delta_b \ll \Delta_L$ in their position cannot significantly affect their population.

4.8 Summary

In summary, we considered mechanical and magnetic effects in the ballistic small junctions formed in scanning tunneling microscope experiments where tip and surface are in a superconducting state and in the similar systems of two-dimensional electron gas connecting two superconductors. We predicted and illustrated that superconductivity induces in quantum wires phase-dependent forces and magnetic response correlated with the supercurrent. At special values $\phi_r = \pi + 2\pi r$ of the phase difference $\phi = \phi_1 - \phi_2$ of the order parameter between two superconductors, force and magnetization become maximal.

The superconductivity induced forces and magnetization for any single transverse mode of the junctions are very small, but since for *transparent* junctions the resonance conditions are identical for all transverse modes, the magnetization and total force of the junction at resonances at low temperatures is proportional to the number of transverse modes and, if the the number of transverse modes is big, the total magnetization of the junction will be large enough to be detected in experiments.

CHAPTER V

AHARONOV-BOHM EFFECT AND PLASMA OSCILLATIONS IN SUPERCONDUCTING TUBES AND RINGS

5.1 Introduction.

In this part of the thesis we consider collective excitations of charge density, so called plasma oscillations, in the small low-dimensional multiply connected superconducting structures in a magnetic field. More precisely, we consider two similar types of systems: *i*) an infinitely long thin superconducting cylinder and *ii*) thin superconducting ring (see Fig.35). By varying the parameters of the cylinder and the ring we expect to recover results for simpler cases - plasma oscillations in a thin infinite superconducting thread and plasma oscillations in a thin superconducting plane, (these cases have been studied earlier in [109]) . For example, by increasing the radius of the thin-walled superconducting cylinder the curvature of its walls decreases and if the wavelength of the excitations is much smaller than radius of the cylinder, the cylinder starts to behave like a flat superconducting 2D plane. On the other hand, if one decreases the radius of the cylinder, making it smaller than the wavelength of the collective excitation, the cylinder behaves like a 1D thread. We are studying the possibility to observe both 1D and 2D regimes for the same sample. Similarly with the ring - it can be transformed into the infinite straight wire by increasing its radius to infinity. Therefore the result that we get can be considered as generalizations of the results achieved in [109].

The cylinder and ring geometries are also interesting to us because they allow us to study the Aharonov-Bohm effect [110] for collective excitations in quasi-low-dimensional superconductors. The Aharonov-Bohm effect was studied previously for various collective

excitations in different kinds of small rings and tubes. For the normal rings, the Aharonov-Bohm effect usually manifests itself in periodic dependence of the transmission coefficient for an electron traversing the ring on the magnetic flux Φ through the ring and in such effects as persistent current in the normal rings and in quantization of magnetic flux through the ring. The period of oscillations in the clean normal rings and cylinders is equal to hc/e [111]. For the dirty (with impurities) rings and cylinders, the situation is more complicated. Due to the *weak localization* effects [112, 113], the period of Aharonov-Bohm oscillations in the dirty cylinder is $hc/2e$.

For the dirty rings, the period of the Aharonov-Bohm effect depends on the parameters of the ring, but in general, for moderately resistive mesoscopic rings one can observe both periods hc/e and $hc/2e$ (with different amplitudes) [113, 114, 115].

The Aharonov-Bohm effect can also be found in the semiconductors with a hopping conductivity mechanism. Even more amazing is that the Aharonov-Bohm effect can be observed for the neutral collective excitations such as electron-hole pairs (excitons) [116, 117] or for the systems without free carriers such as Pierls dielectrics [118] where collective excitations are the charge density waves (instantons) [119]. In this work we study the Aharonov-Bohm effect for the acoustic plasmons in the thin superconducting wires and thin superconducting films.

5.2 Collective excitations in superconductors.

There are two types of collective excitations that can exist in superconductors. The first type is so-called Carlson-Goldman mode [120]. In this mode the superconductor current oscillations are balanced by the current of normal electrons and the charge densities produced by superconducting and normal electrons are mutually compensated. This mode can exist only at temperatures that are very close to a critical temperature; at lower temperatures it is damped due to Ohmic dissipation of normal electrons. The other type of collective excitations are plasma oscillations which are very similar to the plasma oscillations in the normal metals. It is necessary to say, however, that unlike in the case of the normal metals, such plasma excitations cannot exist in the bulk samples of superconductors because

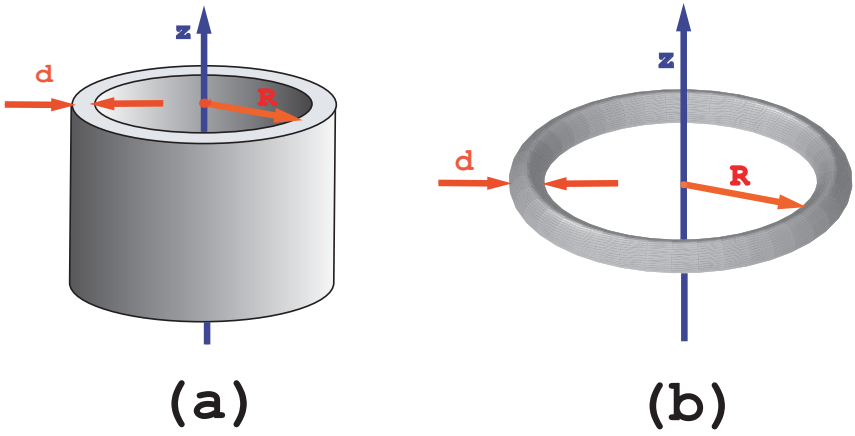

Figure 35: Superconducting cylinder and ring. We assume that width of the cylindrical shell and diameter of the wire of the ring are thin $d \ll R$ and $d \ll \xi_0$ where ξ_0 is the correlation length of the superconductor.

typical frequencies of plasma oscillations in the bulk, $10^{16}\ Hz$, are far above the superconducting gap Δ ($\sim 10^{10} - 10^{11}\ Hz$). However, in small systems like superconducting wires, thin films and tubes, Coulomb interaction (which is responsible for high frequencies in the bulk) is not so efficient and the dispersion relation for plasma excitations has sound-like (acoustic) character. These excitations are very similar to acoustic plasma excitations in the normal (non-superconducting) films [121, 122] and in graphene structures such as carbon nanotubes and fullerenes (see [123, 124]), the only difference between these plasma oscillations and plasma oscillations in superconductors is that oscillations in superconductors are the oscillations of condensate. In what follows we will consider only acoustic type of plasma excitations which have frequencies below the gap ($\omega < k_B\Delta/\hbar \sim k_B\sqrt{T_c}$). The existence of such (acoustic) plasmons in superconductors was predicted theoretically by I.O. Kulik [109]. In his work he considered plasma excitations in the thin infinite filament and plasma excitations in the infinite plane. For these two geometries he found that the dispersion relation for the filament is linear function of wave vector k along the wire ($\omega \sim k$) whereas for the infinite plane frequency of plasmons is proportional to the square root of the wave vector ($\omega \sim \sqrt{k}$) His predictions were verified later in a series of experiments (see,

for example, [125, 126]). The method, used by Kulik to describe superconducting thread and superconducting plane is based on the Ginzburg Landau theory - a phenomenological theory of superconductivity, which he modified to take into account Ohmic disipation due to oscillations of normal electrons. In our work we use the same phenomenological approach.

In the next chapter I note some important relations from the macroscopic theory of superconductivity and rederive the formula for supercurrent in the thin superconducting film. This formula will be important for us later.

5.3 Ginzburg-Landau Theory. Current in thin superconducting film or thin superconducting wire.

Superconducting state of the cylinder and the ring can be described within Ginzburg-Landau theory (see e.g. [82, 127]), which is probably the most popular phenomenological theory for superconductors. In the heart of this theory lies an expression for the superconductor free energy density in terms of the order parameter ψ:

$$f_S(\mathbf{r},T) = f_N(\mathbf{r},T) + a|\psi(\mathbf{r})|^2 + \frac{b}{2}|\psi(\mathbf{r})|^4 + \frac{1}{2m}\left|\left(-i\hbar\nabla - \frac{2e}{c}\mathbf{A}\right)\right|^2 + \frac{H^2}{8\pi} \qquad (222)$$

Minimizing the total free energy $F_s = \int d^3r f_S$ with respect to the order parameter ψ and with respect to vector potential $\mathbf{A}$, we obtain two relations. The first relation is called Ginzburg-Landau equation

$$\frac{1}{2m}\left(-i\hbar\nabla - \frac{2e}{c}\mathbf{A}\right)\psi + a\psi + b|\psi|^2\psi = 0\ . \qquad (223)$$

Solution of this equation gives order parameter ψ. And the second equation is the expression for superconducting current density

$$\mathbf{j} = -i\frac{e\hbar}{m}\left(\psi^*\nabla\psi - \psi\nabla\psi^*\right) - \frac{4e^2}{mc}|\psi|^2\mathbf{A} \qquad (224)$$

These equations became an extremely powerful tool in the macroscopic theory of superconductivity. Ginzburg - Landau theory predicts existence of two characteristic lengths in a superconductor - the coherence length ξ and the magnetic field penetration depth λ. The coherence length $\xi = \sqrt{\hbar^2/(2m|a|)}$ is approximately equal to the spatial extent of Cooper pairs in the superconductor and is a characteristic length over which density of Cooper

pairs changes in space. The magnetic penetration depth $\lambda = \sqrt{\frac{mb}{4e^2|a|}}$ is the characteristic distance of exponential decay of magnetic field inside the superconductor due to the Meissner effect. Both coherence length and magnetic penetration depth are much larger than any microscopic lengths in a superconductor. For example, for aluminum $\xi \approx 1600\ nm$ and $\lambda \approx 16\ nm$, whereas for niobium $\xi \approx 38\ nm$ and $\lambda \approx 39\ nm$, in both cases these lengths are much larger than the crystal lattice constant $\sim 0.1\ nm$. It is therefore experimentally possible to lower the effective dimensionality of the superconducting system from 3D to 2D or to 1D by reducing its size d in one or two dimensions till it becomes smaller than the coherence length and penetration depth.

Let us consider a thin superconducting film. Let us assume that the width of the film is much smaller than coherence length ($d \ll \xi$) and is much smaller than London penetration depth ($d \ll \lambda$). For such a film amplitude of the order parameter is constant in the direction perpendicular to the surface. Thus the order parameter can be written in the form

$$\psi = |\psi| e^{i\phi(r)} \tag{225}$$

where amplitude $|\psi|$ is constant. Substituting (225) into equation (224) we get the expression that connects superconducting current to velocity of condensate electrons (Cooper pairs)

$$\mathbf{j} = 2e|\psi|^2 \mathbf{v} \qquad \text{where} \qquad \mathbf{v} = \frac{1}{m}\left(\hbar\nabla\phi - \frac{2e}{c}\mathbf{A}\right) \tag{226}$$

similarly one can get the expression for free energy density

$$f_S = f_N + |\psi|^2\left(a + \frac{b}{2}|\psi|^2 + \frac{1}{2}mv^2\right) + \frac{H^2}{8\pi}\ . \tag{227}$$

which after minimization gives expression for order parameter

$$|\psi|^2 = -\frac{1}{b}(a + \frac{m}{2}v^2) \tag{228}$$

The uniform solution of Ginzburg-Landau equation for the case when magnetic fields and currents are absent is $\psi_0^2 = -a/b$ and from definition of the Ginzburg-Landau coherence length $\xi = \hbar/\sqrt{2ma}$, the expression for current in the thin film becomes

$$\mathbf{j} = e|\psi_0|^2\left(1 - \left(\frac{\xi m\mathbf{v}}{\hbar}\right)^2\right)\mathbf{v} \tag{229}$$

The current is linearly proportional to velocity at small velocities, but at higher velocities Cooper pairs start to dissociate spontaneously into quasi-particles and this will decrease supercurrent. The maximum current v_m can be found from the requirement $\partial j_s(v)/\partial v = 0$, and is equal to $v_m = \hbar/\sqrt{3}\xi m$. At higher velocities the order parameter and, therefore, supercurrent become zero.

5.4 Dissipation of energy by normal electrons.

To describe superconductivity we can adopt a very simple two-fluid phenomenological model. This model divides the electrons of a superconductor into two groups: some of the electrons are called "superconducting electrons", others - "normal electrons". Superconducting electrons move without any dissipation of energy, whereas normal electrons interact with impurities inside material and dissipate energy. The parameter that characterizes dissipation of normal electrons is τ - the average time between inelastic collisions of a normal electron in a superconductor. Unless this collision time is very small there is no significant difference between normal and superconducting electrons since both superconducting and normal electrons contribute to the electron density. On the other hand, if collision times are small ($\omega\tau \ll 1$) the normal carriers almost do not participate in the plasma oscillations. In the intermediate regime, when the collision times are neither too small nor too large the total current in the thin superconducting film or thin superconducting thread is the sum of the current created by superconducting electrons and the current created by the normal electrons [109]:

$$\mathbf{j} = eN_s\mathbf{v}\left(1 - \frac{v^2}{v_c^2}\right) + \sigma_n\mathbf{E} \tag{230}$$

The first term in this expression describes supercurrent, whereas the second term describes current due to normal electrons. The second term is responsible for all dissipation in our system and the higher the normal conductivity σ, the more dissipation of the energy of the plasma oscillations occur. This initially odd looking result can be explained qualitatively by the following arguments: in the situation when collision time is small the coherent motion in a plasma wave is created by superconducting electrons, whereas normal electrons are only partly involved in this motion and the sooner they are brought into equilibrium by

collisions, the better they follow the motion of other electrons in the plasma wave, and, as a result, the system evolves more adiabatically with less dissipation.

The two-fluid model, though simple and physically clear, describes superconductor very qualitatively. Phenomenologically introduced concentration of superconducting electrons N_s and conductivity due to normal electrons σ do not tell us how to calculate their temperature and frequency dependence. Quantitatively the two-fluid model is rather unsatisfactory for evaluation of the dissipation in the superconductor. In what follows we consider very dirty materials, we totally neglect the normal conductivity, i.e. we will neglect all dissipation in the system.

5.5 Aharonov Bohm effect.

Aharonov-Bohm effect is a quantum-mechanical phenomenon which can be observed in various multiply connected systems. This is the phenomenon when a charged particle is affected by electromagnetic fields in regions where these fields are zero [110]. Due to requirement of gauge invariance for the electromagnetic field, the wave function of the charged particle acquires a phase shift when traveling in the regions of space with nonzero vector potential, even if the associated field strengths are zero in those regions. The effect

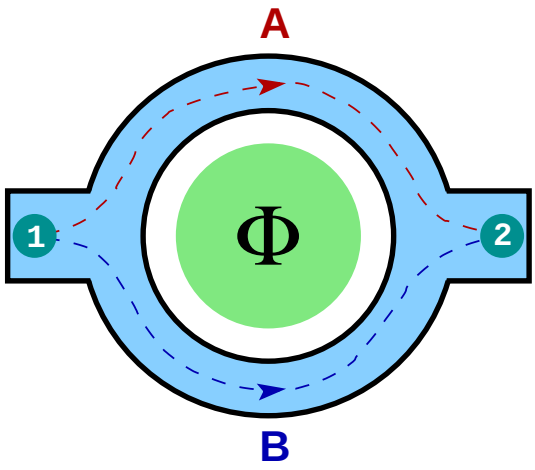

Figure 36: Aharonov-Bohm effect. Although electrons move in the space where magnetic field is zero, they feel the presence of the magnetic flux via vector potential that affects phases of the wave functions of the electrons, changing conditions for the interference of waves going along different paths.

is usually demonstrated on the system where electrons propagate from point 1 to point 2 along different paths in the ring-shaped waveguide (e.g. mesoscopic metallic ring) with magnetic solenoid with flux Φ, inserted in the hole (see Fig.36). There is no magnetic or electrical field that can affect the motion of the electrons in the classical way, nevertheless conductance of the system shows fluctuations with the total magnetic flux through the hole. The reason for these fluctuations is the following. The electrons moving along the path A and path B (see Fig.36), accumulate phases

$$\phi_A = \frac{e}{\hbar}\int_A \mathbf{A}\cdot d\mathbf{x} \qquad \text{and} \qquad \phi_B = \frac{e}{\hbar}\int_B \mathbf{A}\cdot d\mathbf{x} \tag{231}$$

Conductance of the system between points 1 and 2 is proportional to the probability of electron transmission from point 1 to point 2 which equals to the square of the absolute value of sum of amplitudes of electron propagation along paths A and B

$$|\psi(2)|^2 = |\psi_A(2)+\psi_B(2)|^2 = |\chi_A|^2 + |\chi_B|^2 + 2\mathrm{Re}\left[\chi_A\chi_B^* e^{i(\phi_A-\phi_B)}\right] \tag{232}$$

where amplitudes

$$\chi_A = \psi(1)\exp\left(\frac{i}{\hbar}\int_A \mathbf{p}d\mathbf{x}\right) \qquad \text{and} \qquad \chi_B = \psi(1)\exp\left(\frac{i}{\hbar}\int_B \mathbf{p}d\mathbf{x}\right) \tag{233}$$

correspond to phase shifts in the absence of the magnetic flux through the hole of the ring. The interference term in the Eq.(232) can be rewritten in the form

$$P_I = 2\mathrm{Re}\left[\chi_A\chi_B^*\exp\left(i\frac{e}{\hbar}\oint \mathbf{A}\cdot d\mathbf{x}\right)\right] = 2\mathrm{Re}\left[\chi_A\chi_B^*\exp\left(i\pi\frac{\Phi}{\Phi_0}\right)\right] \ . \tag{234}$$

From this equation we see that the transition probability depends on the magnetic flux through the hole of the waveguide despite the fact that electrons never enter the region with magnetic field. As follows from the formula (234), the period of oscillations is $\Phi = 2\Phi_0 = hc/e$. In other systems it can be different. In particular, it turns out that for superconducting cylinders or rings, the period of oscillations is equal to Φ_0.

5.6 Aharonov-Bohm effect in superconductors. Quantization of flux, and quantization of fluxoid. Little-Parks Effect.

Due to the fact that electrons in superconductors couple and form Copper pairs with total charge $2e$, the Aharonov-Bohm effect in a superconductor has two times smaller period than

that in the normal metal. Here we want to mention two very famous effects in superconductors that are related to the Aharonov-Bohm effect. One of these effects is quantization of magnetic flux and the other is the quantization of fluxoid [127, 82].

Quantization of flux can be observed in superconducting rings or cylinders with width of the walls or diameter of cross section large enough ($d \gg \lambda$) to screen external magnetic field. Deep inside the superconductor, the amplitude $|\psi|$ of the order parameter is constant. If we integrate the velocity vector of superconducting electrons $\mathbf{v} = \frac{1}{m}(\hbar\nabla\theta - \frac{2e}{c}\mathbf{A})$, which is proportional to the superconducting current, over the contour which goes inside the superconductor and never approaches close to the surface, we will get zero, since the superconducting current in the bulk of superconductor far from the surface is zero. One can write this mathematically as

$$\oint \left(\hbar\nabla\theta - \frac{2e}{c}\mathbf{A}\right) d\mathbf{x} = 0 \tag{235}$$

or, equivalently,

$$\Phi = \frac{\hbar c}{2e}[\theta] = \Phi_0\ 2\pi n \tag{236}$$

where $[\theta]$ is the total increment of the phase of the order parameter on the contour around the hole. Since order parameter $\psi(\mathbf{x})$ is a single-valued function of coordinate, the total increment of phase should be equal to $[\theta] = 2\pi n$, $n = 0, \pm 1, \pm 2, \ldots$. Equation (236) gives us the relation for allowed magnetic flux values. It says that flux through the hole of the cylinder or ring can take only values that are the multiple of the flux quantum $\Phi_0 = \dfrac{ch}{2e}$.

In thin superconducting cylinder or in a thin superconducting ring, (i.e. when the thickness is comparable to penetration depth) screening currents are insufficient to make current $j = 0$ inside superconductor and as a result the flux through the hole of the cylinder or ring is not quantized, but many properties of the junction remain very sensitive to the flux and are periodic functions of the flux. For example, if we integrate formula (229) over the circle lying within the cylinder (or the ring) and enclosing the hole, we find that

$$\oint \mathbf{v} d\mathbf{x} = \frac{\hbar}{m}[\theta] - \frac{2e}{mc}\oint \mathbf{A} d\mathbf{x} \tag{237}$$

where $[\theta]$ is the increment of phase of the order parameter over the contour (since order parameter should be single-valued $[\theta] = 2\pi n$, where $n = 0, \pm 1, \pm 2, \ldots)$ [1]. After some simplifications expression (237) can be written in the form

$$2\pi R v = \frac{2\pi\hbar}{m}\left(n - \frac{\Phi}{\Phi_0}\right) \tag{238}$$

Although number n can take arbitrary integer values, according to formula (227) the minimum of free energy is achieved when velocity v is minimal, therefore, the actual dependence of absolute value of the velocity on the flux Φ is given by the formula [82]

$$v = \min_n \left(\frac{\hbar}{mR}\left|n - \frac{\Phi}{\Phi_0}\right|\right) \tag{239}$$

taking into account equation (228) we see that magnetic flux can influence the critical temperature of the ring. Indeed, since $a \approx \alpha(T - T_c)$ (where T_c is the critical temperature of bulk superconductor without magnetic field), and from the requirement $|\psi| = 0$ at critical temperature, we find that

$$T_c^* = T_c - \min_n \left(\frac{\hbar^2}{2mR^2\alpha}\left|n - \frac{\Phi}{\Phi_0}\right|^2\right) \tag{240}$$

The transition temperature is not the only parameter that is affected by the flux. In this part of Thesis we study how dispersion relations of plasma oscillations change with magnetic flux through the hole.

5.7 The dispersion relation for plasma oscillations in a hollow superconducting cylinder.

This chapter explains details of our calculation of dispersion relation of plasmons in the thin superconducting cylinder. Let us take the symmetry axis of the cylinder as a coordinate axis z of cylindrical system of coordinates and let $\mathbf{r} = (r, \theta)$, to be radius-vector perpendicular to this axis z. Since the motion of charge carriers is restricted to be within the material of the cylinder the charge and current densities can be written in the form

$$\rho = \rho_2 \delta(r - R) \qquad \mathbf{j} = \mathbf{j}_2 \delta(r - R) \tag{241}$$

[1] Equation (237) can be represented in the form similar to the form of equation (236) where instead of flux Φ one has so-called "fluxoid", defined as $\tilde{\Phi} = \Phi + \frac{mc}{2e}\oint \mathbf{v} d\mathbf{x}$

where $\delta(r-R)$ is Dirac delta function and $\mathbf{j}_2$ and ρ_2 are two-dimensional (areal) current and charge densities. Both current flows and uncompensated charges will produce electrical and magnetic fields around the cylinder. To find the dispersion relation for plasmons in the cylinder we have to solve Maxwell equations for electromagnetic fields created by charge and current oscillations. For the oscillations with frequency ω and wave numbers k_z, m we can write densities and potentials in the form

$$\rho_2(R) = \tilde{\rho}\ e^{i\omega t}e^{-im\varphi}e^{-ik_z z} \qquad \mathbf{j}_2(R) = \tilde{\mathbf{j}}\ e^{i\omega t}e^{-im\varphi}e^{-ik_z z} \tag{242}$$

$$\varphi(r) = \tilde{\varphi}(r)\ e^{i\omega t}e^{-im\varphi}e^{-ik_z z} \qquad \mathbf{A}(r) = \tilde{\mathbf{A}}(r)\ e^{i\omega t}e^{-im\varphi}e^{-ik_z z} \tag{243}$$

Substituting formulas (242) and (243) into the Maxwell equations, we find that Fourier components $\tilde{\varphi}(r)$ and $\tilde{\mathbf{A}}(r)$ of field potentials obey relations

$$\frac{1}{r}\frac{\partial}{\partial r}\left(r\frac{\partial\tilde{\varphi}}{\partial r}\right) - \left[\kappa^2 + \frac{m^2}{r^2}\right]\tilde{\varphi} = -4\pi\tilde{\rho}\ \delta(r-R) \tag{244}$$

$$\frac{1}{r}\frac{\partial}{\partial r}\left(r\frac{\partial\tilde{\mathbf{A}}}{\partial r}\right) - \left[\kappa^2 + \frac{m^2}{r^2}\right]\tilde{\mathbf{A}} = -\frac{4\pi}{c}\tilde{\mathbf{j}}\ \delta(r-R) \tag{245}$$

where $\kappa = \sqrt{k_z^2 - (\omega/c)^2}$ is the modified wave vector that takes into account retardation effects. From the requirement that potentials $\tilde{\mathbf{A}}$ and $\tilde{\varphi}$ must be continuous and finite everywhere, one readily gets for the field on the surface expressions

$$\begin{cases} \tilde{\varphi} = -4\pi\tilde{\rho}RI_m(R\kappa)K_m(R\kappa) \\ \\ \tilde{\mathbf{A}} = -\frac{4\pi}{c}\tilde{\mathbf{j}}RI_m(R\kappa)K_m(R\kappa) \end{cases} \tag{246}$$

For the Fourier components of the electric fields inside the cylinder we find that

$$\tilde{E}_z = 4\pi i\left(\frac{\omega}{c^2}\tilde{j}^z - k_z\tilde{\rho}\right)RI_m(\kappa R)K_m(\kappa R) \tag{247}$$

$$\tilde{E}_\theta = 4\pi i\left(\frac{\omega}{c^2}\tilde{j}^\theta - \frac{m}{R}\tilde{\rho}\right)RI_m(\kappa R)K_m(\kappa R) \tag{248}$$

To proceed further we need make some assumptions about electrons in superconductors. At first, since the number of electrons on the surface of a superconducting cylinder remains constant, electrons should obey the continuity equation

$$\frac{\partial\tilde{\rho}}{\partial t} = -\mathrm{div}\tilde{\mathbf{j}} \tag{249}$$

At second, by modeling the electrons as classical particles with mass m_e, we assume that they are described by the Newtonian mechanics, namely, the equation of motion of an electron in superconductor is

$$m_e \frac{\partial \mathbf{v}}{\partial t} = eE \tag{250}$$

Substituting continuity equation and equation of motion written in Fourier representation

$$\tilde{\rho} = \frac{m}{\omega R}\tilde{j}^{\theta} + \frac{k_z}{\omega}\tilde{j}^{z} \qquad\qquad \tilde{\mathbf{v}} = -i\frac{e}{\omega m_e}\tilde{\mathbf{E}} \tag{251}$$

into the formulas (247) and (248) we derive the expression between currents and velocities of electrons in the superconductor, which can be written in the matrix form

$$\begin{pmatrix} \tilde{v}_z \\ \tilde{v}_\theta \end{pmatrix} = \begin{pmatrix} a_{zz} & a_{z\theta} \\ a_{\theta z} & a_{\theta\theta} \end{pmatrix} \begin{pmatrix} \tilde{j}_z \\ \tilde{j}_\theta \end{pmatrix} \tag{252}$$

where components of the matrix $a_{\alpha\beta}$ are given by the formulas

$$a_{zz} = \frac{4\pi e R}{m_e \omega^2}\left(\frac{\omega^2}{c^2} - k_z^2\right) I_m(R\kappa) K_m(R\kappa) \tag{253}$$

$$a_{\theta\theta} = \frac{4\pi e R}{m_e \omega^2}\left(\frac{\omega^2}{c^2} - \frac{m^2}{R^2}\right) I_m(R\kappa) K_m(R\kappa) \tag{254}$$

$$a_{\theta z} = a_{z\theta} = -\frac{4\pi e k_z m}{m_e \omega^2} I_m(R\kappa) K_m(R\kappa) \tag{255}$$

Until now we did not use the fact that our cylinders are superconducting. In fact equations (252) and (253) are the same as for normal tubes. To take into account superconductivity we have to use material equation (230) between current and velocity of superconducting electrons. This relation is nonlinear. We are interested only in small oscillations when the amplitude of velocity changes in the plasma wave is much smaller than the critical velocity v_c. For such small oscillations we can linearize (230) around some homogeneous state $\mathbf{u}$

$$\mathbf{v} = \mathbf{u} + \delta\mathbf{v}\ , \qquad \mathbf{u} = (u_z, u_\theta) = const \tag{256}$$

The Fourier transformed linearized relation between perturbations of velocity $\delta\mathbf{v} = (\delta v_z, \delta v_\theta)$ and the perturbations of the current density $\delta\mathbf{j} = (\delta j_z, \delta j_\theta)$ can be written as well as (252) in the matrix form

$$\begin{pmatrix} \delta\tilde{j}_z \\ \delta\tilde{j}_\theta \end{pmatrix} = \begin{pmatrix} b_{zz} & b_{z\theta} \\ b_{\theta z} & b_{\theta\theta} \end{pmatrix} \begin{pmatrix} \delta\tilde{v}_z \\ \delta\tilde{v}_\theta \end{pmatrix} \tag{257}$$

with matrix coefficients

$$b_{zz} = N_s ed\left(1 - \frac{u_\theta^2 + 3u_z^2}{v_c^2}\right) \tag{258}$$

$$b_{\theta\theta} = N_s ed\left(1 - \frac{u_z^2 + 3u_\theta^2}{v_c^2}\right) \tag{259}$$

$$b_{z\theta} = b_{z\theta} = 2N_s ed\frac{u_z u_\theta}{v_c^2} \tag{260}$$

Combining equations (252) and (257) we get a lineal algebraic system of equations

$$\begin{pmatrix} a_{zz} & a_{z\theta} \\ a_{\theta z} & a_{\theta\theta} \end{pmatrix} \begin{pmatrix} b_{zz} & b_{z\theta} \\ b_{\theta z} & b_{\theta\theta} \end{pmatrix} \begin{pmatrix} \delta\tilde{v}_z \\ \delta\tilde{v}_\theta \end{pmatrix} = \begin{pmatrix} \delta\tilde{v}_z \\ \delta\tilde{v}_\theta \end{pmatrix} \tag{261}$$

which can be written in more compacter as $\left(\tilde{\mathbf{A}}\tilde{\mathbf{B}} - \tilde{\mathbf{I}}\right)\delta\tilde{\mathbf{v}} = 0$ where $\tilde{\mathbf{I}}$ is the identity matrix. This system has nontrivial solutions if the determinant of the matrix $\tilde{\mathbf{C}} = \tilde{\mathbf{A}}\tilde{\mathbf{B}} - \tilde{\mathbf{I}}$ is zero. The coefficients of matrices $\tilde{\mathbf{A}}$ and $\tilde{\mathbf{B}}$ are functions of k, m and ω, the condition $\Delta(k_z, m, \omega) = \det(\tilde{\mathbf{A}}\tilde{\mathbf{B}} - \tilde{\mathbf{I}}) = 0$ gives in the implicit form the desired dispersion relation for the plasma excitations in the cylinder.

A general relation for the plasma frequency can be approximately written in the form

$$\begin{aligned} \omega^2 &= \omega_s^2\left(\frac{d}{R}\right) I_m(\kappa R)K_m(\kappa R) \times \\ &\times \left[k_z^2 R^2\left(1 - \frac{3u_z^2 + u_\theta^2}{v_c^2}\right) + m^2\left(1 - \frac{u_z^2 + 3u_\theta^2}{v_c^2}\right) - 4mk_z R\frac{u_z u_\theta}{v_c^2}\right] \end{aligned} \tag{262}$$

where $\omega_s = \omega_0\sqrt{N_s/N}$, N is total number of electrons, N_s number of superconducting electrons and $\omega_0 = \sqrt{4\pi e^2 N/m_e}$ is a frequency of plasma oscillations in a bulk piece of normal metal. Deriving equation (262), we neglected terms of the order $\omega_s^2\frac{Rd}{c^2} \ll 1$.

There are two very important cases when the dispersion relation for plasma oscillations can be written explicitly in the simple form. These limiting cases correspond to plasma wave propagation in a one-dimensional infinite superconducting filament and plasma oscillations in two-dimensional infinite flat superconducting plane. The first case is realized at small wave vectors ($k_z R \ll 1$). For low-energy excitations the wavelength of the excitation is larger than the radius of the cylinder and the fields around it are the same as around a 1D wire. Moreover since size, d, of the cross section of the cylinder that we get in this procedure is smaller than the coherence length, the motion of Cooper pairs in it will be effectively

one-dimensional and we reproduce the result of Ref.[109] - the linear dispersion relation. To reproduce result of Ref.[109] up to numerical coefficient, the radius of the cylinder R should be taken equal to the width of the film d of superconductor so that the cylinder becomes a thin wire without a hole inside.

$$\omega_{1D} = \omega_s k_z d \sqrt{\left(1 - \frac{3u_z^2}{v_c^2}\right) \log\left(\frac{2}{\gamma k_z d}\right)}\ , \qquad (k_z R \ll 1) \tag{263}$$

The second limiting case is realized if the wavelenght of plasma oscillation is much smaller than the radius of the cylinder.

$$\omega_{2D}^2 = \frac{\omega_s^2 k_z d}{2}\left(1 - \frac{3u_z^2}{v_c^2}\right)\ , \qquad (Rk_z \gg 1) \tag{264}$$

The frequency of plasmons in this case is not linear anymore, it grows as a square root of wave number ($\omega \sim \sqrt{k_z}$). Formula (262) as well as its limiting cases (263) and (264) at the limit $u_z^2/v_c^2 \to 0$ reproduce results [124] for normal clean metallic cylinders and rings. Notice that frequency of plasma oscillations can be decreased by passing electric current through the tube. The relation for the velocity of the superconducting electrons as a function of the current can be found by inverting the Eq. (229). In the first approximation, for $u_z \ll v_c$ one may write $u_z = \dfrac{j_z}{e|\psi|^2} \approx \dfrac{j_z}{eN_s}$. By increasing the current and making it close to the critical current of electrons in the film j_{max} one can lower the frequency of plasmons to make it below the energy gap in the range of the wave vectors big enough to allow observation of the crossover from 1D ($qR \ll 1$) to 2D ($qR \gg 1$) behavior. Frequencies of charge density oscillations can also be lowered by making the temperature very close to the critical temperature of the superconductor and thus decreasing the number of superconducting electrons N_s.

5.8 Aharonov-Bohm effect for plasma oscillations in the thin superconducting cylinder.

Let us consider what happens when the superconducting thin cylinder is placed in the magnetic field. (Or, if the radius of the cylinder is large enough, one can put a solenoid inside the cylinder.) The external field is parallel to the symmetry axis of the cylinder and is weak enough so it does not destroy the superconductivity in the system. From the formula

Eq.(239), the average circular velocity u_θ of electrons in the cylinder is a periodic function of magnetic flux.

$$u_\theta = \min_n \left[\frac{\hbar}{m_e R} \left(n - \frac{\Phi}{\Phi_0} \right) \right] \tag{265}$$

where Φ is the magnetic flux through the cylinder and $\Phi_0 = \pi\hbar c/e$ is the quantum of magnetic flux. In order to observe the periodicity of the circular velocity, the radius of the cylinder should be large enough to make possible even for weak fields that do not destroy the superconductivity to create fluxes Φ of the order of several flux quanta. This requirement can be expressed mathematically as $R^2 H_c \gg \Phi_0$, where H_c is the critical magnetic field.

The expression for the velocity u_θ should be inserted into the general formula (262). We consider only the case $m = 0$. For the cylinders with small diameter modes with $m > 0$ have frequencies that are higher than energy gap in the superconductor

$$\omega^2 = \omega_s^2 Rd \left(1 - 3\frac{u_z^2}{v_c^2} - \frac{\hbar^2}{m_e^2 R^2 v_c^2} \min_n \left[\left(n - \frac{\Phi}{\Phi_0} \right)^2 \right] \right) k_z^2 I_0(k_z R) K_0(k_z R) \tag{266}$$

The dispersion relation (266) is a periodic function of magnetic flux. The period of oscillations of the frequency is equal to the quantum of magnetic flux Φ_0. Figure 37**(a)** shows the reduced frequency of plasma oscillations as a function of magnetic flux for a fixed temperature $T = 8.5K$ for different values of the current along the tube. Higher currents correspond to smaller density of superconducting electrons in the samples, and, as a consequence, to smaller frequencies of plasmons. Figure 37**(b)** shows reduced frequency of plasma oscillations as a function of magnetic flux for a fixed current along the tube ($I_z = 0.5mA$) for different temperatures. The temperature $T = 8.5K$ is close to the critical temperature of the superconductor ($T_{Nb} = 9.3K$), according to Ginzburg-Landau theory the number of the superconducting electrons depends on the temperature as $N_S = 2N(1 - T/T_c)$, and the gap in the spectrum as $\Delta \approx T_c\sqrt{1 - T/T_c}$ (see e.g. [127]). We substitute these expressions into the formula for critical velocity $v_c = \Delta/p_F$ and into the expression for plasma frequency due to superconducting electrons $\omega_s = \omega_0\sqrt{N_s/N}$ (where $\omega_0 = \sqrt{4\pi e^2 N/m_e}$) and use them in the formula (266). Reduced frequency grows with the temperature because gap Δ in the spectrum of the superconductor decreases faster than the frequency of plasmons ω.

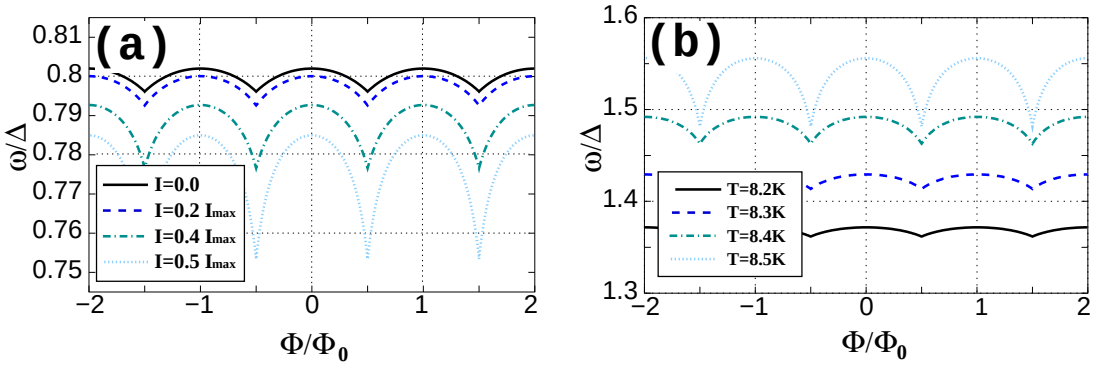

Figure 37: Aharonov Bohm oscillations of dispersion relation for plasmons in the thin superconducting cylindrical tube. The parameters of the tube are the following: radius $R = 5 \times 10^{-4} cm$, width of the walls $d = 10^{-7} cm$, tube is made from niobium ($T_c = 9.3K$). Both figures correspond to plasmons in the zero circular mode $k = 0$ and to longitudinal wave vector $k_z = 0.01/R$. Figure **(a)** shows reduced frequency of plasma oscillations as a function of magnetic flux for a fixed temperature $T = 8.5K$ for different values of the current along the tube. Figure **(b)** shows reduced frequency of plasma oscillations as a function of magnetic flux for a fixed current along the tube ($I_z = 0.5mA$) for different temperatures.

5.9 Thin superconducting ring in magnetic field.

Let us consider a superconducting ring made from a wire of diameter d such that its radius R is much larger than its diameter d i.e. ($R \gg d$). If current through the ring is quite small, we can neglect interaction between different parts of the wire and consider the ring as a straight superconducting wire with periodic boundary conditions imposed. Let us take some point on the ring as origin of a local coordinate system and let x be the coordinate along the wire and ρ the coordinate perpendicular to the wire.

It can be readily deduced from the previous formulas for the cylinder that small perturbations of linear charge density $\delta\tilde{Q}_k(\omega)$ and small perturbations of electrostatic potential $U_k(\omega)$ satisfy the relation

$$\delta\tilde{U}_k(\omega) = \delta\tilde{Q}_k(\omega) \log\left(\frac{k^2 + k_c^2}{k^2}\right) . \tag{267}$$

where $k = 1, 2, 3, \ldots$ is the discrete wave number of plasma oscillations along the ring and k_c is the cut-off parameter $k_c \sim R/d$. Using the expressions between the scalar potential and electric field $\tilde{E}_k(\omega) = ik\tilde{U}_k(\omega)/R$, equation of motion $\omega\tilde{v}_k(\omega) = -ie\tilde{E}_k(\omega)/m_e$ and continuity equation $k\tilde{I}_k(\omega) = \omega\tilde{Q}_k(\omega)R$ written in Fourier components we find the connection

of carrier velocity perturbations to the perturbations of the current

$$\delta\tilde{v}_k(\omega) = \delta\tilde{I}_k(\omega)\frac{ek^2}{\omega^2 m_e R^2}\log\left(\frac{k^2+k_c^2}{k^2}\right). \tag{268}$$

Combining this relation with the linearized equation for the superconducting current

$$\delta I = eN_s S\left(1-\frac{3u_0^2}{v_c^2}\right)\delta v \tag{269}$$

where now S is the cross section of the wire of the ring, and $u_0 = \min_n\left[\frac{\hbar}{m_e R}\left(n-\frac{\Phi}{\Phi_0}\right)\right]$ is the uniform background velocity due to the flux, and using the same arguments and procedures as for the thin cylinder in a magnetic field we get the dispersion relation for plasma oscillations in the ring:

$$\omega^2 = \frac{N_s e^2 k^2 S}{m_e R^2}\left(1-\frac{3\hbar^2}{m_e^2 R^2 v_c^2}\min_n\left[\left(n-\frac{\Phi}{\Phi_0}\right)^2\right]\right)\log\left(\frac{k^2+k_c^2}{k^2}\right) \tag{270}$$

For small wave numbers $k \ll 1$ spectrum of plasmons is acoustic ($\omega \sim ck$) with velocities that are periodic function of magnetic flux. Figure 38**(a)** shows frequency of plasmons as a function of circular wave number k (discrete). Due to induced circular currents, and as a result, reduced density of superconducting electrons, higher flux Φ through the ring gives lower frequencies ω. Figure 38**(b)** shows frequencies of the plasmons in the ring as a function of magnetic flux for several circular modes k.

5.10 Summary.

In summary we considered low frequency acoustic plasma oscillations in superconducting multiply-connected low-dimensional structures. We predict that for plasma oscillations in superconducting tubes it is possible to observe two different dimensionality regimes. For the small wave vectors ($qR \ll 1$) dispersion relation for plasmons is linear, the same as for a thin superconducting wire, whereas for the large wave vectors ($qR \gg 1$) frequency is proportional to the square root of wave vector, which is similar to the dispersion relation for an infinite superconducting plane. In both regimes, velocities (and, therefore, energies) of plasmons demonstrate periodic behavior of magnetic flux with the flux quantum period $hc/2e$. Acoustic plasma oscillations in the thin ring show similar periodic behavior. This

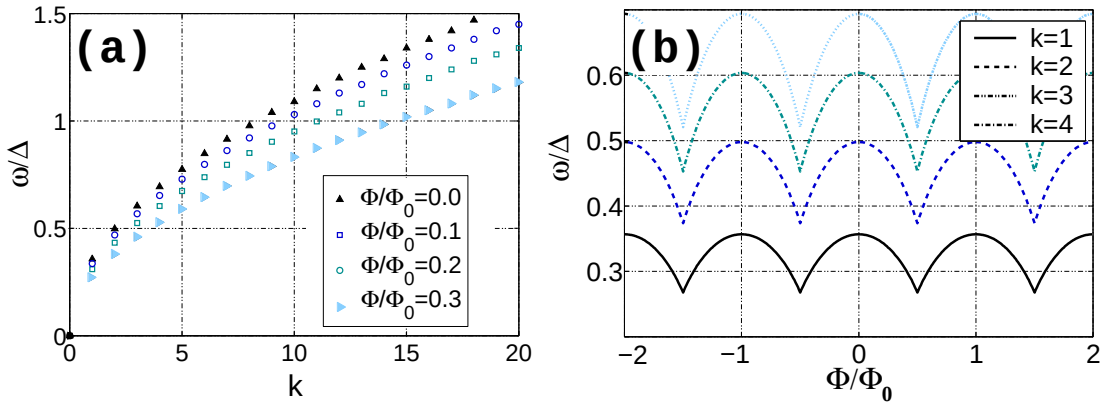

Figure 38: Frequency of plasma oscillations in a superconducting ring. The results are shown for the niobium ring with the radius $R = 2 \times 10^{-3} cm$. The cross sectional area of the wire (from which the ring is made from) is $S_0 = 5 \times 10^{-14} cm$. Figure **(a)** shows frequency as a function of the mode number. Figure **(b)** shows frequency as a function of magnetic flux.

periodicity is a manifestation of the Aharonov-Bohm effect for plasma oscillations in superconductors and is analogous to the Little-Parks effect. We derived dispersion relations of plasma oscillations for both cylinders and rings and found that the relative amplitude of frequency or velocity variations due to Aharonov-Bohm effect is proportional to $(\xi_0/R)^2$, where ξ_0 is the superconducting coherence length.

CHAPTER VI

CONCLUSION

In this thesis we considered four different problems. The first problem that we considered was the behavior of few strongly repelling atoms in harmonic and ring trap at zero temperature. We solved this problem numerically and found that the ground state of the system of few strongly repelling bosons can not be described by single-orbital theories such as Gross-Pitaevskii theory, since at high repulsion strength bosons occupy different localized orbitals, forming a crystalline structure similar to the crystalline structures of electrons in quantum dots. The wave function of the ground state that we found using our method has good angular momentum and has lower energy at all repulsion strengths and is more compact in space than the Gross-Pitaevskii wave function. The crystalline structure of our wave function is hidden (the function is rotationally symmetric) but it can be revealed via a conditional probability density. Our description of few strongly interacting bosons can be considered as a first attempt to get detailed understanding of the mechanism of destruction of the condensate and as a prediction of new possible quantum phases of trapped bosons at zero temperature.

The second part of this thesis addressed a problem of thermopower in one-dimensional quantum wires. We considered thermopower induced by nonlinearities of the dispersion relation of electrons and by impurities. Within the Luttinger Liquid model we found analytical expressions for both cases. It turns out that thermopower decreases with the increase of repulsion between electrons. For both dispersion-induced thermopower and for impurity-induced thermopower electron-electron interaction leads to simple renormalization of the thermopower. For the impurity-induced thermopower the renormalization coefficient is $C_i = 3g/(2+g)$ and for dispersion-induced thermopower $C_d = g(g^2+1)/2$, where $g^{-1} = \sqrt{1 + U_0/\pi v_F}$. All results that we obtained are valid for an infinite quantum

wire. The real quantum wires are, however, finite and connected to the macroscopic electron reservoirs (leads). Thermoelectric characteristics of a finite piece of a quantum wire connected to macroscopic leads depend strongly on the properties of the contact between the wire and leads. So far we have not been able to derive an analytical expression for the thermopower of the finite system using existing models of the contact. Our work is, however, a significant step toward solution of this problem.

The third problem, that we considered, was the problem of the force and magnetization in S/N/S and S/2DEG/S junctions. We showed that at certain values of the superconducting phase difference between superconductors, due to the properties of Andreev levels all transverse modes in the normal narrow part of the S/N/S or S/2DEG/S junction can contribute in unison to the force or magnetization resulting in giant oscillations of the magnitude of the force and magnetization. Although force and magnetization due to superconductivity are small, they are within measurable ranges of values.

And, finally, the fourth part of the thesis deals with plasma excitations in the small and thin superconducting tubes and rings. We have found analytical expressions for the frequency of plasmons as a function of longitudinal wave vector and circular wave number. We predict the Aharonov-Bohm effect for plasmons, which manifests itself in the periodic variations of frequency as a function of the magnetic flux. Moreover, we have found that for low frequency plasmons, the dispersion relation is approximately linear, like for plasma oscillations in the superconducting wire, whereas for high frequencies the dispersion relation is similar to the dispersion relation in the thin superconducting plane, i.e. frequency is proportional to the square root of wave vector.

Some of the results of the first part (dealing with bosons) were published in the Ref. [128] and other results are submitted for publication. The results of the part about thermopower in the Luttinger Liquid were published in Refs. [129] and [61]. The results of the third part about force and magnetization in the S/N/S junction were published in [105] and the results of the fourth part are being prepared for publication.

APPENDIX A

EXPRESSIONS FOR MATRIX ELEMENTS.

In this appendix we give explicit expressions for matrix coefficients of various operators, that we used in our numerical solution. Hamiltonian $\hat{H}_B$ of the system of particles in the magnetic field $\mathbf{A} = \frac{1}{2}[\mathbf{B}, \mathbf{r}]$ is

$$H_B = \sum_{i=1}^{N} \left(\frac{1}{2m_a} \left(\mathbf{p}_i - \frac{e}{c}\mathbf{A} \right)^2 + \frac{m_a}{2}\omega_0^2 \mathbf{r}_i^2 \right) + \sum_{i<j} U^{(2)}(\mathbf{r}_i - \mathbf{r}_j) \tag{271}$$

Hamiltonian $\hat{H}_\Omega$ of the system in the rotating frame can be rewritten in the form

$$H_\Omega = \sum_{i=1}^{N} \left(\frac{1}{2m_a} \left(\mathbf{p}_i - m\Omega[\mathbf{z}, \mathbf{r}_i] \right)^2 + \frac{m_a}{2}(\omega_0^2 - \Omega^2)\mathbf{r}_i^2 \right) + \sum_{i<j} U^{(2)}(\mathbf{r}_i - \mathbf{r}_j) \tag{272}$$

As it was shown in the text, the orbital of the single particle in the rotating frame as well as in the magnetic field can be quite accurately described by the function

$$\phi_i(\mathbf{r}) = \sqrt{\frac{1}{\pi\lambda^2}} \exp\left(-\frac{(\mathbf{r} - \mathbf{R}_i)^2}{2\lambda^2} - i(\mathbf{b}, [\mathbf{R_i}, \mathbf{r}]) \right) \tag{273}$$

where vector $\mathbf{b} = m\mathbf{\Omega}/\hbar$ for the case of rotating frame, and $\mathbf{b} = -e\mathbf{B}/2\hbar c$ for the case of the system in magnetic field. In the momentum representation

$$\phi_i(\mathbf{p}) = \frac{\lambda}{\hbar\sqrt{\pi}} \exp\left(-\frac{p^2\lambda^2}{2\hbar^2} - i\frac{(\mathbf{R}_i, \mathbf{p})}{\hbar} \right) \tag{274}$$

The overlap matrix $S_{ij} = (i|j) = \int \phi_i^*(\mathbf{r})\phi_j(\mathbf{r})d\mathbf{r}$ between two orbitals is

$$\begin{aligned} S_{ij} = (i|j) = \frac{1}{\pi\lambda^2} \int d\mathbf{r} \exp\left(-\frac{(\mathbf{r} - \mathbf{R}_i)^2}{2\lambda^2} - \frac{(\mathbf{r} - \mathbf{R}_j)^2}{2\lambda^2} + i(\mathbf{b}, [(\mathbf{R}_i - \mathbf{R}_j), \mathbf{r}]) \right) = \\ = \exp\left(-\frac{1}{4\lambda^2}(1 + b^2\lambda^4)(\mathbf{R}_i - \mathbf{R}_j)^2 + i(\mathbf{b}, [\mathbf{R}_i, \mathbf{R}_j]) \right) \end{aligned} \tag{275}$$

other matrix elements, needed for computation of the energy of the system, are

$$(i|p^2|j) = \frac{\hbar^2}{\lambda^2} \left(1 + \frac{1}{4\lambda^2} \left(-(\mathbf{R}_i - \mathbf{R}_j)^2 + b^2\lambda^4(\mathbf{R}_i + \mathbf{R}_j)^2 + 4i\lambda^2(\mathbf{b}, [\mathbf{R}_i, \mathbf{R}_j]) \right) \right) S_{ij} \tag{276}$$

$$(i|r^2|j) = \lambda^2 \left(1 + \frac{1}{4\lambda^2} \left((\mathbf{R}_i + \mathbf{R}_j)^2 - b^2\lambda^4(\mathbf{R}_i - \mathbf{R}_j)^2 + 4i\lambda^2(\mathbf{b}, [\mathbf{R}_i, \mathbf{R}_j]) \right) \right) S_{ij} \tag{277}$$

$$(i|r|j) = \sqrt{\pi\lambda^2}\exp\left(-\frac{\mathbf{R}_{ij}^2}{2\lambda^2}\right)\left[\left(1+\frac{\mathbf{R}_{ij}^2}{\lambda^2}\right)I_0\left(\frac{\mathbf{R}_{ij}^2}{\lambda^2}\right)+\frac{\mathbf{R}_{ij}^2}{\lambda^2}I_1\left(\frac{\mathbf{R}_{ij}^2}{\lambda^2}\right)\right]S_{ij} \qquad (278)$$

where $\mathbf{R}_{ij} = (\mathbf{R}_i + \mathbf{R}_j + i\lambda^2[\mathbf{b},(\mathbf{R}_i - \mathbf{R}_j)])/2$, and function $I_0(z)$ and $I_1(z)$ are the modified Bessel function of the first kind of the zero and first order.

Matrix element of the angular momentum operator is

$$\begin{aligned}(i|\hat{L}_z|j) &= -i\hbar(i|(x\partial_y - y\partial_x)|j) = \\ &= -\frac{\hbar}{2\lambda^2 b}\left(i(\mathbf{b},[\mathbf{R}_i,\mathbf{R}_j])(1+b^2\lambda^4) + 2b^2\lambda^2(\mathbf{R}_i,\mathbf{R}_j)\right)S_{ij}\end{aligned} \qquad (279)$$

Matrix elements of interaction terms:

1) contact potential $U^{(2)}(\mathbf{r}_i - \mathbf{r}_j) = U_0\delta(\mathbf{r}_i - \mathbf{r}_j)$

$$\begin{aligned}(ij|U^{(2)}|kl) = \frac{U_0}{2\pi\lambda^2}\exp\left(-\frac{R_i^2+R_j^2+R_k^2+R_l^2}{2\lambda^2}\right)\exp\left(\frac{(\mathbf{R}_i+\mathbf{R}_j+\mathbf{R}_k+\mathbf{R}_l)^2}{8\lambda^2}\right)\times \\ \times\exp\left(\frac{-b^2\lambda^2}{8}(\mathbf{R}_i+\mathbf{R}_j-\mathbf{R}_k-\mathbf{R}_l)^2\right)\exp\left(\frac{i}{2}(\mathbf{b},[(\mathbf{R}_i+\mathbf{R}_j),(\mathbf{R}_k+\mathbf{R}_l)])\right)\end{aligned} \qquad (280)$$

2) Coulomb potential $U^{(2)}(\mathbf{r}_i - \mathbf{r}_j) = e^2/|\mathbf{r}_i - \mathbf{r}_j|$

$$\begin{aligned}(ij|U^{(2)}|kl) = \frac{e^2}{\lambda}\sqrt{\frac{\pi}{2}}\exp\left(-\frac{1}{2\lambda^2}(R_i^2+R_j^2+R_k^2+R_l^2)\right)\times \\ \times\exp\left(\frac{1}{8\lambda^2}(i\lambda^2\mathbf{G}+\mathbf{R}_i+\mathbf{R}_j+\mathbf{R}_k+\mathbf{R}_l)^2\right)\exp\left(\frac{D^2}{8}\right)F\left(\frac{D^2}{16}\right)\end{aligned} \qquad (281)$$

where we introduced vectors $\mathbf{G} = [\mathbf{b},(\mathbf{R}_i + \mathbf{R}_j - \mathbf{R}_k - \mathbf{R}_l)]$, and $\mathbf{D} = \frac{1}{\lambda}(\mathbf{R}_i - \mathbf{R}_j + \mathbf{R}_k - \mathbf{R}_l) - i\lambda[\mathbf{b},(\mathbf{R}_i - \mathbf{R}_j - \mathbf{R}_k + \mathbf{R}_l)]$, and where $F(x) = e^{-x}I_0(x)$.

APPENDIX B

EXPRESSIONS FOR DENSITIES.

One particle density i.e. the probability to find any particle in some position $\mathbf{r}$ multiplied by the number of particles, *for unprojected wave function*, is given by the equation

$$\rho(\mathbf{r}) = \frac{\langle \Psi_N | \sum_{i=1}^{N} \delta(\mathbf{r} - \mathbf{R}_i) | \Psi_N \rangle}{\langle \Psi_N | \Psi_N \rangle} \tag{282}$$

this formal expression can be rewritten in terms of orbital matrix elements (here we use notation $|i) = |\phi_i)$)

$$\rho(\mathbf{r}) = \frac{N!}{\langle \Psi_N | \Psi_N \rangle} \sum_{k,l} (k|\mathbf{r})(\mathbf{r}|l)\mathrm{perm}(S_l^k). \tag{283}$$

Substituting overlap matrix elements (see Eq.275) into this formula we get

$$\rho(\mathbf{r}) = \frac{1}{\pi\lambda^2} \sum_{kl} \exp\left(-\frac{(\mathbf{r} - \mathbf{R}_k)^2 + (\mathbf{r} - \mathbf{R}_l)^2}{2\lambda^2} + i(\mathbf{r}, [(\mathbf{b}, \mathbf{R}_k - \mathbf{R}_l)]) \right) \frac{\mathrm{perm}(S_l^k)}{\mathrm{perm}(S\ )} \tag{284}$$

The expression for momentum distribution can be calculated similarly

$$\rho(\mathbf{p}) = \frac{\lambda^2}{\pi\hbar^2} \sum_{kl} \exp\left(i\frac{(\mathbf{R}_l - \mathbf{R}_k)\mathbf{p}}{\hbar} \right) \exp\left(-\frac{\lambda^2 p^2}{\hbar^2} \right) \frac{\mathrm{perm}(S_l^k)}{\mathrm{perm}(S\ )}. \tag{285}$$

The conditional probability, which is the probability to find the second particle in some position r if the first particle is in the position r_0, *for unprojected wave function*, can be written as

$$\rho(\mathbf{r}|\mathbf{r_0}) = \frac{\langle \Psi_N | \sum_{i \neq j} \delta(\mathbf{r} - \mathbf{R}_i)\delta(\mathbf{r_0} - \mathbf{R}_j) | \Psi_N \rangle}{\langle \Psi_N | \Psi_N \rangle} \tag{286}$$

which, as can be easily found, is equivalent to

$$\rho(\mathbf{r}|\mathbf{r_0}) = \frac{N!}{\langle \Psi_N | \Psi_N \rangle} \sum_{k \neq m, l \neq n} (k|\mathbf{r})(\mathbf{r}|l)(m|\mathbf{r_0})(\mathbf{r_0}|n)\mathrm{perm}(S_{ln}^{km}) \tag{287}$$

$$\rho(\mathbf{r}|\mathbf{r_0}) = \sum_{k\neq m, l\neq n} \exp\left(-\frac{(\mathbf{r}-\mathbf{R}_k)^2 + (\mathbf{r}-\mathbf{R}_l)^2 + (\mathbf{r}_0-\mathbf{R}_m)^2 + (\mathbf{r}_0-\mathbf{R}_n)^2}{2\lambda^2}\right) \times$$
$$\times \exp\left(\frac{i(\mathbf{r},[(\mathbf{b},\mathbf{R}_k-\mathbf{R}_l)]) + i(\mathbf{r}_0,[(\mathbf{b},\mathbf{R}_n-\mathbf{R}_m)])}{2\lambda^2}\right) \frac{\mathrm{perm}(S^{km}_{ln})}{\mathrm{perm}(S)} \quad (288)$$

Notice again that formulas (282)-(284), as well as (285) and Eqs.(286)-(288) stand for *unprojected* wave function. The expressions for a single-particle probability density and a conditional probability density for *projected* wave function are more cumbersome and are not shown here. Computation of densities of projected wave function requires derivation of the matrix elements and overlaps between equal or non-equal bosonic wave functions.

APPENDIX C

GAUSSIAN ORBITALS AND THE LLL.

In this appendix we provide a proof that Gaussian orbitals with width $\lambda = l_\Omega\sqrt{2}$ are in the lowest Landau level. We start from the formula (47) and show that it is a superposition of the Darwin-Fock single-particle wave functions with zero nodes, i.e. it is a superposition of the Lowest Landau level states. Introducing complex variables $z = x + iy$ and $Z = X + iY$, one can write

$$\begin{aligned}
\psi(\mathbf{r}) &= \frac{1}{\sqrt{2\pi}l_\Omega}\exp\left(-\frac{1}{4l_\Omega^2}((x-X)^2+(y-Y)^2) - \frac{i}{2l_\Omega^2}(xY-yX)\right) = && (289)\\
&= \frac{1}{\sqrt{2\pi}l_\Omega}\exp\left(-\frac{zz^*+ZZ^*-2zZ^*}{4l_\Omega^2}\right) = && (290)\\
&= \frac{1}{\sqrt{2\pi}l_\Omega}\exp\left(-\frac{zz^*+ZZ^*}{4l_\Omega^2}\right)\sum_{l=0}^{\infty}\left(\frac{zZ^*}{2l_\Omega^2}\right)^l = && (291)\\
&= \sum_{l=0}^{\infty} C_l(Z^*)\psi_l(z) && (292)
\end{aligned}$$

where coefficients C_l are equal to

$$C_l(Z^*) = \frac{1}{\sqrt{l!}}\left(\frac{Z^*}{\sqrt{2}l_\Omega}\right)^l e^{-\frac{ZZ^*}{4l_\Omega^2}} = \frac{1}{\sqrt{l!}}\left(\frac{X-iY}{\sqrt{2}l_\Omega}\right)^l \exp\left(-\frac{X^2+Y^2}{4l_\Omega^2}\right) \qquad (293)$$

and functions

$$\psi_l(z) = \frac{1}{\sqrt{2\pi l!}l_\Omega}\left(\frac{z}{\sqrt{2}l_\Omega}\right)^l e^{-\frac{zz^*}{4l_\Omega^2}} = \frac{1}{\sqrt{2\pi l!}l_\Omega}\left(\frac{x+iy}{\sqrt{2}l_\Omega}\right)^l \exp\left(-\frac{x^2+y^2}{4l_\Omega^2}\right) \qquad (294)$$

are (see Eq. (43)) the Darwin-Fock single particle wave functions with zero nodes, i.e. wave functions from the lowest Landau level. Thus, shifted gaussians with $\lambda = l_\Omega\sqrt{2}$ are the linear combinations of the states from the lowest Landau level only. If $\lambda \neq l_\Omega\sqrt{2}$, the above decomposition can not be made - the expansion will necessary include states from the higher Landau levels. This means that by allowing Gaussians to change their width we are taking into account effects related to higher Landau levels, i.e. we are going beyond the lowest Landau level approximation.

APPENDIX D

TRANSPORT COEFFICIENTS.

In this appendix we show details of perturbational calculation of transport coefficients. The density operators $\rho_{N,J}(t,x)$ in momentum representation take the form (see e.g. Ref. [156])

$$\rho_N(x,t) = \frac{N_0}{L} + \frac{1}{2\pi}\int_{-\infty}^{+\infty} dp \sqrt{\frac{g\epsilon_p}{s}}\left[b_p e^{-i(px-\epsilon_p t)} + b_p^\dagger e^{i(px-\epsilon_p t)}\right], \tag{295}$$

$$\rho_J(x,t) = \frac{J_0}{L} + \frac{1}{2\pi}\int_{-\infty}^{+\infty} dp \sqrt{\frac{\epsilon_p}{sg}}\mathrm{sgn}(p)\left[b_p e^{-i(px-\epsilon_p t)} + b_p^\dagger e^{i(px-\epsilon_p t)}\right], \tag{296}$$

where L is the size of the system ($L \to \infty$), N_0 is the number of extra (above the Fermi level) electrons, J_0 is the zero-mode current, b_p and $b_p^\dagger$ are the standard bosonic annihilation and creation operators ($[b_p, b_{p'}^\dagger] = \delta_{p,p'}$), and $\epsilon_p = s|p|$ is the energy of bosonic excitation with momentum p.

By making use of Eqs.(295) and (296) it is straightforward to calculate the Matsubara Green functions for the density operators ($L \to \infty$)

$$\langle \hat{T}_\tau \rho_N(-i\tau,x)\rho_N(0,y)\rangle = -\frac{g}{2\pi s^2\beta}\sum_n e^{i\bar{\omega}_n\tau}\bar{\omega}_n \frac{\cosh\left[\frac{\bar{\omega}_n}{s}(x-y-\frac{L}{2})\right]}{\sinh\left[\frac{\bar{\omega}_n}{s}\frac{L}{2}\right]}, \tag{297}$$

$$\langle \hat{T}_\tau \rho_J(-i\tau,x)\rho_J(0,y)\rangle = -\frac{1}{2\pi s^2 g\beta}\sum_n e^{i\bar{\omega}_n\tau}\bar{\omega}_n \frac{\cosh\left[\frac{\bar{\omega}_n}{s}(x-y-\frac{L}{2})\right]}{\sinh\left[\frac{\bar{\omega}_n}{s}\frac{L}{2}\right]}, \tag{298}$$

$$\langle \hat{T}_\tau \rho_N(-i\tau,x)\rho_J(0,y)\rangle = -\frac{1}{2\pi s^2\beta}\sum_n e^{i\bar{\omega}_n\tau}\bar{\omega}_n \frac{\sinh\left[\frac{\bar{\omega}_n}{s}(x-y-\frac{L}{2})\right]}{\sinh\left[\frac{\bar{\omega}_n}{s}\frac{L}{2}\right]}. \tag{299}$$

Here $\rho_{N,J} \equiv \rho_{N,J}(0,0)$ and $\bar{\omega}_n = i2\pi n/\beta$ is the Matsubara frequency ($\beta = T^{-1}$, $n = 0, \pm1, \pm2, ...$). One readily gets from Eqs.(297)-(299)

$$\langle \rho_N\rho_N\rangle = \frac{g}{\pi sL}\sum_m \frac{\varepsilon_m}{e^{\beta\varepsilon_m}-1}, \qquad \langle \rho_J\rho_J\rangle = \frac{1}{\pi sgL}\sum_m \frac{\varepsilon_m}{e^{\beta\varepsilon_m}-1}, \qquad \langle \rho_J\rho_N\rangle = 0 \quad . \tag{300}$$

In perturbation theory the kinetic coefficients can be represented as the time-ordered product of the ρ_N and ρ_J density operators. In particulary, for $\sigma^{(2)}$ in the static limit, $\omega \to 0$

(see Eq.(128)), one gets

$$\sigma^{(2)} = A\frac{e\pi^3 s^3 g}{6} \lim_{\substack{\bar{\omega}\to 0 \\ L\to\infty}} \frac{1}{\bar{\omega}} \int_0^\beta d\lambda \int_0^\beta d\tau_1 \int_0^L dx_1 \exp(i\lambda\bar{\omega}) \times \tag{301}$$
$$\times \Big(\langle \hat{T}_\tau \rho_J(-i\lambda, x)\rho_N(-i\lambda, x)\rho_J(0, x)\rho_N(-i\tau_1, x_1)\rho_N(-i\tau_1, x_1)\rho_N(-i\tau_1, x_1)\rangle +$$
$$+3\langle \hat{T}_\tau \rho_J(-i\lambda, x)\rho_N(-i\lambda, x)\rho_J(0, x)\rho_J(-i\tau_1, x_1)\rho_J(-i\tau_1, x_1)\rho_N(-i\tau_1, x_1)\rangle \Big) \ .$$

Wick's theorem allows us to reduce the time-ordered product of operators to the sum of the product of Green's functions. In our case the thermoelectric coefficient takes the form

$$\sigma^{(2)} = A\frac{e\pi^3 s^3 g}{2} \lim_{\substack{\bar{\omega}\to 0 \\ L\to\infty}} \frac{1}{\bar{\omega}} \int_0^\beta d\lambda \int_0^\beta d\tau_1 \int_0^L dx_1 \exp(i\lambda\bar{\omega}) \times \tag{302}$$
$$\times \Big(\langle \hat{T}\rho_J(-i\lambda, x)\rho_J(0, x)\rangle \langle \hat{T}\rho_N(-i\lambda, x)\rho_J(-i\tau_1, x_1)\rangle \Big) \left(\langle \rho_J \rho_J \rangle + \langle \rho_N \rho_N \rangle \right) \ ,$$

where $\bar{\omega} = i\omega$. The substitution of the Green's functions into the last equation yields

$$\sigma^{(2)} = \frac{Ae}{s^2\beta^2} \frac{\pi(g^2+1)}{6} \tag{303}$$

APPENDIX E

SEMI-INFINITE LUTTINGER LIQUID.

Here we derive following Ref.[151] the expressions for the momentum representation of the bosonic fields $\Phi(x)$ and $\Theta(x)$ for a LL with an open boundary. The impurity potential at $x = 0$ is modeled by the boundary which reflects electrons perfectly. Thus one may regard the LL wire as consisting of two independent (in the absence of tunneling) segments. Let us continue the fermion field $\Psi_{r_m}(x)$ from the segment "1(2)" to the segment "2(1)". The fermion field Ψ must satisfy the condition

$$\Psi_{L,m}(x) = -\Psi_{R,m}(-x) \tag{304}$$

on each segment $m = 1, 2$. Hence the densities $\rho_{N,J,L,R}$ and the field operators have to obey the relations: $\rho_L(x) = \rho_R(-x)$, $\rho_N(x) = \rho_N(-x)$, $\rho_J(x) = -\rho_J(-x)$, $\Theta(x) = \Theta(-x)$, $\Phi(x) = -\Phi(-x)$. It is natural to consider that for the case of noninteracting electrons ($g = 1$) the fields Θ and Φ are the stationary waves

$$\Theta_m^{(0)}(x) = i \int_{-\infty}^{+\infty} dp \sqrt{\frac{2v_F}{\epsilon_p}} (b_p - b_p^\dagger) \cos(\frac{\epsilon_p}{v_F} x), \qquad \Phi_m^{(0)}(x) = \int_{-\infty}^{+\infty} dp \sqrt{\frac{2v_F}{\epsilon_p}} (b_p + b_p^\dagger) \sin(\frac{\epsilon_p}{v_F} x) \ , \tag{305}$$

where b_p and $b_p^\dagger$ are bosonic annihilation and creation operators ($[b_p, b_{p'}^\dagger] = \delta_{p,p'}$), and $\epsilon_p = v_F|p|$. Substituting Eq.(305) into the Luttinger liquid Hamiltonian Eq.(118) we observe that the Hamiltonian is not diagonal in the annihilation and creation operators. It is diagonalized by the Bogoliubov's transformation, and the transformed fields $\Theta_m(x)$ and $\Phi_m(x)$ take the form

$$\Theta_m(x) = \hat{U}\Theta_m^0(x)\hat{U}^{-1} = i \int_{-\infty}^{+\infty} dp \sqrt{\frac{2s}{g\epsilon_p}} (b_p - b_p^\dagger) \cos(\frac{\epsilon_p}{s} x) \ , \tag{306}$$

$$\Phi_m(x) = \hat{U}\Phi_m^0(x)\hat{U}^{-1} = \int_{-\infty}^{+\infty} dp \sqrt{\frac{2sg}{\epsilon_p}} (b_p + b_p^\dagger) \sin(\frac{\epsilon_p}{s} x) \ , \tag{307}$$

where the unitary operator $\hat{U}$ is

$$\hat{U} = \exp\left(\frac{1}{2}\varphi \int_{-\infty}^{+\infty} dq \;\; [b_q^\dagger b_{-q}^\dagger - b_q b_{-q}]\right) \; . \tag{308}$$

Here $\tanh(2\varphi) = (1-g^2)/(1+g^2)$. The energy ϵ_p in Eqs.(B3),(B4) is now the energy of plasmons $\epsilon_p = s|p|$ in a Luttinger liquid.

APPENDIX F

INTEGRALS OF THE GAMMA FUNCTIONS.

In this appendix, for completeness, we list the analytical expressions for the integrals of the Euler Gamma functions appearing in the evaluation of the Luttinger liquid thermopower:

$$\int_{-\infty}^{+\infty} dx|\Gamma(\alpha+ix)|^2|\Gamma(\beta+ix)|^2 = 2\pi\frac{\Gamma^2(\alpha+\beta)\Gamma(2\alpha)\Gamma(2\beta)}{\Gamma(2(\alpha+\beta))} \tag{309}$$

$$\int_{-\infty}^{+\infty} dx\left\{x\left|\Gamma\left(\alpha+\frac{i}{2}(x+z)\right)\right|^2\left|\Gamma\left(\beta+\frac{i}{2}(x-z)\right)\right|^2\right\} = 2\pi z\frac{\Gamma^2(\alpha+\beta+iz)\Gamma(2\alpha)\Gamma(2\beta)}{(\alpha+\beta)\Gamma(2(\alpha+\beta))} \tag{310}$$

$$\int_{-\infty}^{+\infty} dx\left\{x^2\left|\Gamma(\alpha+ix)\right|^2\left|\Gamma(\beta+ix)\right|^2\right\} = \frac{2\pi\alpha\beta}{(2\alpha+2\beta+1)}\frac{\Gamma^2(\alpha+\beta)\Gamma(2\alpha)\Gamma(2\beta)}{\Gamma(2(\alpha+\beta))} \tag{311}$$

The first integral can be found in the tables of integrals (see, e.g., Ref. [163]), it follows from Barnes' Lemma (see proof in [164]). The two other integrals (310) and (311) are readily derived from Eq.(309) using property $\Gamma(1+z) = z\Gamma(z)$.

REFERENCES

[1] M. H. Anderson, J. R. Ensher, M. R. Matthews, C. E. Wieman, and E. A. Cornell., "Observation of Bose-Einstein Condensation in a Dilute Atomic Vapor.," *Science* **269**, 198 (1995).

[2] T. Schneider and R. BlÜmel., "Bose-Einstein condensates of bosonic Thomson atoms.," *Journal of Physics B: At. Mol. Opt. Phys.* **32**, 5017 (1999).

[3] K. W. Madison, F. Chevy, W. Wohlleben, and J. Dalibard, "Vortex Formation in a Stirred Bose-Einstein Condensate.," *Phys. Rev. Lett.* **84**, 806 (2000).

[4] T. Kinoshita, T. Wenger, and D. S. Weiss., "Observation of a One-Dimensional Tonks-Girardeau Gas.," *Science* **305**, 1125 (2004).

[5] K. Huang, *Statistical Mechanics* (Wiley, New York, 1987).

[6] M. Olshanii, "Atomic Scattering in the Presence of an External Confinement and a gas of Impenetrable Bosons.," *Phys. Rev. Lett.* **81**, 938 (1998).

[7] D. S. Petrov, M. Holzmann, and G. V. Shlyapnikov, "Bose-Einstein Condensation in Quasi-2D Trapped Gas.," *Phys. Rev. Lett.* **84**, 2551 (2000).

[8] S.-H. Kim, C. Won, S. D. Oh, and W. Jhe, "Two-Dimensional Gross-Pitaevskii Equation: Theory of Bose-Einstein Condensation and Vortex State.," arXiv:cond-mat/9904087 **3** (1999).

[9] S.-H. Kim, S. D. Oh, and W. Jhe, "Two-Dimensional Condensation of Dilute Bpse Atoms in a Harmonic Trap.," *Journal of the Korean Physical Society* **37**, 665 (2000).

[10] M. Girardeau, "Relationship between Systems of Impenetrable Bosons and Fermions in One Dimension.," *Journal of Mathematical Physics* **1**, 516 (1960).

[11] L. Tonks, "The Complete Equation of State of One, Two and Three-Dimensional Gases of Hard Spheres.," *Physical Review* **50**, 955 (1936).

[12] B. Paredes, A. Widera, V. Murg, O. Mandel, S. Fölling, I. Cirac, G. V. Shlyapnikov, T. W. Hänsch, and I. Bloch, "Tonks-Girardeau gas of ultracold atoms in an optical lattice.," *Nature* **305**, 277 (2004).

[13] edited by G. M. d'Ariano, A. Montorsi, and M. G. Rasetti, *Integrable Systems in Statistical Mechanics* (World Scientific, Singapore, 1985).

[14] E. B. Kolomeisky, T. J. Newman, J. P. Straley, and X. Qi, "Low-Dimensional Bose Liquids: Beyond Gross-Pitaevskii approximation.," *Phys. Rev. Lett.* **85**, 1146 (2000).

[15] A. Szabo and N. S. Ostlund, *Modern Quantum Chemistry* (Macmillan Publishing Co., New York, 1982).

[16] F. W. Bobrowicz and W. A. Goddard III, *"The Self-Consistent Field Equations for Generalized Valence Bond and Open-Shell Hartree-Fock Wave Functions" in Methods of Electronic Structure Theory* (Addison-Wesley, New York, 1977).

[17] I. William A. Goddard, "Improved Quantum Theory of Many-Electron Systems. I. Construction of Eigenfunctions of S^2 Which Satisfy Pauli's Principle.," *Physical Review* **157**, 73 (1967).

[18] I. William A. Goddard, "Improved Quantum Theory of Many-Electron Systems. II. The Basic Method.," *Physical Review* **157**, 81 (1967).

[19] G. Brown, *Unified Theory of Nuclear Models and Forces.* (Elsevier, New York, 1971).

[20] P. Ring and P. Schuck, *The Nuclear Many-Body Problem.* (Springler-Verlag, New York, 1980).

[21] P. Lowdin, "Normal constants of motion in quantum mechanics treated by projection technique.," *Rev. Mod. Phys.* **34**, 520 (1962).

[22] C. Yannouleas and U. Landman, "Spontaneous Symmetry Breaking in Single and Molecular Quantum Dots.," *Phys. Rev. Lett.* **82**, 5325 (1999).

[23] C. Yannouleas and U. Landman, "Spontaneous Symmetry Breaking in Single and Molecular Quantum Dots.," *Phys. Rev. Lett.* **85**, 2220(E) (2000).

[24] C. Yannouleas and U. Landman, "Group theoretical analysis of symmetry breaking in two-dimensional quantum dots.," *Physical Review B* **68**, 035325 (2003).

[25] C. Yannouleas and U. Landman, "Strongly correlated wavefunctions for artificial atoms and molecules.," *Journal of Physics: Condensed Matter* **14**, L591 (2002).

[26] B. Paredes, P. Fedichev, J. I. Cirac, and P. Zoller, "1/2-Anyons in small Atomic Bose-Einstein Condensates.," *Phys. Rev. Lett.* **87**, 010402 (2001).

[27] M. Popp, B. Paredes, and J. I. Cirac, "Adiabatic path to fractional quantum Hall states of a few bosonic atoms.," *Physical Review A* **70**, 053612 (2004).

[28] N. K. Wilkin and J. M. F. Gunn, "Condensation of "Composite Bosons" in a Rotating BEC.," *Phys. Rev. Lett.* **84**, 6 (2000).

[29] S. A. Trugman and S. Kivelson, "Exact results for the fractional quantum Hall effect with general interactions.," *Physical Review B* **31**, 5280 (1985).

[30] A. G. Morris and D. L. Feder, "Validity of the Lowest Landau Level approximation for rotating Bose gases.," *arXiv:cond-matt* **v1**, 0602037 (2006).

[31] M. Girardeau and E. M. Wright, "Quantum mechanics of one-dimensional trapped Tonks gases.," *Laser Physics* **12**, 8 (2002).

[32] A. Lorke, R. J. Luyken, A. O. Govorov, and J. P. Kotthaus, "Spectroscopy of Nanoscopic Semiconductor Rings.," *Phys. Rev. Lett.* **84**, 2223 (2000).

[33] S. Gupta, K. W. Murch, K. L. Moore, T. P. Purdy, and D. M. Stamper-Kurn, "Bose-Einstein Condensation in a Circular Waveguide.," *Phys. Rev. Lett.* **95**, 143201 (2005).

[34] P. Verkerk and D. Hennequin, "An Optical Lattice of Ring Traps.," *arXiv:cond-matt* **v1**, 0306155 (2003).

[35] P. F. Kartsev, "Rotating Bose-Einstein condensate with attractive interaction in one dimension: Single-L states and mesoscopics.," *Physical Review A* **68**, 063613 (2003).

[36] D. Butts and D. Rokhsar, "Predicted signatures of rotating Bose-Einstein condensates.," *Nature* **397**, 327 (1999).

[37] M. Greiner, O. Mandel, T. Esslinger, T. Hansch, and I. Bloch, "Quantum phase transition from a superfluid to a Mott insulator in a gas of ultracold atoms.," *Nature* **415**, 39 (2002).

[38] B. Paredes, A. Widera, V. Murg, O. Mandel, S. Folling, I. Cirac, G. Shlyapnikov, T. Hansch, and I. Bloch, "Tonks-Girardeau gas of ultracold atoms in an optical lattice.," *Nature* **429**, 277 (2004).

[39] M. Schellekens, R. Hoppeler, A. Perrin, J. Gomes, D. Boiron, A. Aspect, and C. Westbrook, "Hanbury Brown Twiss Effect for Ultracold Quantum Gases.," *Science* **310**, 648 (2005).

[40] R. G. Wheeler, K. K. Choi, A. Goel, R. Wisnieff, and D. E. Prober, "Localization and Electron-Electron Interaction Effects in Submicron-Width Inversion Layers.," *Phys. Rev. Lett.* **49**, 1674 (1982).

[41] Y. Hirayama, S. Tarucha, Y. Suzuki, and H. Okamoto, "Fabrication of a $GaAs$ quantum-well-wire structure by Ga focused-ion-beam implantation and its optical properties.," *Physical Review B* **37**, 2774 (1988).

[42] J. R. Kirtley, Z. Schlesinger, T. N. Theis, F. P. Milliken, S. L. Wright, and L. F. Palmateer, "Voltage-controlled dissipation in the quantum Hall effect in a laterally constricted two-dimensional electron gas.," *Physical Review B* **34**, 5414 (1986).

[43] T. J. Thornton, M. Pepper, H. Ahmed, D. Andrews, and G. J. Davies, "One-Dimensional Conduction in the 2D Electron Gas of a $GaAs - AlGaAs$ Heterojunction.," *Phys. Rev. Lett.* **56**, 1198 (1986).

[44] H. Z. Zhang, H. P. Wei, D. C. Tsui, and G. Weimann, "Gate-controlled transport in narrow $GaAs/Al_xGa_{1-x}As$ heterostructures.," *Physical Review B* **34**, 5635 (1986).

[45] C. Kane and M. Fisher, *Edge State Transport (in "Perspectives in the Quantum Hall effect".)* (edited by S. Das Sarma and A. Pinczuk (Wiley), New York, 1997).

[46] S. Iijima, "Helical microtubules of graphitic carbon.," *Nature.* **354**, 56 (1991).

[47] T. W. Ebbesen and P. M. Ajayan, "Large-scale synthesis of carbon nanotubes.," *Nature.* **358**, 220 (1992).

[48] A. Thess, R. Lee, P. Nikolaev, H. Dai, P. Petit, J. Robert, C. Xu, Y. H. Lee, S. G. Kim, A. G. Rinzler, D. T. Colbert, G. E. Scuseria, D. Tomanek, J. E. Fischer, and R. E. Smalley, "Crystalline ropes of metallic carbon nanotubes.," *Science.* **273**, 483 (1996).

[49] Z. F. Ren, Z. P. Huang, J. W. Xu, J. H. Wang, P. Bush, M. P. Siegal, and P. N. Provencio, "Synthesis of Large Arrays of Well-Aligned Carbon Nanotubes on Glass.," *Science.* **282**, 1105 (1998).

[50] E. H. Lieb and F. Y. Wu, "Absence of Mott transition in an exact solution of the short-range, one band model in one dimension.," *Phys. Rev. Lett.* **20**, 1445 (1968).

[51] J. M. Luttinger, "An exactly soluble model of many-fermion system.," *Journal of Mathematical Physics.* **4**, 1154 (1963).

[52] D. C. Mattis and E. H. Lieb, "Exact solution of a many-fermion system and its associated boson field.," *Journal of Mathematical Physics.* **6**, 304 (1965).

[53] F. D. M. Haldane, "Luttinger Liquid theory of one-dimensional quantum fluids. I. Properties of the Luttinger model and their extension to the general 1D interacting spinless Fermi gas.," *Journal of Physics C: Solid State Physics* **14**, 2585 (1981).

[54] E. Miranda, "Introduction to bosonization.," *Brazilian Journal of Physics* **33**, 3 (2003).

[55] R. Landauer, "Electrical resistance of disordered one-dimensional lattices.," *Philosophical magazine.* **21**, 863 (1970).

[56] J. M. Ziman, *Principles of the Theory of Solids* (Cambridge University Press, Cambridge, England, 1986).

[57] C. Kane and M. Fisher, "Transport in a one-channel Luttinger Liquid.," *Phys. Rev. Lett.* **68**, 1220 (1992).

[58] C. Kane and M. Fisher, "Transmission through barriers and resonant tunneling in an interacting one-dimensional electron gas.," *Physical Review B* **46**, 15233 (1992).

[59] C. Kane and M. Fisher, "Thermal Transport in a Luttinger Liquid.," *Phys. Rev. Lett.* **76**, 3192 (1996).

[60] I. V. Krive, E. N. Bogachek, A. G. Scherbakov, and U. Landman, "Interaction enhanced thermopower in a Luttinger Liquid.," *Physical Review B* **63**, 113101 (2001).

[61] I. Romanovsky, I. Krive, E. Bogachek, and U. Landman, "Thermopower of an infinite Luttinger Liquid.," *Physical Review B* **65**, 075115 (2002).

[62] J. Rammer and H. Smith, "Quantum field-theoretical methods in transport theory of metals.," *Review of Modern Physics.* **58**, 323 (1986).

[63] I. M. Lifshits, M. Y. Azbel, and M. I. Kaganov, *Electron theory of metals.* (Consultants Bureau, New York, 1973).

[64] A. Furusaki and N. Nagaosa, "Single-barrier problem and Anderson localization in a one-dimensional interacting electron system.," *Physical Review B* **47**, 4631 (1993).

[65] M. Bockrath, C. D.H., J. Lu, A. Rinzler, R. Smalley, T. Balents, and P. McEuen, "Luttinger Liquid behaviour in carbon nanotubes.," *Nature.* **397**, 598 (1999).

[66] D. Maslov and M. Stone, "Landauer conductance of Luttinger Liquids with leads.," *Physical Review B* **52**, R5539 (1995).

[67] V. V. Ponomarenko, "Renormalization of the one-dimensional conductance in the Luttinger-liquid model.," *Physical Review B* **52**, R8666 (1995).

[68] I. Safi and H. J. Schulz, "Transport in an inhomogeneous interacting one-dimensional system.," *Physical Review B* **52**, R17040 (1995).

[69] R. Fazio, F. W. J. Hekking, and D. E. Khmelnitskii, "Anomalous Thermal Transport in Quantum Wires.," *Phys. Rev. Lett.* **80**, 5611 (1998).

[70] I. V. Krive, "Thermal transport through Luttinger Liquid constriction.," *Low Temperature Physics* **24**, 377 (1998).

[71] R. Egger and H. Grabert, "Applying voltage sources to a Luttinger Liquid with arbitrary transmission.," *Physical Review B* **58**, 10761 (1998).

[72] U. Landman, W. Luedtke, N. Burnham, and R. Colton, "Atomistic mechanisms and dynamics of adhesion, nanoindentation, and fracture.," *Science* **248**, 454 (1990).

[73] N. Agrait, Yeyati, A. Levy, van Ruitenbeek, and J. M., "Quantum properties of atomic-sized conductors.," *Physics Reports* **377**, 81 (2003).

[74] G. Rubio, N. Agrat, and S. Vieira, "Atomic-Sized Metallic Contacts: Mechanical Properties and Electronic Transport.," *Phys. Rev. Lett.* **76**, 2302 (1996).

[75] C. A. Stafford, D. Baeriswyl, and J. Bürki, "Jellium Model of Metallic Nanocohesion.," *Phys. Rev. Lett.* **79**, 2863 (1997).

[76] C. Yannouleas and U. Landman, "On mesoscopic forces and quantized conductance in model metallic nanowires.," *Journal of Physical Chemistry B* **101**, 5780 (1997).

[77] C. Yannouleas, E. Bogachek, and U. Landman, "Energetics, forces, and quantized conductance in jellium-modeled metallic nanowires.," *Physical Review B* **57**, 4872 (1998).

[78] D. Leckband and J. Israelachvili, "Intermolecular forces in biology.," *Quarterly Reviews of Biophysics.* **34**, 105 (2001).

[79] I. Kulik, "Macroscopic quantization and proximity effect in S-N-S junctions.," *Soviet Physics JETP-USSR* **30**, 944 (1970).

[80] D. L. Maslov, M. Stone, P. M. Goldbart, and D. Loss, "Josephson current and proximity effect in Luttinger Liquids.," *Physical Review B* **53**, 1548 (1996).

[81] J. Caux, H. Saleur, and F. Siano, "Josephson current in Luttinger Liquid-superconductor junctions.," *Phys. Rev. Lett.* **88**, 106402 (2002).

[82] P. de Gennes, *Superconductivity of metals and alloys.* (Benjamin, New York, 1966).

[83] C. Ishii, "Josephson currents through junctions with normal metal barriers.," *Progress of Theoretical Physics* **44**, 1525 (1970).

[84] J. J. J. Bardeen, "Josephson current flow in pure $S/N/S$ junctions.," *Physical Review B* **5**, 72 (1972).

[85] J. Bardeen, "Tunnelling from a Many-Particle Point of View.," *Phys. Rev. Lett.* **6**, 57 (1961).

[86] J. Bardeen, "Tunneling Into Superconductors.," *Phys. Rev. Lett.* **9**, 147 (1962).

[87] C. Beenakker and H. van Houten, "Josephson current through a superconducting quantum point contact shorter than the coherence length.," *Phys. Rev. Lett.* **66**, 3056 (1991).

[88] P. Samuelsson, J. Lantz, V. Shumeiko, and G. Wendin, "Nonequilibrium Josephson effect in mesoscopic ballistic multiterminal $S/N/S$ junctions.," *Physical Review B* **62**, 1319 (2000).

[89] C. Stafford, D. Baeriswyl, and J. Burki, "Jellium model of metallic nanocohesion.," *Phys. Rev. Lett.* **79**, 2863 (1997).

[90] D. Leckband and J. Israelachvili, "Forces in Biology.," *Quarterly Reviews of Biophysics* **34**, 105 (2001).

[91] P. Sandström and I. Krive, "Coulomb blockade effects on quantization of charge and persistent current in a Luttinger Liquid ring.," *Annals of Physics* **257**, 18 (1997).

[92] A. Furusaki, H. Takayanagi, and M. Tsukada, "Theory of quantum conduction of supercurrent through a constriction.," *Phys. Rev. Lett.* **67**, 132 (1991).

[93] H. Blom, A. Kadigrobov, A. M. Zagoskin, R. I. Shekhter, and M. Jonson, "Dissipative electron transport through Andreev interferometers.," *Physical Review B* **57**, 9995 (1998).

[94] G. Gogadze and I. Kulik, "Oscillatory and resonant effects in $S/N/S$ junctions in a magnetic field.," *Soviet Physics JETP-USSR* **33**, 984 (1971).

[95] A. Kadigrobov, R. Shekhter, M. Jonson, and Z. Ivanov, "Resonant transmission of normal electrons through Andreev states in ferromagnets.," *Physical Review B* **60**, 14593 (1999).

[96] A. Buzdin, L. Bulaevskii, and S. Panyukov, "Critical current oscillations as a function of the exchange field and thickness of the ferromagnetic metal (F) in an $S/F/S$ Josephson junction.," *JETP Letters* **35**, 178 (1982).

[97] H. Takayanagi, T. Akazaki, and J. Nitta, "Observation of Maximum Supercurrent Quantization in a Superconducting Quantum Point Contact.," *Phys. Rev. Lett.* **75**, 3533 (1995).

[98] S. den Hartog, B. van Wees, Y. Nazarov, T. Klapwijk, and G. Borghs, "Giant Andreev Backscattering through a Quantum Point Contact Coupled via a Disordered Two-Dimensional Electron Gas to Superconductors.," *Phys. Rev. Lett.* **79**, 3250 (1997).

[99] E. V. Bezuglyi, A. S. Rozhavsky, I. Vagner, and P. Wyder, "Combined effect of Zeeman splitting and spin-orbit interaction on the Josephson current in a superconductor-two-dimensional electron gas-superconductor structure.," *Physical Review B* **66**, 052508 (2002).

[100] A. Andreev, "The thermal conductivity of the intermediate states in superconductors.," *Soviet Physics JETP-USSR* **19**, 1228 (1964).

[101] A. M. Zagoskin, *Quantum Theory of Many-Body Systems.* (Springer, New York, 1998).

[102] G. Gogadze and A. Kosevich, "Quantum levels and quasi-local states of S/I/N/I/S structures.," *Low Temperature Physics* **24**, 540 (1998).

[103] O. Cakir and I. Kulik, "Josephson effect in superconductive S/N/S heterostructures with barriers.," *Physical Review B* **67**, 174514 (2003).

[104] P. Bagwell, "Suppression of the Josephson current through a narrow, mesoscopic, semiconductor channel by a single impurity.," *Physical Review B* **46**, 12573 (1992).

[105] I. Krive, I. Romanovsky, E. Bogachek, and U. Landman, "Phase-Controlled Force and Magnetization Oscillations in Superconducting Ballistic Nanowires.," *Phys. Rev. Lett.* **92**, 126802 (2004).

[106] S. Laux, D. Frank, and F. Stern, "Quasi-one-dimensional electron states in a split-gate $GaAs/AlGaAs$ heterostructure.," *Surface Science* **196**, 101 (1988).

[107] J. Davies and J. Nixon, "Fluctuations in submicrometer semiconducting devices caused by the random positions of dopants.," *Physical Review B* **39**, 3429 (1989).

[108] A. Kadigrobov, A. Zagoskin, R. Shekhter, and M. Jonson, "Giant conductance oscillations controlled by supercurrent flow through a ballistic mesoscopic conductor.," *Physical Review B* **52**, R8662 (1995).

[109] I. Kulik, "Oscillations of surface charge in superconductors.," *Soviet Physics JETP* **65**, 1008 (1975).

[110] Y. Aharonov and D. Bohm, "Significance of Electromagnetic Potentials in the Quantum Theory.," *Physical Review* **115**, 485 (1959).

[111] I. Kulik, "Flux quantization in a normal metal.," *JETP Letters-USSR.* **11**, 275 (1970).

[112] B. Al'tshuler, A. Aronov, B. Spivak, J. Sharvin, and D. Sharvin, "Observation of the Aharonov-Bohm effect in hollow metal cylinders.," *JETP Letters* **35**, 588 (1982).

[113] B. Al'tshuler, A. Aronov, and B. Spivak, "The Aaronov-Bohm effect in disordered conductors.," *JETP Letters* **33**, 94 (1981).

[114] M. Büttiker, Y. Imry, R. Landauer, and S. Pinhas, "Generalized many-channel conductance formula with application to small rings.," *PRB* **31**, 6207 (1984).

[115] R. Webb, S. Washburn, C. Umbach, and R. Laibowitz, "Observation of h/e Aharonov-Bohm Oscillations in Normal-Metal Rings.," *Phys. Rev. Lett.* **54**, 2696 (1985).

[116] I. Krive and A. Krokhin, "Excitonic mechanism of Aharonov-Casher oscillations.," *Physical Review A* **186**, 162 (1994).

[117] R. Römer and M. Raikh, "Aharonov-Bohm effect for an exciton.," *Physical Review B* **62**, 7045 (2000).

[118] I. Kulik, A. Rozhavskii, and E. Bogachek, "Magnetic flux quantization in dielectrics.," *Pis'ma Zh. Eksp. Teor. Fiz.* **47**, 251 (1988).

[119] E. Bogachek, I. Krive, I. Kulik, and A. Rozhavsky, "Instanton Aharonov-Bohm effect and macroscopic quantum coherence in charge-density-wave systems.," *Physical Review B* **42**, 7614 (1990).

[120] R. Carlson and A. Goldman, "Propagating Order-Parameter Collective Modes in Superconducting Films.," *Phys. Rev. Lett.* **34**, 11 (1975).

[121] R. Ritchie, "Plasma Losses by Fast Electrons in Thin Films.," *Physical Review* **106**, 874 (1957).

[122] R. Ferrell, "Predicted Radiation of Plasma Oscillations in Metal Films.," *Physical Review* **111**, 1214 (1964).

[123] C. Yannouleas, E. Bogachek, and U. Landman, "Dimensionality crossovers of the σ plasmon in coaxial carbon nanotubes.," *Physical Review B* **50**, 7977 (1994).

[124] C. Yannouleas, E. Bogachek, and U. Landman, "Collective excitations of multishell carbon microstructures: Multishell fullerenes and coaxial nanotubes.," *Physical Review B* **53**, 10225 (1996).

[125] O. Buisson, P. Xavier, and J. Richard, "Observation of Propagating Plasma Modes in a Thin Superconducting Film.," *Phys. Rev. Lett.* **73**, 3153 (1994).

[126] F. Parage, M. Doria, and O. Buisson, "Plasma modes in periodic two-dimensional superconducting-wire networks.," *Physical Review B* **58**, R8921 (1998).

[127] A. Abrikosov, *Fundamentals of the Theory of Metals.* (North-Holland, Amsterdam, 1988).

[128] I. Romanovsky, C. Yannouleas, and U. Landman, "Crystalline boson phases in harmonic traps: Beyond the Gross-Pitaevskii mean field.," *Phys. Rev. Lett.* **93**, 230405 (2004).

[129] I. Krive, I. Romanovsky, E. Bogachek, A. Scherbakov, and U. Landman, "Thermoelectric effects in a Luttinger Liquid.," *Low Temperature Physics* **27**, 821 (2001).

[130] S. Cornish, N. Claussen, J. Roberts, E. A. Cornell, and C. E. Wieman, "Stable ^{85}Rb Bose-Einstein Condensates with Widely Tunable Interactions.," *Phys. Rev. Lett.* **85**, 1795 (2000).

[131] C. Yannouleas and U. Landman, "Trial wave function with long-range Coulomb correlations for two-dimensional N-electron systems in high magnetic fields.," *Physical Review B* **66**, 115315 (2002).

[132] E. H. Lieb and W. Liniger, "Exact Analysis of an interacting Bose Gas. I. General Solution and the Ground State.," *Physical Review* **130**, 1605 (1963).

[133] O. E. Alon, A. I. Streltsov, and L. S. Cederbaum, "Fragmentation of Bose-Einstein condensates in multi-well three-dimensional traps.," *Physics Letters A* **347**, 88 (2005).

[134] S.-C. Cheng, "Variational Hartree-Fock Ground-State Energy for a Two-Dimensional Wigner Crystal Induced by a Strong Magnetic Field.," *Chineese Journal of Physics* **35**, 718 (1997).

[135] J. Kainz, S. A. Mikhailov, A. Wensauer, and U. Rossler., "Quantum dots in high magnetic fields: Calculation of ground-state properties.," *Physical Review B* **65**, 115305 (2002).

[136] A. Kamlan, "An Approximation for Rotation-Projected Expectatio Values of the Energy for Deformed Nuclei and a Derivation of the Cranking Variational Equation.," *Zeitschrift fur Physik* **216**, 52 (1968).

[137] E. Anisimovas, A. Matulis, and F. M. Peeters., "Currents in a many-particle parabolic quantum dot under a strong magnetic field," arXiv:cond-mat/0408672 **1** (2004).

[138] A. Puente, L. Serra, and R. G. Nazmitdinov, "Roto-vibrational spectrum and Wigner crystallization in two-electron parabolic quantum dots.," arXiv:cond-mat/0308430 **2** (2004).

[139] M. J. Holland, "Atomic beads on strings of light.," *Nature* **429** (2004).

[140] E. L. Bolda, E. Tiesinga, and P. S. Julienne, "Pseudopotential model of ultracold atomic collisions in quasi-one- and two-dimensional traps.," *Physical Review A* **68**, 032702 (2003).

[141] J. Anandan and J. Suzuki, "Quantum mechanics in a Rotating Frame.," arXiv:quant-ph/0305081 **2** (2003).

[142] Z. Idziaszek and T. Calarco, "Two atoms in an anisotropic harmonic trap.," *Physical Review A* **71**, 050701(R) (2005).

[143] P. Capuzzi, N. H. March, and M. P. Tosi, "Wigner bosonic molecules with repulsive interactions and harmonic confinement," *Physics Letters A* **339**, 207 (2005).

[144] V. M. Bedanov and F. M. Peeters, "Ordering and phase transitions of charged particles in a classical finite two-dimensional system.," *Physical Review B* **49**, 2667 (1994).

[145] P. A. Maksym, "Quantum states of interacting electrons in a 2D elliptical quantum dot.," *Physica B* **249 − 251**, 233 (1998).

[146] P. A. Maksym, "Eckardt frame theory of interacting electrons in quantum dots.," *Physical Review B* **53**, 10871 (1995).

[147] S. M. Reimann and M. Manninen, "Electronic structure of quantum dots.," *Reviews of Modern Physics* **74**, 1283 (2002).

[148] H. J. Metcalf and P. van der Straten, *Laser Cooling and Trapping* (Springer, New York, 1999).

[149] J. K. Jain and R. K. Kamilla, *Composite Fermions: Particles of the Lowest Landau Level (in the book "Composite fermions: A unified view of the Quantum Hall Regime", edited by O. Heinonen).* (World Scientific, Singapore, 1998).

[150] D. Schmeltzer, "Bozonization in one and two dimensions.," *Physical Review B* **47**, 11980 (1993).

[151] M. Fabrizio and A. Gogolin, "Interacting one dimensional electron gas with open boundaries.," *Physical Review B* **51**, 17827 (1995).

[152] L. I. Glazman, I. M. Ruzin, and B. I. Shklovskii, "Interacting one dimensional electron gas with open boundaries.," *Physical Review B* **45**, 8454 (1992).

[153] M. I. Visscher and G. E. W. Bauer, "Mesoscopic charge-density wave junction.," *Physical Review B* **54**, 2798 (1996).

[154] J. Voit and H. J. Schulz, "Electron-phonon interaction and phonon dynamics in one-dimensional conductors: Spinless fermions.," *Physical Review B* **36**, 968 (1987).

[155] G. Ingold and Y. Nazarov, *"Single Charge Tunneling" (in NATO ASI series B)*volume 294 (edited by H. Grabert and M. H. Devoret (Plenum), New York, 1992).

[156] A. Gogolin, A. Nersesyan, and A. Tsvelik, *Bosonization Approach to Strongly Correlated Systems.* (Cambridge University Press, Cambridge, England, 1998).

[157] C. Lau, N. Markovic, M. Bockrath, A. Bezryadin, and M. Tinkham, "Quantum phase slips in superconducting nanowires.," *Phys. Rev. Lett.* **87**, 217003 (2001).

[158] I. Krive, S. Kulinich, R. Shekhter, and M. Jonson, "Charge and spin effects in mesoscopic Josephson junctions.," *Low Temperature Physics* **30**, 738 (2004).

[159] E. Bogachek and I. Kulik, "Vector potential induced diamagnetism and flux quantization in normal metals.," *Fiz. Nizk. Temp.* **9**, 398 (1983).

[160] E. Bogachek and G. Gogadze, "Quantum electromagnetic-waves in cylindrical conductors.," *Zhurnal Eksperimentalnoi i Teoreticheskoi Fiziki* **67**, 621 (1974).

[161] J. Mooij and G. Schön, "Propagating plasma mode in thin superconducting filaments.," *Phys. Rev. Lett.* **55**, 114 (1985).

[162] F. Dunmore, "Observation of below-gap plasmon excitations in superconducting $YBa_2Cu_3O_7$ films.," *Physical Review B* **52**, R731 (1995).

[163] I. S. Gradshtein and I. M. Ryzhik, *Tables of Integrals, Series and Products.* (Academic, New York, 1980).

[164] E. Whittaker and G. Watson, *A course of modern analysis. (vol. 2)* (University Press, Cambridge, 1927).

LIST OF PUBLICATIONS

1. Krive I.V., Romanovsky I.A., Bogachek E.N., Scherbakov A.G., Landman U., *"Thermoelectric effects in a Luttinger liquid"*, Low Temperature Physics, vol. 27 (9-10): p. 821, Sep-Oct 2001

2. Romanovsky I.A., Krive I.V., Bogachek E.N., Landman U., *"Thermopower of an infinite Luttinger liquid"*, Physical Review B, vol. 65, Issue 7, p.075115, Feb 2002

3. Krive I.V., Romanovsky I.A., Bogachek E.N., Landman U., *"Phase-Controlled Force and Magnetization Oscillations in Superconducting Ballistic Nanowires"*, Physical Review Letters, vol. 92, Issue 12, p. 126802, Mar 2004

4. Romanovsky I.A., Yannouleas C., Landman U., *"Crystalline boson phases in harmonic traps: Beyond the Gross-Pitaevskii mean field"*, Physical Review Letters, vol. 93, Issue 23, p. 230405, Dec 2004

5. Romanovsky I.A., Yannouleas C., Landman U., *"Bosonic molecules in rotating traps"*, submitted for publication in PRL

6. Romanovsky I.A., Bogachek E.N., Krive I.V., Landman U., *"Giant magnetization of a superconductor – two-dimensional electron gas – superconductor structure."*, in preparation

7. Bogachek E.N., Romanovsky I.A., Landman U. *"Aharonov-Bohm effect and plasma oscillations in superconducting tubes and rings."*, in preparation

LIST OF PRESENTATIONS

1. Romanovsky I.A., Krive I.V., Bogachek E.N., Landman U., *"Thermopower of an infinite Luttinger liquid."*, Bull. Amer. Phys. Soc. **47**, No. 1, 358 (2002).

2. Krive I.V., Romanovsky I.A., Bogachek E.N., Landman U., *"Phase-controlled Force and Magnetization Oscillations in Superconducting Ballistic Wires."*, Bull. Amer. Phys. Soc. **48**, No. 1, 125 (2003).

3. Bogachek E.N., Romanovsky I.A., Landman U. *"Plasma oscillations and Aharonov-Bohm effect in superconducting tubes and rings."*, Bull. Amer. Phys. Soc. **49**, No. 1, 871 (2004).

4. Romanovsky I.A., Yannouleas C., Landman U., *"Crystalline Phases of Bosons in Harmonic Traps."*, Bull. Amer. Phys. Soc. **50**, No.1, 132 (2005).

5. Romanovsky I.A., Bogachek E.N., Krive I.V., Landman U., *"Giant magnetization of superconductor – two-dimensional electron gas – superconductor structure."*, Bull. Amer. Phys. Soc. **50**, No.1, 210 (2005)

6. Romanovsky I.A., Yannouleas C., Landman U., *"Crystalline phases of bosons in rotating traps: Tonks-Girardeau gas on a ring."*, Bull. Amer. Phys. Soc. **51**, No. 1, 1294 (2006).